Effect of Intraocular Pressure on Chick Eye Geometry, Finite Element Modeling, and Myopia

by

Reno Genest

A thesis
presented to the University of Waterloo
in fulfillment of the
thesis requirement for the degree of
Master of Applied Science
in
Mechanical Engineering and Vision Science

Waterloo, Ontario, Canada, 2010

Author's Declaration

I hereby declare that I am the sole author of this thesis. This is a true copy of the thesis, including any required final revisions, as accepted by my examiners.

I understand that my thesis may be made electronically available to the public.

Abstract

In most cases, myopia is characterized by an increase in axial length of the eye, but the exact mechanisms for the axial elongation are still unknown. Higher intraocular pressure (IOP) has been associated with myopia and could be involved in eye enlargement. Also, some investigators have argued that the mechanical stresses generated by the ocular muscles during near work cause the eye to stretch out of shape. The purpose of this work was to investigate the effect of IOP on eye geometry, build a finite element model of the corneo-scleral shell of a chick eye, and verify if the eye could elongate due to increased IOP and hence become myopic.

In the present study, myopia was induced in the right eye of chicks using -15 dioptre (D) goggles. The in-vitro pressure-volume curves of normal and myopic chick eyes were obtained using a computer controlled syringe pump and a digital pressure gauge. The axial length and horizontal equatorial diameter of the chick eyes as pressure increased were measured from digital photographs. To build the finite element model, normal chick eyes were frozen, sliced using a microtome, and photographed. The image sequence was aligned using MATLAB software and imported into SolidWorks® and Mimics software packages for three-dimensional (3D) reconstruction. Three 3D models were constructed and imported into Abaqus/CAE® software for finite element analysis. Isotropic, homogeneous, linear elastic and exponentially stiffening material properties were used for the finite element models. The results of the finite element models were compared with the experimental data.

The results showed that normal chick eyes elongated in the axial direction and initially contracted in the horizontal equatorial direction as IOP increased. Myopic chick eyes did not elongate as much in

the axial direction and did not contract as much in the horizontal equatorial direction compared with normal eyes. The volumetric deformation of myopic eyes was similar to normal eyes suggesting that growth and remodelling of the ocular tissues was involved in experimental myopia in the chick. The 3D reconstructed geometry of a chick eye was similar to a real eye although small geometric inaccuracies were present. The finite element model with isotropic, homogeneous, and exponentially stiffening material properties agreed well with the experimental strains in spite of the fact that the anisotropy of the ocular tissues was not included in the finite element model. This suggests that the oblate geometry of the chick eye was the main parameter dictating its deformation under increased IOP.

The natural tendency of chick eyes is to elongate in the axial direction as IOP increases and this suggests that IOP could play a role in myopia onset and progression. The way chick eyes deformed as pressure increased is probably due to their oblate geometry. The finite element model could be used in the future to study the effect of different parameters such as ocular muscle forces and ocular tissues material properties on eye geometry. This way, an eye configuration more prone to eye elongation and myopia could be determined.

Acknowledgements

I would like to thank my supervisors Dr. Naveen Chandrashekar and Dr. Elizabeth L. Irving for their help and guidance and for giving me the opportunity to carry out this project. I would also like to thank my fellow graduate students for their help and support.

Dedication

This thesis is dedicated to my parents and my sister.

Table of Contents

List of Figures

List of Tables

Chapter 1: Introduction

The eye is a very complex and important organ allowing animals to see objects in their surroundings. The sense of sight is a tremendous advantage for survival enabling living creatures to effectively search for food and detect obstacles or predators. Modern humans rely on their eyes (Figure 1) to perform a variety of daily activities such as reading, driving, cooking, etc. One requirement necessary for good vision is that the optical power of the eye matches its axial length such that parallel rays of

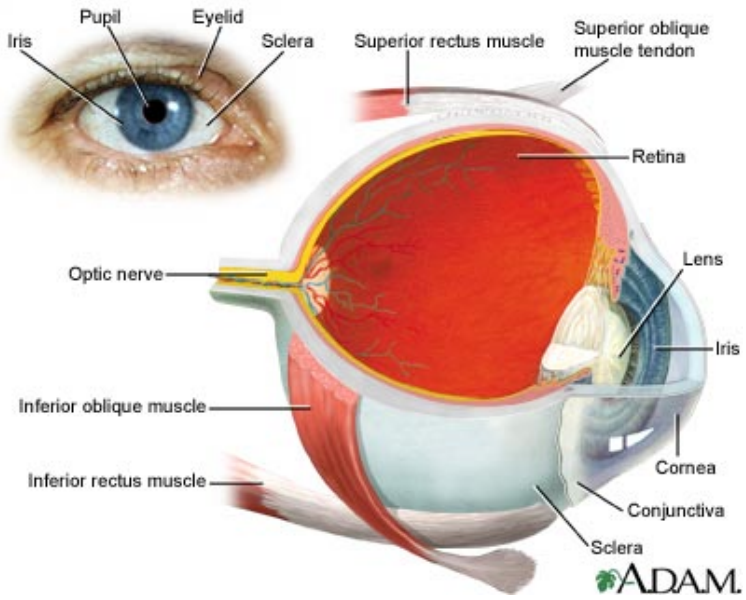

Figure 1: The human eye (Howstuffworks.com, 2010).

light entering the eye are focused precisely on the retina. This condition is called emmetropia (Figure 2). However, many people all around the world are affected by myopia, a refractive error of the eye that occurs when the axial dimension of the eye is too long causing light to be focused in front of the retina (Figure 2). The result is that distant objects appear blurry. Myopia is normally corrected by the use of eyeglasses or contact lenses having a negative power. The negative lenses are placed in front of the eye so that the plane of focus is brought to the retina. Although clear vision is achieved, negative

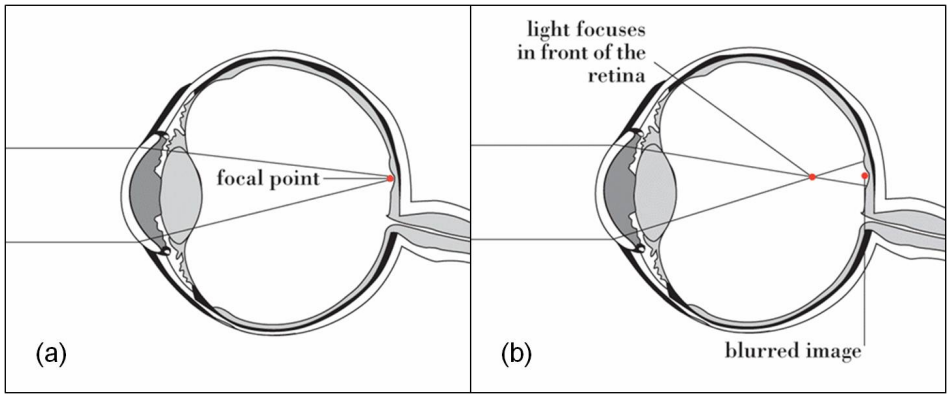

Figure 2: Diagram of (a) an emmetropic eye and (b) a myopic eye (Fendalton Eye Clinic, 2010).

lenses do not prevent the eye from getting longer and myopia from getting worst (Gwiazda, 2009). The exact mechanisms for the axial elongation of the eye are still unknown but a few theories have been proposed. One of them is the mechanical theory of myopia where the eye is thought to stretch out of shape due to the mechanical stress induced on the eyeball by the intraocular pressure (IOP) and the ocular muscles (Greene, 1980).

In this thesis, the effect of IOP on chick eye geometry is studied to determine the preferred deformation mode of the eye under elevated IOP and verify whether the eye could elongate and become myopic. Also, myopia is induced in chick eyes and their pressure-volume behavior is compared to normal eyes. Finally, a finite element model of the corneo-scleral shell of a chick eye is constructed and compared with experimental data. In the future, the finite element model could be used to study the effect of different parameters such as ocular muscle forces and ocular tissues mechanical properties on eye geometry and help understand myopia onset and progression. In this study, chicks are used for convenience; they grow fast, are easy to obtain, and inexpensive. Also, it is possible to experimentally induce myopia in chicks within a few days.

1.1 Anatomy of the human eye

1.1.1 Geometry of the eye

The overall geometry of the adult human eye is somewhat spherical. It can be idealized as two spheres with their centers 5 mm apart (Le Grand and El Hage, 1980a). A sphere with a radius of 12 mm can represent the posterior portion of the eye while the anterior part can be characterized by a smaller sphere having a radius of 8 mm (Figure 3). Of course, this is an idealization. In reality, the back of the eye is slightly flattened and the eye is not a body of revolution: its radius of curvature changes around the eye. For instance, the horizontal equatorial radius is normally larger in the nasal side compared with the temporal side. In a study of eye shape, Atchison et al. (2004) used MRI to measure the eye of 22 emmetropes (absence of refractive error) and found on average that the eyes were 23.0 mm long, 22.7 mm wide, and 22.4 mm high. They also noted a lot of variation between subjects; the axial length (anteroposterior direction) of the eye ranged from 21.4 to 24.3 mm, the width from 20.6 to 24.6 mm and the height ranged from 20.4 to 24.0 mm.

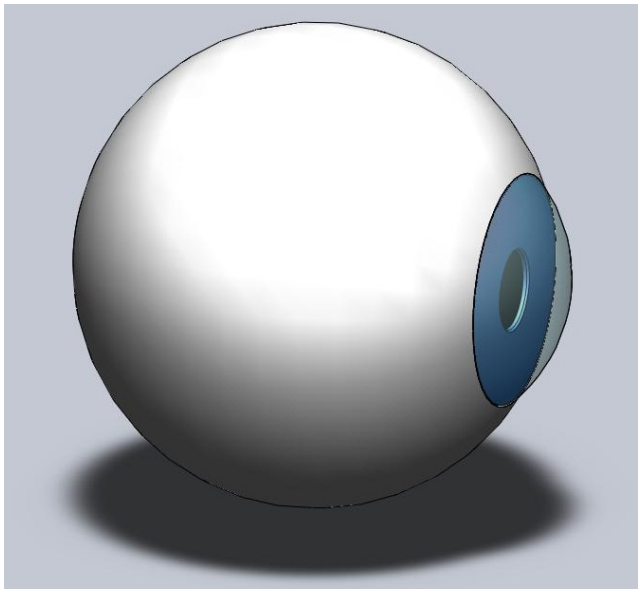

Figure 3: Idealized geometry of a human eye.

1.1.2 Corneo-scleral shell

The outer coat of the eye, often referred to as the corneo-scleral shell, is a tough fibrous tissue that encloses and protects the intraocular structures (McBrien and Gentle, 2003; Ethier et al., 2004). The corneo-scleral shell is composed of the cornea anteriorly and the sclera posteriorly (Figure 4). The cornea and the sclera meet at the limbus. The outer coat of the eye contains up to 90% collagen (McBrien and Gentle, 2003), giving it its strength. An important function of the corneo-scleral shell is to maintain a fixed axial length such that the light is focused on the retina at all time. Thus, the outer coat of the eye has to resist the variation in intraocular pressure, which is the fluid pressure inside the eye, and the forces generated by the extraocular muscles during eye movements. It also has to provide a rigid structure for the ciliary muscle to ensure accurate accommodation.

The cornea is transparent due to its avascularity and to the highly regular arrangement of its collagen fibers. The stroma, which is the main part of the cornea, consists of layers of lamellae stacked together. Each layer has its own preferred direction and within each lamella, the collagen fibrils are near equidistant and almost perfectly parallel to each other (Pinsky et al., 2005). The thickness of the cornea is around 500 μm in the center and increases to about 650 μm at the periphery. The sclera is the white part of the eye which is opaque due to the irregular arrangement of its collagen fibers. A preferred collagen fiber orientation in the sclera can be found near the extraocular muscle attachment sites (Thale et al., 1996) and around the optic nerve (Thale and Tillmann, 1993). The thickness of the sclera is lowest anteriorly and increases steadily to reach a maximum of around 1.25 mm at the back of the eye (Le Grand and El Hage, 1980a). The sclera is the main load-bearing component of the eye (Girard et al., 2008).

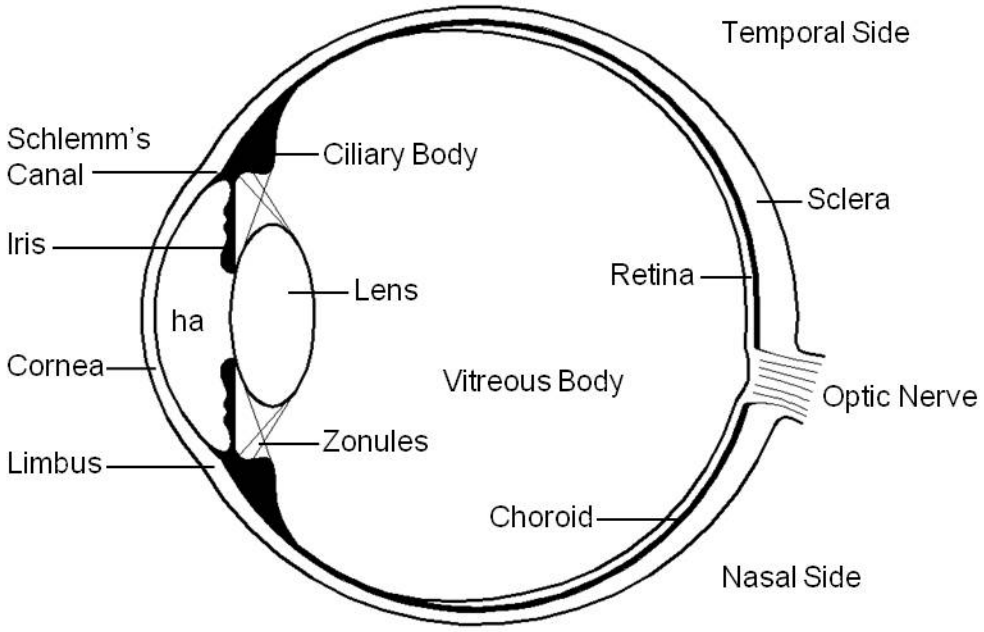

Figure 4. Diagram of a horizontal section of a human eye. ha: aqueous humor.

1.1.3 Middle tunic

The middle tunic is composed of the iris, the ciliary body, and the choroid. These structures are highly vascularized and pigmented. The iris is a circular structure that gives the eye its color. The iris lies between the lens and the cornea. Muscles within the iris relax and contract to control the size of the pupil and therefore the amount of light entering the eye based on the ambient illumination. In high illumination the pupil diameter can contract to 2 mm whereas complete darkness produces a pupil diameter of about 8 mm (Le Grand and El Hage, 1980a).

The ciliary body is composed of the ciliary muscle and the ciliary processes. The ciliary muscle is divided into three types based on the orientation of the muscle fibers: longitudinal, radial, and circular. The main function of the ciliary muscle is accommodation which is required to bring near

objects into focus. During accommodation, the ciliary muscle contracts pulling the ciliary body forward and inward (Tamm et al., 1991). The inward movement causes a release of tension of the zonules leading to a change in shape of the lens. The main function of the ciliary process is the production of aqueous humor which is a liquid that nourishes avascular tissues such as the lens and the cornea. Aqueous humor fills the space of the anterior chamber which lies between the posterior surface of the cornea and the anterior surface of the iris and the lens. Aqueous humor flows from the ciliary processes around the iris and drains mainly into Schlemm's canal located at the angle of the iris and the limbus (Figure 5). Proper balance between aqueous humor production and outflow is critical for the maintenance of normal intraocular pressure (IOP).

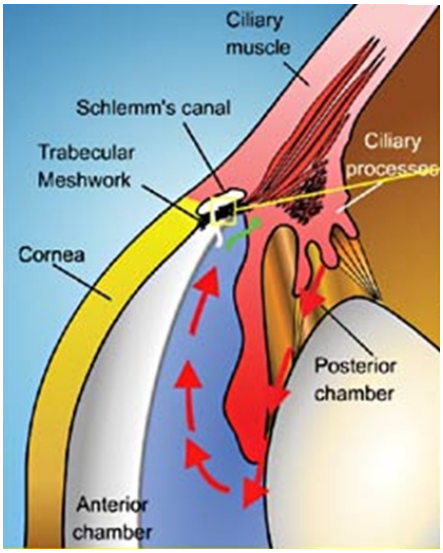

Figure 5: Aqueous humor flow (Ferrer, 2006). Copyright © 2006 Prous Science, S.A. All rights reserved.

The choroid is a layer of highly vascularized tissues located between the retina and the sclera. The main function of the choroid is to supply oxygen and nutrients to the outer retina where the energy-demanding photoreceptors (rods and cones) are located. The blood vessels in the choroid swell and

contract with the cardiac cycle which causes variation in choroidal thickness producing a change in IOP known as the ocular pulse (Ethier et al., 2004).

1.1.4 The lens

The lens is a transparent optical component capable of adjusting its refractive power to focus light coming from different distances. The lens is suspended by the zonules which are attached to the ciliary body. When focusing on a near object, the tension on the zonules is released causing the lens to fatten and change its curvature which results in an increase in dioptric power. The result is a close object focused on the retina and a clear image. With accommodation at rest, the lens accounts for roughly 1/3 of the total refractive power of the eye and its dioptric power range available for accommodation is around 10 dioptres (D) in young adults (Allen and O'Leary, 2006). The dioptre is commonly used in optometry as a measure of the optical power of a lens and is equal to the reciprocal of the focal length in metres. For instance, a 4 D lens brings parallel rays of light into focus at a distance of 1/4 metres behind the lens. The dioptre is also used to specify the optical power of the eye.

1.1.5 Vitreous body

The vitreous body is a transparent gel that fills the space of the vitreous chamber which lies between the posterior surface of the lens and the anterior surface of the retina. Its main functions are to support and inflate the eye; to provide nutrients and eliminate cellular waste; and to maintain the vitreous pressure. Studies in monkeys showed that during accommodation, the vitreous pressure increases while the anterior chamber pressure (IOP) decreases such that a pressure gradient across the lens is present (Young, 1981).

1.1.6 Retina

The retina is the innermost layer of the eye consisting of light sensitive tissue. Light striking the retina is converted into nerve impulses sent to the brain via the optic nerve.

1.2 Chicken eye anatomy

The chicken eye has the same basic structures as the human eye depicted in section 1.1. It has a cornea, a sclera, a choroid, ciliary body, a lens and so on, but there are several differences as well. First, the geometry of the chicken eye is oblate, that is, its axial length is shorter than its equatorial diameter. Also, the cornea and the lens are tilted toward the beak (Walls, 1942). The sclera of chickens consists of two layers: an inner cartilaginous layer and a thinner outer fibrous layer (Phillips et al., 2000) whereas the human sclera only has a fibrous layer. The sclera of a chicken eye is concave near the attachment site of the ciliary muscle and the concavity coincides with a bony structure: the scleral ossicles. The scleral ossicles are embedded in the sclera and appear to act as reinforcement to support the concavity (Walls, 1942). There is also a plate of bone around the optic nerve probably to reinforce this region of the sclera weakened by the optic nerve canal. Although there is no bone or cartilage in the human eye, the collagen fibers of the peripapillary sclera (near the optic nerve) are oriented circumferentially relative to the optic nerve entrance port (Greene, 1980). Another difference is that the ciliary muscle of chickens is striated (McBrien et al., 1993) while the ciliary muscle of humans is smooth. During accommodation in chickens, the ciliary muscle contracts pulling the ciliary body forward effectively pushing on the lens and squeezing it to change its shape (Sivak, 2004) as opposed to releasing the tension on the zonules as in humans. Contraction of the ciliary muscle in the chicken also leads to a change in central corneal curvature (Glasser and Howland, 1996). In addition, the choroid of a chicken eye is thicker than that of a human and can undergo larger variations in thickness to compensate for imposed defocus compared with primates (Troilo et al., 2000). The retina of chickens is also thicker, at least 1.5 times thicker than most vertebrates (Walls, 1942). At last, chicken eyes have a pecten which is a pigmented structure consisting of blood vessels that extends from the head of the optic nerve into the vitreous (Walls, 1942). The blood supply to the pecten is

different from the choroid. The function of the pecten is unknown but some argued that it supplies additional nutrients to the eye (Walls, 1942).

1.3 Myopia

1.3.1 Definition of myopia

Myopia is a refractive error that occurs when the non-accommodated eye focuses parallel rays of light, coming from far objects, in front of the retina (Figure 2). In other words, the refractive power of the eye is too powerful for the length of the eyeball and the result is a blurred image. The degree of myopia is measured in terms of dioptres (D). For instance, the emmetropic eye has a refractive error of 0 D while myopia in North America is typically defined as a refractive error of -0.50 D or less (Rosenfield and Gilmartin, 1998). In other parts of the world such as Asia, myopia is often defined as a refractive error of -0.25 D or less. Furthermore, myopia is classified as low if the refractive error is between -0.50 D and -3.00 D, mild if it is between -3.00 D and -6.00 D, or high if it is higher than -6.00 D (Rosenfield and Gilmartin, 1998). Myopia can also be classified based on the age at onset. Congenital myopia is either present at birth or develops between the ages of 0 to about 6 years (McBrien and Adams, 1997). Early-onset myopia (EOM) develops between 6 and 18 years of age while late-onset myopia (LOM) occurs between 18 and 25 (Rosenfield and Gilmartin, 1998). Grosvenor (1987) suggested that early adult-onset myopia occurs between the ages of 20 and 40 and that late adult-onset myopia takes place after 40 years.

The cornea and the lens are the two main focusing components of the eye with the cornea accounting for roughly 70 % of the total refractive power of the eye while the lens dictates around 30 % (Le Grand and El Hage, 1980b). There exists variation in cornea and lens between individuals and it is possible that someone may have a combination of cornea and lens that is more powerful than

normal which would result in the light being over focused. However, in most cases of human myopia (> 95%), the total refractive power of the eye is normal while the axial dimension is too long causing light from distant objects to fall in front of the retina (McBrien and Gentle, 2003). Furthermore, the axial elongation appears to be mainly due to an increase in vitreous chamber depth. Young (1981) pointed out that the correlation between axial length and vitreous chamber depth was 0.97 in humans. Also, Greene (1980) stated that the vitreous chamber of myopes is elongated while the posterior sclera is thinned. More recently, Atchison et al. (2004) found that "although myopic eyes tend to expand in all directions relative to emmetropic eyes, they are elongated more in the axial than in the vertical or horizontal dimension".

1.3.2 Prevalence

Myopia affects many people worldwide. In the United States, the prevalence of myopia in 1999-2004 was estimated at 41.6% (Vitale et al., 2009), up from 25% in 1971-1972 (Sperduto et al., 1983). When myopia was defined as a mean spherical equivalent of -0.5 D or less, the prevalence of myopia in 1999-2004 in the United States was around 50.1% (Vitale et al., 2008). A recent report estimated the total annual cost of correcting myopia in the United States to be at least $US 3.8 billion (Vitale et al., 2006). The rate of myopia is increasing in the United States such that the treatment costs for myopia are likely to go up (Bloom et al., 2010). The situation is similar in other parts of the world. In Australia, myopia is also on the rise (Rose et al., 2001) while in Asia, myopia is even more common and reaches levels as high as 95.9% (≤ -0.25 D) among freshmen at the National Taiwan University (Wang et al., 2008a). A report from Singapore showed that not only the prevalence is increasing but also the severity of myopia (Au Eong et al., 1993).

The prevalence of myopia appears to be higher among people who perform more near work such as professionals (Wong et al., 2000), university students (Rosenfield and Gilmartin, 1998), and certain

occupations such as microscopist (Adams and McBrien, 1992). Around the world, the prevalence and severity of myopia increases with increasing education (Rose et al., 2001). In contrast, the prevalence of myopia is low among those who do not perform a lot of close work. In a Danish study, Goldschmidt (1968) showed that the prevalence of myopia was 30.1 % among university students and dropped to 2.9 % among farmers and unskilled laborers. In addition, the prevalence of myopia increases with the degree of urbanization such that lower myopia rates are found in rural areas compared with cities (Rosenfield and Gilmartin, 1998).

The high prevalence of myopia is problematic because the risk of developing eye diseases such as glaucoma and subcapsular cataracts, which can lead to low vision and blindness, is increased in myopia (Rose et al., 2001). As mentioned earlier, the public health cost of visual correction such as spectacles, contact lenses, and refractive surgery is already very high and is likely to go up with increasing rates. The increased severity of myopia poses problems as well because high myopia can lead to blinding conditions such as retinal degeneration or retinal detachment.

1.3.3 Genetic versus environmental factors

One of the theories of myopia is that it is inherited, in other words, myopia genes are passed down from parents to offspring. The evidence to support this theory is that children having two myopic parents are more at risk to develop myopia compared with children having one or no myopic parent (Mutti et al., 2002). However, the rapid increase in myopia prevalence over the last 30 years in the United States and Asia does not support the genetic theory (Rose et al., 2001; Vitale et al., 2009). It is difficult to imagine that mutations occurred so quickly and that the gene pool changed significantly to explain the drastic increase in myopes. A more plausible explanation to the increase in myopia is that a change in the environment causes genetically susceptible individuals to develop myopia. For instance, the prevalence of myopia among the Eskimos in Barrow Alaska was almost zero until the

graded school system was introduced around 1948. From that point on, the prevalence of myopia went up significantly such that 58 % of the children were myopic (≤ -0.25 D) while almost no myopia was present among parents and grandparents when Young et al. (1969) published their study in 1969. In this case, the environmental factor is the graded school system where children do more reading and writing. The two main environmental factors associated with myopia are outdoor activity (Rose et al., 2008; Dirani et al., 2009) and near work (Rosenfield and Gilmartin, 1998) such as reading, writing, and computer work. Outdoor activity appears to be protective against myopia while near work seems to be a contributing factor.

1.3.4 Experimental myopia

Myopia can be induced in animals experimentally by form deprivation and refractive defocus. Form deprivation myopia can be induced in animals such as chicks (McBrien et al., 1993) tree shrews (Phillips et al., 2000) or guinea pigs (McFadden et al., 2004) by placing a translucent goggle in front of the eye. The amount of myopia induced by form deprivation varies from animal to animal. The third way of creating myopia is by refractive defocus where a minus lens is placed in front of the animal's eye. The minus lens creates hyperopic defocus that signals the eye to elongate (Schaeffel et al., 1988; Irving et al., 1992; Wildsoet and Wallman, 1995). Hyperopic defocus occurs when light is focused behind the retina and the eye compensates by elongating. The elongation continues until the refractive power of the eye matches the power of the lens that was placed in front of it. The amount of myopia produced by refractive defocus is very consistent and most eye elongate to match the power of the lens. For instance, a chick treated with a -10 D lens for 7 days will have a refractive error of nearly -10 D upon removal of the lens (Irving et al., 1992). No matter what technique is used to produce myopia, the main correlate of experimental myopia is axial length, which is longer in the myopic eye. The longer axial dimension in experimental myopia is mainly the result of an elongated vitreous chamber although an increase in anterior chamber has also been observed in chicks

(Schaeffel and Howland, 1988). The left eye in Figure 6 is a chicken eye treated with a -20 D lens while the right eye is a normal eye. It is clear from Figure 6 that the myopic eye is axially longer than the normal eye.

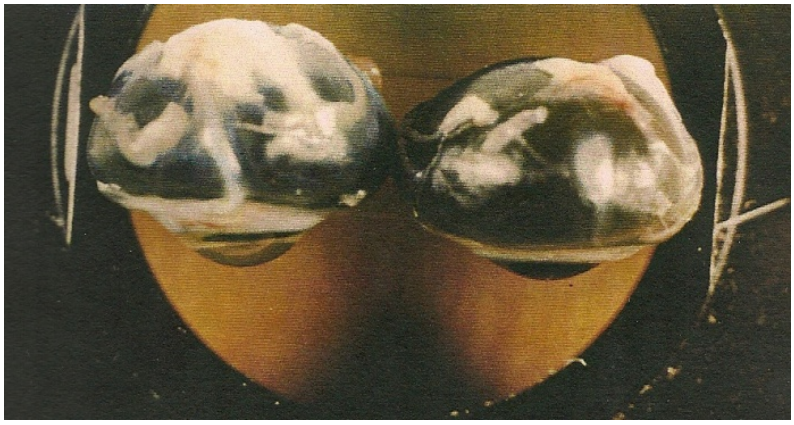

Figure 6. Chicken eye treated with a -20 D lens for two weeks (left eye) compared with a normal eye (Irving, 1993).

1.3.5 Chicken as myopia model

The chicken has been used extensively as a myopia model (Wallman and Adams, 1987; Schaeffel et al., 1988; Irving et al., 1991; McBrien et al., 1993; Wildsoet and Wallman, 1995; Phillips et al., 2000) because it offers many advantages. First, chickens grow very fast and it is possible to induce a significant amount of myopia in chickens in only 7 days. This allows many experiments to be run and a great deal of data to be gathered in a short period of time. Also, chicks are able to walk and get to their water and food tray to drink and eat immediately after hatching so that minimal care is required in this regard. Chickens are relatively small and do not require large spaces which make it easy to control and monitor experiments on a daily basis. At last, chickens are relatively inexpensive and easy to obtain compared with other animals. On the other hand, because of all the anatomical differences

between a chicken eye and a human eye (mentioned previously in section 1.2), there is some difficulty in extrapolating the results obtained with chickens to humans.

1.3.6 Intraocular pressure and myopia

Intraocular pressure refers to the positive gage pressure generated by the aqueous humour in the anterior chamber of the eye. An IOP of 15 mmHg means that the fluid pressure in the eye is 15 mmHg above ambient atmospheric pressure. As mentioned earlier, proper balance between aqueous humour production and outflow is critical to maintain IOP to a typical level. The normal IOP in humans is around 15 mmHg (Puell-Marin et al., 1997; Bonomi et al., 1998; Xu et al., 2005) and can reach values as high as 35 mmHg in patients with glaucoma (Bonomi et al., 1998). IOP can rise even higher; Ku and Greene (1981) reported that the rise in IOP due to rubbing on an in vivo rabbit eye was around 150 mmHg.

Normal IOP is essential for the proper development of the eye and a sustained reduction of IOP causes a significant reduction in eye growth. Indeed, Neath et al. (1991) found that normal embryonic chick eyes elongated at a rate of 1.193 mm/day between embryonic day 4 (E4) and day 10 (E10) and at a slower rate of 0.346 mm/day after E10. When IOP was reduced by intubation, the rate of elongation was 0.356 mm/day for E4-E10 and 0.155 mm/day for E10-E16, a significant reduction. Also, higher than normal IOP in children with congenital glaucoma leads to increased axial length and a thinner sclera (Kiskis et al., 1985). Although, it could be argued that children with congenital glaucoma have a decreased visual acuity which could also cause the eye to elongate similar to form deprivation experimental myopia.

The role of IOP in myopia onset and progression has been studied in the past, but it is unclear whether IOP is higher in myopes compared with emmetropes. Some authors reported higher IOP in

children (Edwards and Brown, 1993; Quinn et al., 1995; Edwards and Brown, 1996) and adult (Tomlinson and Phillips, 1970; Wong et al., 2003; Nomura et al., 2004) myopes suggesting that IOP causes ocular expansion and myopia while others did not find an association between IOP and myopia in children (Lee et al., 2004) and university students (Puell-Marin et al., 1997). For instance, Nomura et al. (2004) measured the IOP of 1855 adult subjects aged 40 to 82 years and found a significant correlation between IOP and advancing degree of myopia, the higher myopes having higher IOP. Furthermore, Edwards and Brown (1993) found a mean IOP of 13.69 mmHg in 30 myopic children aged between 6 and 9 years and a mean IOP of 11.55 mmHg in 30 age-matched emmetropic children, a significant difference. However, Edwards and Brown (1996) found, in a 2 year longitudinal study, that IOP was higher in children myopes only after myopia onset such that higher IOP is an effect of myopia rather than a cause. If this is the case, higher IOP could be involved in myopia progression, but not in myopia onset. Jensen (1992) showed that myopia progressed at a faster rate in children with higher IOP while Manny (2008) found no significant correlation between the rate of myopia progression and IOP. In a chick study, Schmid et al. (2003) found that the IOP of chicks wearing -15 D lenses was higher than those wearing +15 D lenses 50 hours after application of the lenses.

To have a better idea of the importance of IOP in myopia onset and progression, IOP has to be measured while the subject is under the influence of environmental factors such as near work and outdoor activity. A recent study presented at the ARVO 2010 annual meeting demonstrated that vitamin D, which can be obtained from the sun, decreases IOP in monkeys by up to 30% (Gabelt et al., 2010). As accommodation is an important part of near work, it seems logical to study the effect of accommodation on IOP. Many studies reported that IOP decreases during accommodation and this would make it very unlikely that IOP causes eye enlargement and myopia. However, most of these

studies use applanation tonometry such that the pressure in the anterior chamber is measured. Read et al. (2010) found a significant reduction of pressure in the anterior chamber of 1.8 mmHg when subjects were accommodating on a 3 D target compared with when the accommodation was relaxed. The reasons for a decrease in anterior chamber pressure while accommodating are still unknown but one possibility is that aqueous humour outflow facility is increased due to the mechanical effect of the ciliary muscle contraction. A decrease in anterior chamber pressure with accommodation in humans has been known to researchers since the 60's from a study by Armaly and Rubin (1961). However, it is difficult to conceive that an overall decrease in eye pressure would lead to an increase in axial length during accommodation. Indeed, Mallen et al. (2006) found that a transient axial elongation was seen in emmetropes and myopes during accommodation. Interestingly, the increase in axial length during accommodation was found to be greater in myopes than in emmetropes (Mallen et al., 2006) and they suggested that this was "due to reduced ocular rigidity and a more efficient transmission of ciliary muscle force to the choroid and sclera in these subjects" (myopes). The increase in axial length would make more sense if the pressure somewhere in the eye increased with accommodation. Young et al. (1987) implanted a radio pressure transducer in the vitreous chamber of a monkey and found that the pressure was 12 mmHg for a fixation distance of 6 m and that the pressure instantly went up to 24 mmHg when the fixation was suddenly brought to 12 cm. Young (1981) also noted that the pressure in the anterior chamber decreases with accommodation while the pressure in the vitreous increases such that a pressure gradient is created. The fact that the pressure in the vitreous chamber increases with accommodation in monkeys suggests that it could lead to vitreous expansion and myopia. Young (1981) pointed out that the correlation between axial elongation and vitreous elongation was equal to 0.97 in human myopia.

During near work, the eyes do not only have to accommodate to focus on an object, but they also have to converge to maintain a single binocular image. To study the effect of convergence on IOP, Moses et al. (1982) had their subjects focus on targets at 0^o, 10^o, 30^o, and 50^o on a wall 2 meters away (to avoid accommodation) and they found a 2.0 mmHg increase in IOP in both eyes when the gaze shifted from primary 0^o to 50^o nasal. Greene (1980) stated that the extraocular muscles responsible for convergence give rise to a 5 to 14 mmHg increase in IOP.

1.4 Mechanical properties of materials

The mechanical properties of different materials can be obtained by performing different tests. One of these tests is the tension test where a specimen of known dimensions is placed into a hydraulic testing machine and stretched. As the specimen stretches, the force acting on the specimen and the elongation of the specimen are recorded. The force and the elongation are converted into stress and strain so that the mechanical properties of the material can be extracted. In this section, the mechanical properties of steel, which is a common engineering material, are depicted to illustrate basic solid mechanics concepts. Then, the mechanical properties of living tissues are presented.

1.4.1 Mechanical properties of steel

Structural steel is a very common metal used in the fabrication of different structures such as bridges, cars, and buildings. Structural steel is considered a simple material and its mechanical properties are well defined so it is used here for illustration purposes. The stress/strain curve for structural steel is shown in Figure 7 and was obtained by performing a tension test. Note that the strain is not plotted exactly to scale so that the different regions of the curve can be easily identified. The stress used to plot the stress/strain curve is the engineering stress and is defined as follow:

$$\sigma = \frac{F}{A_o} \quad \text{(a)}$$

where σ is the engineering stress, F is the force required to stretch the specimen, and A_o is the initial cross-sectional area of the specimen before the start of the tension test. Similarly, the strain used to plot a conventional stress/strain curve is the engineering strain:

$$\varepsilon = \frac{\Delta L}{L_o} \quad \text{(b)}$$

where ε is the engineering strain, ΔL is the elongation of the test specimen, and L_o is the initial length of the specimen (Craig Jr., 2000). Engineering stress and engineering strain are used throughout this document and are simply referred to as stress and strain.

The region between point A (origin) and point B on the stress/strain curve (Figure 7) is called the elastic region. The relationship between stress and strain in the elastic region is linear and the slope of the line is called the Young's modulus or modulus of elasticity:

$$E = \frac{\Delta\sigma}{\Delta\varepsilon} \quad \text{(c)}$$

where E is Young's modulus, $\Delta\sigma$ is the change in stress, and $\Delta\varepsilon$ is the change in strain (Craig Jr., 2000). Note that Young's modulus is a measure of the stiffness of a material. When steel is stretched within the elastic region, it deforms elastically and returns to its initial geometry when the stress is removed. Point C is called the yield point or elastic limit. When a material is stretched beyond its yield point, it is said to yield and a portion of the deformation remains after the stress is removed. The material is said to undergo plastic deformation and permanent deformation occurs. From point C to point D, the specimen continues to stretch plastically even though the stress stays constant. The stress

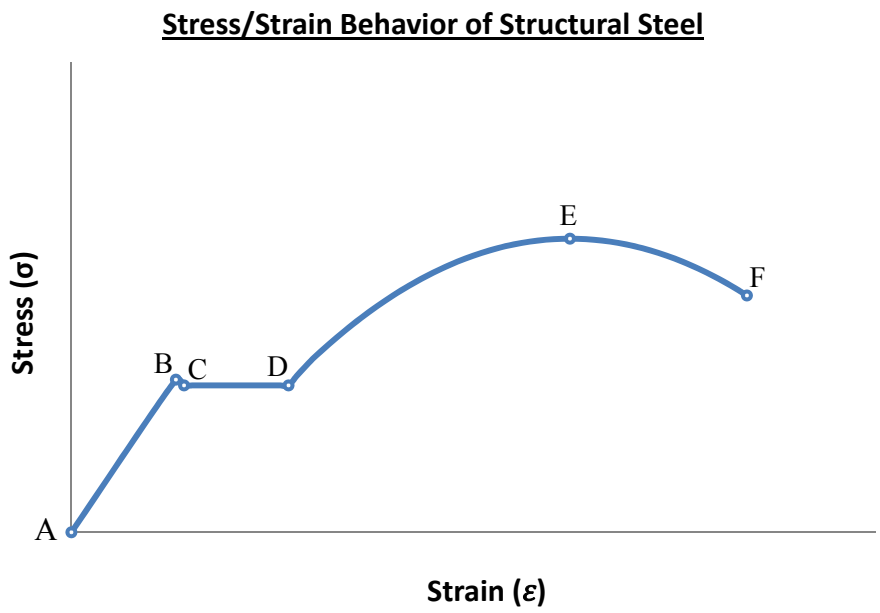

Figure 7: Stress/strain curve for structural steel tested in tension. Curve not shown to scale.

at point E is the maximum stress that the material can withstand and is called the ultimate stress or ultimate strength. At point E, the specimen's cross section starts to significantly contract and the phenomenon is known as necking. Necking continues until the specimen fails at point F.

When a specimen is tested in tension, it elongates in the longitudinal direction (direction of pull), but also tends to contract in the transverse direction (perpendicular to the longitudinal direction) and the ratio of longitudinal strain and transverse strain is known as Poisson's ratio:

$$\nu = -\frac{\varepsilon_{trans}}{\varepsilon_{long}} \qquad \text{(d)}$$

where ν is Poisson's ratio, $\varepsilon_{\text{trans}}$ is the strain in the transverse direction, and $\varepsilon_{\text{long}}$ is the strain in the longitudinal direction (Craig Jr., 2000). Poisson's ratio for structural steel is 0.29.

Structural steel is an isotropic material meaning that its mechanical properties (stress/strain curve) at a given point do not depend on direction. In other words, a piece of steel can be stretched in any direction and its stress/strain curve will remain the same. Also, structural steel is a homogeneous material because its mechanical properties do not change from point to point.

1.4.2 Mechanical properties of biological tissues

Tension testing is also performed on biological tissues to obtain their mechanical properties and the relations for stress, strain, and Poisson's ratio given in section 1.4.1 still apply. However, the mechanical behavior of biological tissues is more complex. Their stress versus strain curve is not linear and bent upward which means that living tissues get stiffer as they stretch (Figure 8). Also, because the stress/strain curve is not linear, Young's modulus cannot be defined and the secant modulus is often used instead. The secant modulus is the slope of a line joining two points on the stress/strain curve. The stress/strain behavior of collagen, which is the main structural constituent of living tissues, can be fitted with an exponential function of the form:

$$\sigma = A[e^{\alpha\varepsilon} - 1] \qquad \text{(e)}$$

where σ is the stress, ε is the stain and A and α are material constants (Ethier et al., 2004). Materials governed by equation (e) are said to be exponentially stiffening and the values of A and α determine the shape of the curve and the stiffness of the material. Also, the mechanical properties of biological tissues are heterogeneous meaning that they change depending on the location. For example, biaxial mechanical testing of the human sclera showed that its stiffness varies from 1 to 7 MPa depending on the location on the globe (Eilaghi et al., 2010b). The same study also showed that the sclera is nearly-

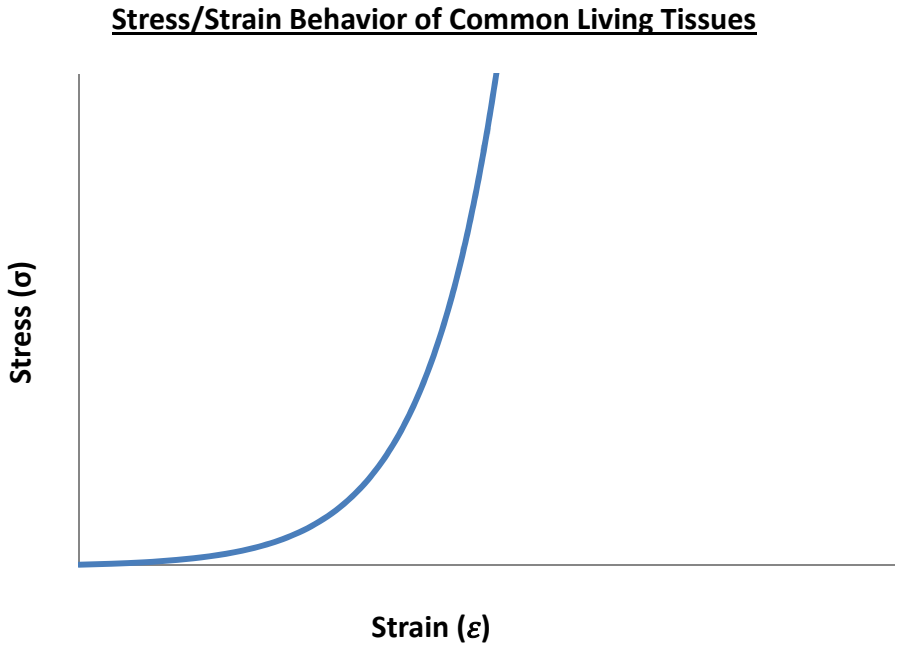

Figure 8: Stress/strain curve for common living tissues. Curve not shown to scale.

isotropic meaning that the mechanical properties at a given point on the sclera do not vary much with direction. Although, in the vicinity of the optic nerve canal and near the extraocular muscle attachment sites where the collagen fibers have a preferred orientation, the sclera is anisotropic and its mechanical properties at a given point vary with direction. The sclera is stiffer in the preferred direction of the collagen fibers and softer perpendicular to it. In general, biological tissues show some degree of anisotropy (Katz and Meunier, 1990; Kuo et al., 2001; Nguyen et al., 2008).

Biological tissues also have viscoelastic material properties which mean that they display characteristics of both elastic and viscous (liquid-like) materials such that their stress/strain relationship depends on loading rate and loading duration (Fung, 1993; Callister Jr., 2003). Indeed,

living tissues are stiffer, that is, they have a steeper stress/strain curve when they are loaded quickly compared with a slower loading rate. Also, living tissues have a tendency to creep and exhibit stress relaxation. Creep is the tendency of a material to deform over time under the influence of a constant stress (Callister Jr., 2003). For instance, when a constant stress is applied to a strip of viscoelastic tissue, there is an instantaneous deformation (elastic strain) and, as time goes by, the strip continues to deform (viscous strain). Creep is influenced by temperature and higher temperatures result in greater creep. The ocular tissues could creep under the influence of the constant stress caused by the IOP, especially if IOP is high and/or the temperature of the eye is elevated. Apparently, coughing causes an increase in IOP and any illness involving coughing and fever (elevated body temperature) could render someone more susceptible to myopia (Grosvenor, 1989). Living tissues also exhibit stress relaxation. During a stress relaxation test, a strip of tissue is stretched to a fixed amount of strain and the stress in the tissue is measured over time. As time goes by, the stress in the tissue decreases even though the strain is kept constant (Callister Jr., 2003). The last feature of viscoelastic materials is hysteresis. The stress/strain curve of living tissues is different during the loading cycle than it is during the unloading cycle which results in energy dissipated as heat (Fung, 1993). This phenomenon is known as hysteresis.

Another peculiarity of ocular tissues is that their material properties are not fixed in time. For example, the sclera gets stiffer with age (Friberg and Lace, 1988) and this may explain why myopia progression slows down and eventually stops with aging.

1.5 Myopia theories

It was shown in section 1.3.3 that genetic factors do not support the rapid increase in myopia observed around the world over the last few decades. If the increase in myopia prevalence is not genetically determined, what causes it? Most humans are hyperopic at birth (Mayer et al., 2001) and between the ages of 0 and 12 months there is a rapid shift toward emmetropia such that the child is below +1.00 D at 12 months of age (Gwiazda et al., 1993a). Between the ages of 1 and 6 years, the refraction of children is rather stable. Interestingly, there is a myopic shift occurring around the age of 6 years old, which is the time when most kids enter primary school. The refraction of children keeps moving in the myopic direction after that point (Gwiazda et al., 1993a). Animal models of myopia have shown that once emmetropia is reached, eye elongation stops. So, why do the eyes of children keeps elongating even though emmetropia is reached? The exact reasons for the increase in myopia prevalence and the continued progression are still unclear, but two main theories have been postulated: the hyperopic defocus theory and the mechanical theory.

1.5.1 Hyperopic defocus

Human children and adults normally exhibit a lag of accommodation when focusing on a close object (Gwiazda et al., 2005; Mutti et al., 2006; Tarrant et al., 2008). This means that the accommodative response is insufficient for the accommodative demand and this results in hyperopic defocus that could stimulate eye growth. People who perform more close work such as reading and writing expose themselves to longer periods of hyperopic defocus which would make them more prone to myopia. However, a study in chicks demonstrated that even small periods of normal vision (total of 3 hours daily), i.e. no minus lens in front of the eye, are enough to counteract the effect of hyperopic defocus caused by -10 D lenses such that myopia does not develop (Schmid and Wildsoet, 1996). It is difficult to imagine that people, especially children, do not get at least 3 hours of normal vision (no hyperopic defocus) each day. Also, when chicks wore minus lenses all day with only four 2-minute periods of

plus lens wear, the eye adapted and compensated for the plus lens (Wallman and Winawer, 2004). This means that myopic defocus is much more powerful than hyperopic defocus in influencing eye growth. Myopic children could abstain from wearing their glasses for 2 minutes four times a day and myopia progression should reverse. But it is not the case, even though early myopes tend to not wear their glasses all the time.

Myopic children and adults have been shown to exhibit a greater lag of accommodation compared with emmetropes (Gwiazda et al., 1993b; Gwiazda et al., 2005; Mutti et al., 2006). Yet, there is still considerable debate on whether a greater lag of accommodation occurs before or after myopia onset and whether a greater lag of accommodation leads to increased rates of myopia progression. In a 10-year longitudinal study with children, Mutti et al. (2006) reported that the lag of accommodation was seen only after myopia onset such that the lag of accommodation is only an effect of myopia rather than a cause. However, Gwiazda et al. (2005) did find a significant difference in lag of accommodation between children who became myopic and those who remained emmetropic even before myopia onset. The hyperopic defocus theory also tries to explain myopia progression, with children having the greater lag of accommodation progressing more rapidly. However, a recent study found no significant correlation between the magnitude of accommodative lag and the rate of myopia progression (Weizhong et al., 2008).

The results of the different studies presented here are not conclusive, but it is possible that lag of accommodation and hyperopic defocus causes myopia and/or myopia progression in certain individuals.

1.5.2 Mechanical stretch

The mechanical stretch theory suggests that the sclera of myopes creeps more than normal (McBrien and Gentle, 2003) and that higher stress concentration causes the eye to stretch out of shape (Greene, 1980). According to this theory, the elongation of the eye is caused by mechanical stretch and not by abnormal ocular growth. The extraocular muscles, the ciliary muscles, along with the IOP exert forces that generate stress on the ocular shell. If the stress on the eyeball is too high and/or if the corneo-scleral shell is mechanically weak (low elastic limit and high propensity to creep), then it might permanently stretch (Ethier et al., 2004). As the extraocular muscles and the ciliary muscles are involved in near work, people who perform more near tasks expose themselves to longer periods of mechanical stress and their eyes would be more susceptible to creep and become myopic. Also, variation in IOP during alternating close and distance viewing conditions could lead to cyclic loading that may result in fatigue deformation.

Measuring the strain or calculating the stress due to IOP, the extraocular muscles, and the ciliary muscles of a living eye is not a simple task. Many pressure-volume experiments have been done with post-mortem eyes where fluid is injected into the eye to raise the IOP (Woo et al., 1972; Pierscionek et al., 2007; Wang et al., 2008b). In this way, it is possible to obtain the pressure-volume characteristic of the eye and ocular rigidity. It is also possible to obtain the strain field of a dead eyeball by sprinkling microspheres on the surface of the eye and tracking them with an optical device (Girard et al., 2008). However, no information about the effect of the ocular muscles is acquired in this manner. Greene (1980) tried to calculate the stress on the corneo-scleral shell due to IOP and the extraocular muscles. He used Laplace's equation to relate ocular stress to IOP:

$$\sigma = \frac{Pr}{2t} \qquad \text{(f)}$$

where σ is the stress in the corneo-scleral shell, P is the IOP, r is the radius of the eye, and t is the thickness of the corneo-scleral shell. The assumptions used to derive Laplace's equation are that the eye is perfectly spherical; the material properties of the eye are isotropic and homogeneous; and the thickness of the shell is constant. Obviously, there are serious limitations to the use of this equation because the eye is not a perfect sphere, its material properties are heterogeneous and anisotropic, and the thickness of the globe varies from point to point. Greene also tried to calculate the stress on the corneo-scleral shell due to the extraocular muscles. He used the equation of a line force acting on a large flat plate to obtain the stress as a function of muscle force:

$$\sigma = \frac{F}{2Wt} \qquad \text{(g)}$$

where σ is the stress in the corneo-scleral shell, F is the force generated by one extraocular muscle, W is the width of the attachment line of the muscle, and t is the thickness of the shell near the muscle attachment. Greene stated that the oblique muscle attachment width can vary from 5 to 14 mm. He calculated that the stress on the eyeball caused by an oblique muscle having an attachment width of 5 mm was 2.8 times higher than when the attachment width was 14 mm. People with narrow extraocular muscle attachment width would experience more mechanical stress and would be more prone to eye deformation and myopia. Also, it can be seen from these equations that people who have a thinner sclera or who generate more force in their ocular muscles would be more at risk to eye deformation. Again there are limitations to this equation because the eye is curved and not flat and the thickness of the globe varies. Greene (1985) stated that: "it is very difficult to include the curvature change effects at the corneo-scleral junction and the different radius and thickness in closed form or even-power series".

Because the eye is a living structure, it is difficult to differentiate between growth, remodelling, and stretch. As a child develops, its eye naturally grows as part of the normal development process regardless of whether the child is myopic or not. In the case of a myopic child, the eye appears to grow at a faster rate than normal such that the eyeball ends up too long. Maybe the myopic eye grows at a normal rate and stretches at the same time. Or perhaps the stresses exerted on the eyeball by the IOP and the extraocular muscles do not just result in passive stretching: maybe stress influences eye growth and development. Indeed, it has been shown that growth and remodelling of all living tissues are affected by stresses induced by gravity, tension, compression, pressure, or shear (Ingber, 1997). For instance, arterial walls are able to change their geometry and material properties to maintain a constant stress level (mechanical homeostasis) under changing blood flow conditions. Arteries are able to sense circumferential stress and increase the thickness of their wall in response to an increase in blood pressure (Humphrey, 2008). Also, it is well known that bones remodel to some extent in response to mechanical stress. For example, physical activity results in an increase in bone mass whereas microgravity experienced by astronauts results in bone atrophy (Hall, 2007). So, it is possible that the stresses imposed on the eye during near work influence growth and remodelling of the eye. Perhaps the hyperopic defocus theory and the mechanical stretch theory happen simultaneously such that they both play a role in myopia onset and progression in humans. On the one hand, you have a visually guided pattern of ocular growth and on the other, a mechanical one. This could explain the partial effectiveness of progressive addition lenses (PALs) in the treatment of myopia (Gwiazda, 2009). PALs remove the hyperopic defocus of near work but do not alleviate the stresses induced by the extraocular muscles.

1.6 Finite element method

The finite element method (FEM) is a numerical technique to obtain approximate solutions to complex physical problems that cannot be solved analytically. Physical problems range from solid and fluid mechanics to heat transfer, electromagnetism, and acoustics. Coupled problems such as solid mechanics with heat transfer can also be solved using FEM. In general solid mechanics problems, forces are applied to a structure and the deformation or displacements of the structure need to be solved for. The geometry of structures is often too complex to be solved analytically and the FEM is used to find an approximate solution. During a structural finite element analysis (FEA), the complex geometry of a structure is decomposed into smaller regions called elements which are easier to analyze (Hutton, 2004). Then, the governing differential equations are approximately solved on each element. Afterwards, the elements are assembled together to obtain the solution over the entire domain of the structure. The process of dividing the geometry into a finite number of elements is called discretization or meshing. Elements can be one-dimensional (1D), two-dimensional (2D), or three-dimensional (3D). In 3D, elements are usually in the shape of a tetrahedron or a hexahedron. It is easier to decompose a complex geometry using tetrahedral elements than hexahedral elements, but for a given mesh density (number of elements per unit volume) hexahedral elements lead to more accurate results. The elements are connected to each other at specific points called nodes and the solution to the field variable is found at the nodes only. For instance, in a structural FEA, the field variable of interest is the displacement field of the structure which is computed at the nodes. Then, interpolation functions are used to interpolate the displacements found at the nodes to obtain the displacement between the nodes. The elemental displacement field for a 3D element can be written as:

$$u_e(x, y, z) = \sum_{i=1}^{n} N_i u_{ei} = N_1 u_{e1} + N_2 u_{e2} + \ldots + N_n u_{en} \qquad \text{(h)}$$

where $u_e(x, y, z)$ is the elemental displacement field, N_i are the interpolation functions, u_{ei} are the displacements at the nodes, and n is the number of nodes in the element (Inal, 2008). In most cases, the interpolation functions are either linear or quadratic. The stiffness of the element is used to relate the elemental forces to the elemental displacements as follow:

$$\{f_e\} = [k_e]\{u_e\} \tag{i}$$

where $\{f_e\}$ are the elemental forces, $[k_e]$ is the elemental stiffness matrix, and $\{u_e\}$ is the elemental displacements at the nodes. This gives a system of equations in terms of the nodal displacements $\{u_e\}$ for the element. The elemental stiffness matrix $[k_e]$ takes into account the configuration of the element and its material properties and can be calculated as follow:

$$[k_e] = \int_v [B]^T[D][B]dv \tag{j}$$

where $[B]$ is the matrix of differential of the interpolation functions, $[B]^T$ is the transpose of the $[B]$ matrix, $[D]$ is the matrix of material properties, and v denotes that the integral has to be evaluated over the volume of the element. Note that different material properties can be assigned to different elements. Then, the elements are assembled together to form a global stiffness matrix and a global system of equations representing the entire geometry of the structure:

$$[K] = \sum_e [k_e]$$

$$\{F\} = [K]\{U\} \tag{k}$$

where $\{F\}$ are the global forces, $[K]$ is the global stiffness matrix of the entire structure, and $\{U\}$ are the global displacements at the nodes. At this point, the system of equations is indeterminate and boundary conditions must be applied in order to obtain a unique solution. In solid mechanics, a

structure must be fixed in space or else it will move as a rigid body under loading. To fix the structure in space in a FEA, a node or many nodes are prescribed a displacement of zero. Then, the system of equations is solved using standard numerical techniques to find the displacements $\{U\}$ at the nodes. In normal engineering problems, the number of equations to be solved simultaneously is often in the thousands such that a computer is required to perform the calculation. Once the global displacements are calculated, it is easy to obtain the strain and stress in the structure using the following formulae:

$$\{\varepsilon\} = [B]\{U\} \quad \text{(l)}$$

$$\{\sigma\} = [D]\{\varepsilon\} \quad \text{(m)}$$

where $\{\varepsilon\}$ is the strain and $\{\sigma\}$ is the stress.

Finite element softwares such as Abaqus/CAE® (Dassault Systèmes SIMULIA, Providence, USA) greatly simplify the implementation of the finite element method. The user has to input the geometry, material properties, loads and boundary conditions, mesh the model and run the simulation. It is possible to import 3D models from computer-aided design (CAD) softwares. Also, different material properties can be assigned to different parts of the model and test data from tensile testing can be imported and fitted with different material models. Different loading types such as force, line load, or pressure can be applied to the model by selecting the appropriate feature. Also, nodes, edges, or surfaces can be constrained in different directions to reflect the physics of the problem. Abaqus/CAE® has a mesh module so that the meshing of the model is automated. The mesh size can be specified and a finer mesh can be created in areas of stress concentration. Then, simulations can be run. It is important to conduct convergence studies to ensure accurate numerical solutions. With a given number of elements, it is not possible to estimate the error in the solution. However, as more

elements are introduced in the model, the solution normally converges to a certain value. So, during a convergence study, simulations are run with more and more elements until the solution barely changes. Using more elements results in more accurate solutions, but the computer time required to perform the calculation is increased.

Because the FEM is capable of solving solid mechanics problems with complex geometries, it is well suited to study the mechanics of the eye and myopia. In fact, the FEM is commonly used in the biomedical field to study the effect of forces on the complex geometry of biological structures such as bones and tissues. The FEM has also been used in glaucoma research to study the effect of elevated IOP on the optic nerve head (Sigal et al., 2004; Eilaghi et al., 2010a). The FEM could be used to study the effect of IOP, extraocular muscles, ciliary muscle, and scleral material properties on eye geometry and help understanding the etiology of myopia.

1.7 Purpose of research

The main purpose of this study was to investigate the effect of intraocular pressure on the geometry of the post-mortem chick eyes. Different studies investigated the effect of IOP on axial eye length (Phillips and McBrien, 2004; Leydolt et al., 2008), but the effect of IOP on equatorial diameter seems to be absent from the literature. What is the natural tendency of the eye to deform under the influence of increasing IOP? Does it expand equally in all directions? Is there a preferred deformation mode? Does the eye elongate and become myopic? The second goal of the present study was to build a finite element model of the corneo-scleral shell of a 7-day old chick eye including proper thickness variations around the eye, simulate increases in IOP, and compare the model with pressure-volume experimental data performed with real 7-day old chick eyes. The last goal of this study was to induce myopia in chicks and obtain the pressure-volume characteristic of myopic eyes and compare it to normal eyes.

Chapter 2: Pressure-volume experiment with normal eyes

2.1 Introduction

The pressure-volume experiment consists of injecting water inside a chick eye, measuring the intraocular pressure, and photographing the eye so that deformation can be quantified. The chick eyes were tested to failure and theoretical equations were fitted to the experimental data in an attempt to obtain overall mechanical properties for chick eyes.

The first goal of the pressure-volume experiment was to determine if post-mortem chick eyes could stretch, elongate and become myopic under increased IOP. By using post-mortem chick eyes, eye growth was taken out of the equation and it was possible to estimate the amount of transient myopia that can be obtained by mechanical stretch alone. The amount of permanent myopia under stretch alone could not be assessed because the elastic limit of chick eyes was not determined. For stresses below the elastic limit, the eye returns to its original shape when the IOP is lowered back to normal but once the elastic limit is exceeded, permanent deformation occurs.

The second goal of the pressure-volume experiment was to obtain experimental data to help build the finite element model. During the experiment, the intraocular pressure inside the chick eye was increased and the strains in the axial and horizontal equatorial directions were computed. Once a finite element model of the corneo-scleral shell of a chick eye is constructed, it is possible to simulate increases in IOP and vary the material properties of the chick eye until the finite element model strains in the axial and equatorial directions best match the experimental strains. This ensures that the model behaves like a real chick eye. At the same time, the overall material properties of the chick eye are extracted. However, it is difficult to obtain material anisotropy (change in stiffness with direction)

and heterogeneity (change in stiffness with location) using this technique. Another way of getting the material properties of ocular tissues is by testing them in simple elongation. A small square of ocular tissue can be cut, flattened, and stretched in the longitudinal and latitudinal directions using a biaxial mechanical tester. By cutting small squares at different locations on the sclera, the change in material properties of the sclera with position (heterogeneity) can be obtained. Using this technique, Eilaghi et al. (2010b) found that the human sclera was almost isotropic away from the optic nerve, heterogeneous, and exhibited nonlinear mechanical properties. However, it has been argued that performing a pressure-volume test on the whole eye is better than testing the sclera in simple elongation because in the former test, the tissues are strained in their natural configuration and the collagen fibers are not severed (Hibbard et al., 1970; Woo et al., 1972).

2.2 Syringe pump apparatus design

In order to perform the pressure-volume experiment, a syringe pump apparatus was designed to inject precise amounts of water into the chick eye, measure intraocular pressure, and photograph the chick eye. The computer-aided design (CAD) software SolidWorks® (Dassault Systèmes SolidWorks Corp., Concord, USA) was used to design the syringe pump apparatus. This allowed for better visualization of all the components in three dimensions and to ensure that the digital cameras were properly aligned such that the chick eye lies in the middle of the field of view. The final design is shown in Figure 9. The apparatus is composed of a computer controlled syringe pump (NE-500, New Era Pump Systems Inc., Wantagh, USA), a 3 ml syringe, and a 26G x ½″ hypodermic needle connected in series using a 1/8″ diameter medical tubing. This arrangement can dispense precise amounts of water to the chick eye attached to the end of the needle. A digital pressure gauge (DPG1000B-30G, Omega, Stamford, USA) having an accuracy of ±0.1 psi (5.17 mmHg) is also connected using a T-connector so that the pressure inside the apparatus is measured. Two digital

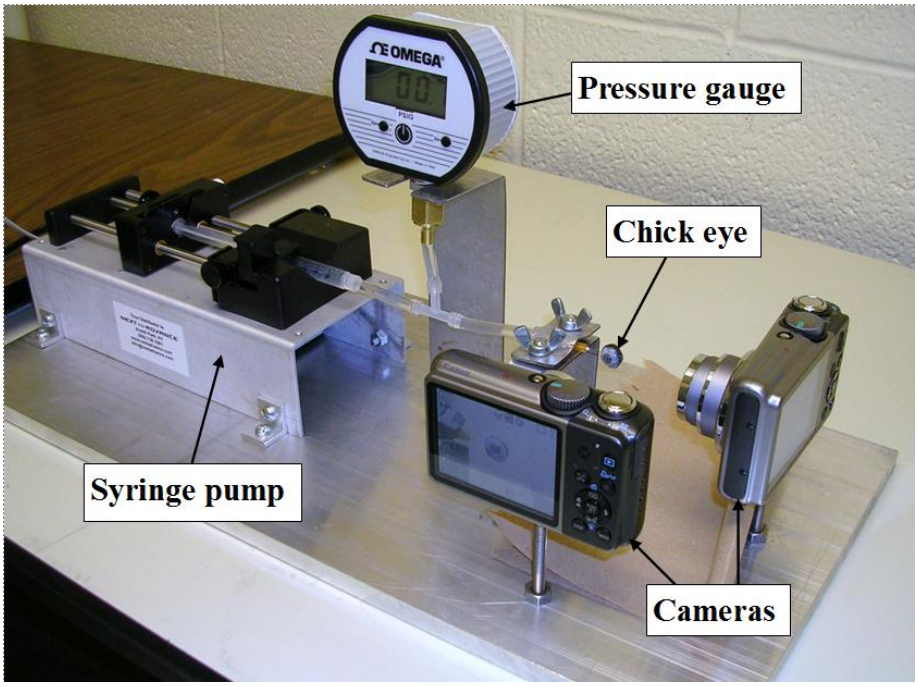

Figure 9. Syringe pump apparatus.

cameras (PowerShot A2000 IS, Canon, Tokyo, Japan) having a resolution of 3648 x 2736 pixels are mounted perpendicular to each other so that both the axial and equatorial deformation of the eye can be photographed.

2.3 Methods

2.3.1 Chicks

The chicks used in this study were Ross 308 obtained from a local poultry plant (Maple Leaf Poultry, New Hamburg, Ontario, Canada) on the day of hatching. The birds were kept in stainless steel brooders for seven days at a temperature of 32 ^{o}C and were subjected to a circadian fluorescent light regime of 14 h light/10 h dark. The chicks were given food and water ad libitum. All the birds were sacrificed by decapitation using a guillotine. The eyes were extracted, the extraocular muscles and fat were removed, and the eyes were stored in phosphate buffered saline (PBS) at 4 ^{o}C for no more than

48 hours before the start of the experiment. Ethics approval for research with animals was granted by the University of Waterloo and the research adhered to the ARVO Statement for the Use of Animals in Ophthalmic and Vision Research.

2.3.2 Experimental procedure

Ten chick eyes from 6 birds (2 eyes from each of 4 birds and 1 eye from each of 2 birds) were obtained and ready to be mounted on the needle of the syringe pump apparatus. As a first step, the syringe, medical tubing, T connector, and needle were connected together and filled with tap water by submersion. The system was carefully examined for trapped air bubbles that could bias the volume measurements. The remaining end of the T connector was coupled to the digital pressure gauge. The pressure gauge was placed on its holder, the syringe was secured on the syringe pump, and the needle fastened to the needle holder (Figure 9). The syringe pump was activated to take out any lag and to make sure that fluid was coming out of the needle. A chick eye was cannulated at the intersection of the equator and the 90 degree meridian, which is the middle point of the eye to ensure that the eye did not rotate on the needle during experimentation. Furthermore, the eye was cannulated with the optic nerve aligned with the needle so that each eye was in the same orientation (Figure 10). During the experiment, the eye was attached to the needle only with nothing else to hold it (Figure 9 and Figure 10). The puncture was sealed with cyanoacrylate glue and the two cameras were mounted on their respective holders. Two pictures of the chick eye were taken at zero pressure, one showing the front and one showing the side of the eye. The zoom setting on both cameras was kept constant so that only one calibration per camera was needed which sped up the measurement process. The infusion rate of the syringe pump was set to 2000 microliters/minute and was kept constant throughout the experiment. Twenty microliters (μl) of fluid were injected into the eye in 0.6 second and then the

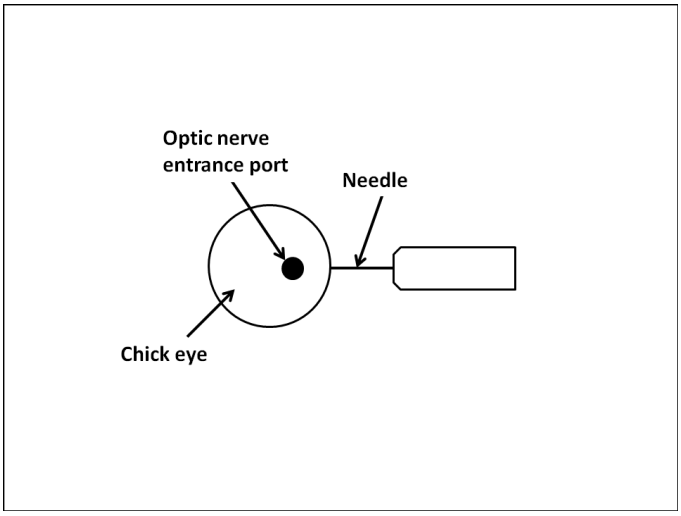

Figure 10. Posterior view of the chick eye and the needle position.

pressure was recorded. Two pictures of the chick eye were taken each time the pressure went up by a noticeable amount (~5 mmHg). This procedure was repeated until 340 microliters of fluid was injected into the eye. At this point, the intraocular pressure was around 100 mmHg. Then, a single 60-microliter injection of fluid was administered followed by injections of 100 microliters until the eye failed. Mechanical failure of the eye was determined when rupture of the sclera caused the intraocular pressure to go down to zero. Intraocular pressure was raised beyond the physiological range and the eyes were tested to failure to obtain the complete pressure-volume curve. Note that the physiological range is also part of the data. Each injection of 100 microliters took 3 seconds to complete at an infusion rate of 2000 microliters/minute. This experiment was executed rapidly with just enough time between injections to record the pressure and take the pictures such that minimal creep could occur. Slow rates of injection have a significant effect on the pressure-volume curve due to creep and leakage through different orifices such as Schlemm's canal or blood vessels (Lyon et al., 1970). The time elapsed between when the eye was taken out of the PBS solution and when it failed was no more

than 30 minutes so that the eye did not dry out. In addition, the cornea is permeable (Ethier et al., 2004) and fluid droplets could be seen at its surface when the IOP exceeded 70 mmHg. Consequently, the surface of the eye was carefully wiped down before taking the pictures to ensure that the edge of the eye could be identified for optimum measurements. On average, 50 photographs were taken for each eye, that is, 2 photographs (front and side view) per pressure value. The photographs were imported into the ImageJ software (U. S. National Institutes of Health, Bethesda, USA) to measure the axial length and the horizontal equatorial dimension (Figure 11). Note that a white sheet of paper was placed behind the chick eye to increase the contrast between the eye and the background. After all the chick eyes were tested, the needle was replaced by a plug at the end of the medical tubing and water was injected in the syringe pump apparatus in a similar fashion, that is, 20 µl increments followed by 100 µl increments. This was done to evaluate the mechanical behaviour of the system alone without the chick eye attached to it.

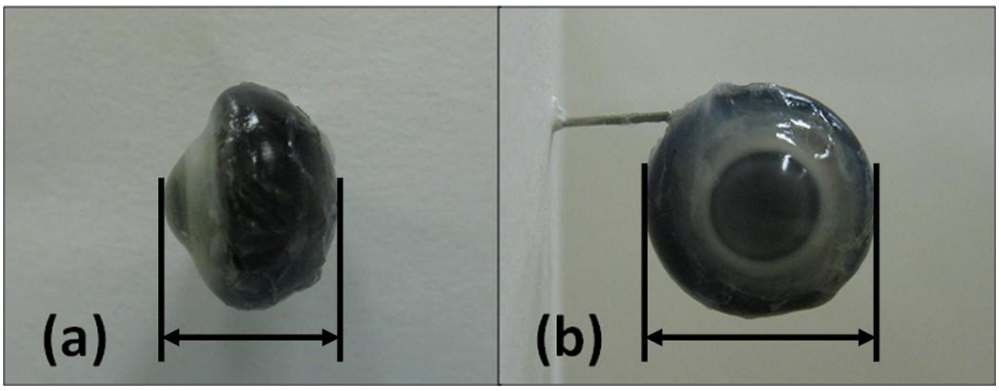

Figure 11. Photographs of a chick eye showing (a) the axial length and (b) the horizontal equatorial dimension.

The thickness of the corneo-scleral shell was measured from a photograph of the midsection of a frozen chick eye. A 7-day old chick eye was frozen with carbon dioxide and sliced using a microtome. Photographs of the remaining block were taken at regular intervals. The photograph of

the midsection was imported into the ImageJ software for measuring the thickness of the sclera and the cornea. More details on the microtome experiment are given in Chapter 4.

2.3.3 Theoretical fit

The pressure-volume curve was least square fitted using a formula derived by Greene (1985) for human eyes. The equation assumes an exponentially stiffening sphere of constant thickness and isotropic and homogeneous mechanical properties:

$$p(V) = \frac{2tA}{r_o}\left[e^{\frac{\alpha(V-V_o)}{3V_o(1-\nu)}} - 1\right] \quad \text{(n)}$$

where p(V) is the intraocular pressure, t is the average thickness of the corneo-scleral shell (t=0.15 mm, average corneal and scleral thickness measured on a 7-day old chick eye), r_o is the initial radius of the eye (average of axial length and equatorial diameter), V-V_o is the volume injected, V_o is the initial volume of the spherical eye, ν is Poisson's ratio (ν=0.47 (Uchio et al., 1999)), and A and α are material constants for exponentially stiffening materials (see Appendix A for more details). The A and α constants describe the stress-strain behaviour of exponentially stiffening materials such as tissues just like Young's modulus describes the stress-strain behaviour of constant stiffness materials like metals.

Strain is a dimensionless measure of deformation and was chosen in this experiment to take away the variability due to differences in initial eye dimensions. The equation for strain is:

$$\varepsilon = \frac{L - L_o}{L_o} = \frac{\Delta L}{L_o} \quad \text{(o)}$$

where ε is the strain, L is the eye dimension (axial length or horizontal equatorial dimension) at a given pressure p, and L_o is the eye dimension immediately after cannulation when p=0 mmHg, and ∆L is the elongation. The axial strain-pressure curve was fitted using the following equation:

$$\varepsilon_x(p) = \frac{1}{\alpha} \ln \left| \frac{r_o p}{2tA} + 1 \right| \qquad \text{(p)}$$

where $\varepsilon_x(p)$ is the axial strain, r_o is the initial radius of the spherical eye, p is the IOP, t is the thickness of the corneo-scleral shell and A and α are constants defining exponentially stiffening materials (Appendix A).

2.4 Results

2.4.1 Pressure-volume relationship

The average experimental and theoretical pressure-volume relationships are shown in Figure 12. The experimental curve is not linear; as the intraocular volume increases, the eye gets stiffer. The theoretical curve was calculated assuming a spherical eye, constant wall thickness, isotropic, homogeneous and exponentially stiffening mechanical properties. On average, the chick eyes failed when the IOP reached 869 mmHg with a standard deviation of 95 mmHg. Most eyes failed at the back of the eye near the optic nerve entrance port, a few failed at the limbus, and none failed at the needle insertion point. This makes sense because there is a stress concentration near the optic nerve entrance port (Greene, 1980) and at the junction of the cornea and the sclera. The theoretical curve was obtained by fitting the experimental pressure-volume curve with equation (n); as a result, values for A=4473 mmHg and α=1.45 were found for chick eyes. The values of A and α represent the average mechanical properties of the whole eye which include the sclera, choroid, retina, cornea, etc. Very good agreement was found between the theoretical and experimental pressure-volume curves confirming the exponentially stiffening mechanical behavior of ocular tissues. When examining the

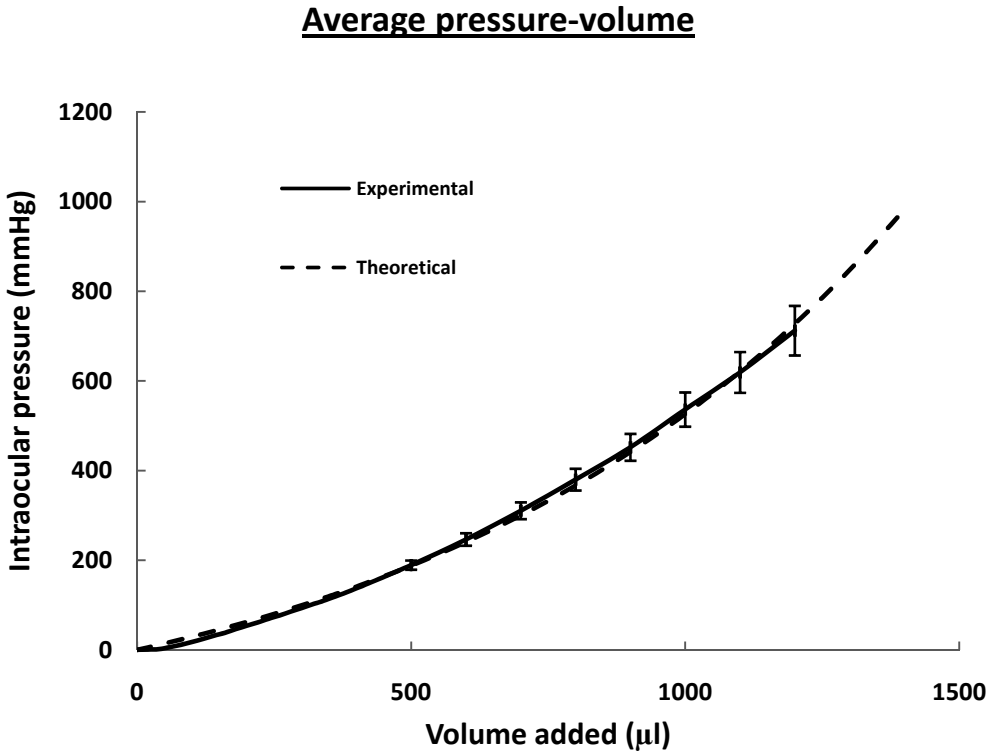

Figure 12. Average pressure-volume curve of 7-day old chick eyes (n=10, ±SD).

pressure-volume curve of individual eyes, the eyes from the same bird had similar pressure-volume curves suggesting similar geometry and mechanical properties (Figure 13). Only two birds are shown for clarity.

The pressure-volume curve of the syringe pump apparatus with the plug at the end of the medical tubing instead of the needle-chick eye assembly is shown in Figure 14. The pressure of the system itself increased more rapidly than when the chick eye was attached at the end and this shows that the syringe pump apparatus is stiffer when the plug is in place. Also, the syringe pump apparatus gets stiffer as more water is injected and this is a characteristic of the polymer material making the

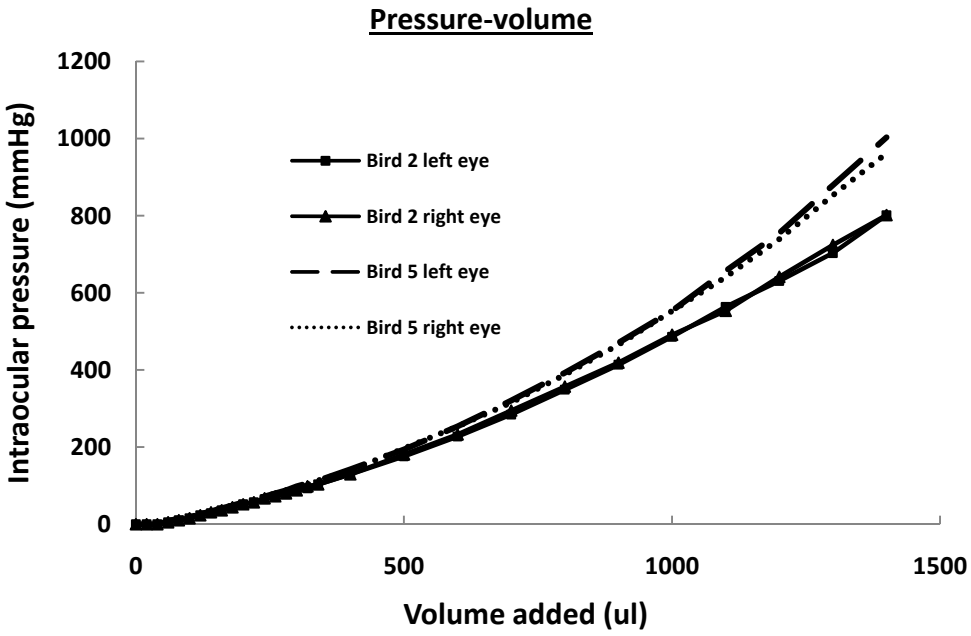

Figure 13. Individual pressure-volume curves for eyes from the same bird.

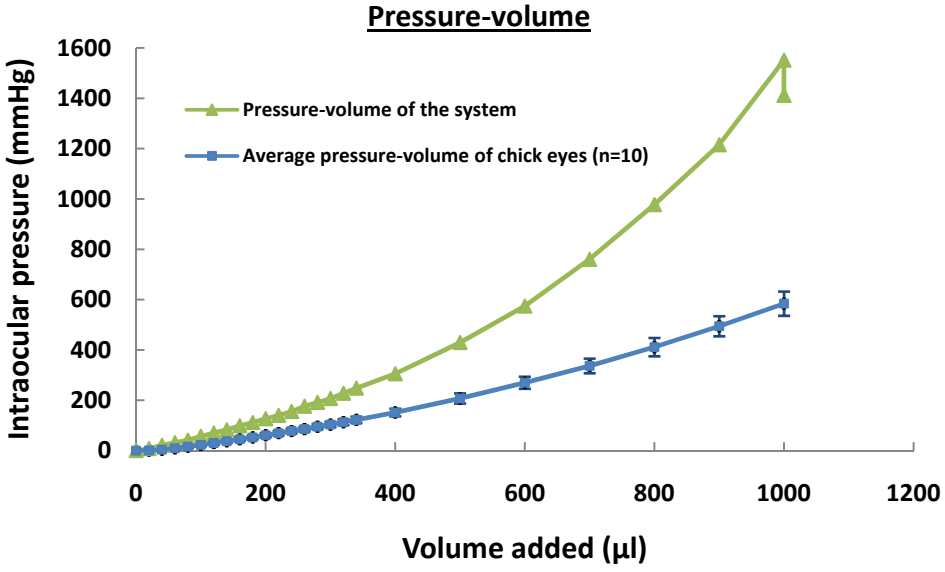

Figure 14. Pressure-volume characteristic of the syringe pump apparatus.

medical tubing. When the volume injected into the system was kept constant at 1000 µl for 15 minutes, the pressure in the system decreased. In other words, the system exhibited stress relaxation.

2.4.2 Strain-pressure relationship

The way chick eyes deform as pressure increases is somewhat counterintuitive. As expected, the axial length increases when pressure increases, but not at a constant rate. This is depicted by the positive and nonlinear axial strain curve (Figure 15). Interestingly, almost 60% of the total axial deformation occurs by the time intraocular pressure reaches 100 mmHg. Furthermore, the average axial strain when the intraocular pressure is equal to 100 mmHg corresponds to an axial elongation of about 1 mm. This axial elongation of 1 mm is equivalent to ≈25 dioptres of myopia, using the conversion given by Irving et al. (1992) for 7-day old chick eyes. Also, the average axial elongation at failure was 1.70 mm which represents 44 dioptres of myopia. Remember that strain was calculated based on initial dimensions when the IOP was equal to 0 mmHg. Now, the normal intraocular pressure for 7-day old chicks is around 20 mmHg (Prashar et al., 2007) and the axial elongation from 20 mmHg to failure is 1 mm which would produce a maximum refractive error of 25 dioptres by stretch alone. Note that these amounts of myopia do not represent the amount of permanent myopia that would be acquired by stretch alone. To determine the amount of acquired myopia at an IOP of say 100 mmHg, the intraocular pressure would have to be raised to 100 mmHg and lowered back down to 20 mmHg before measuring the axial length of the chick eye. This was not done in the present study since the eyes were tested to failure.

Perhaps the most surprising aspect of chick eye deformation is the horizontal equatorial dimension contracting as pressure increases from 0 to 140 mmHg (Figure 15). After that point, the horizontal equatorial strain starts to increase to become positive at a pressure of 540 mmHg. If the reference dimension is taken when the IOP is 20 mmHg instead of 0 mmHg, the horizontal equatorial strain

becomes positive at a pressure of 385 mmHg. At any given point, the axial strain is at least 10 times greater than the horizontal equatorial strain.

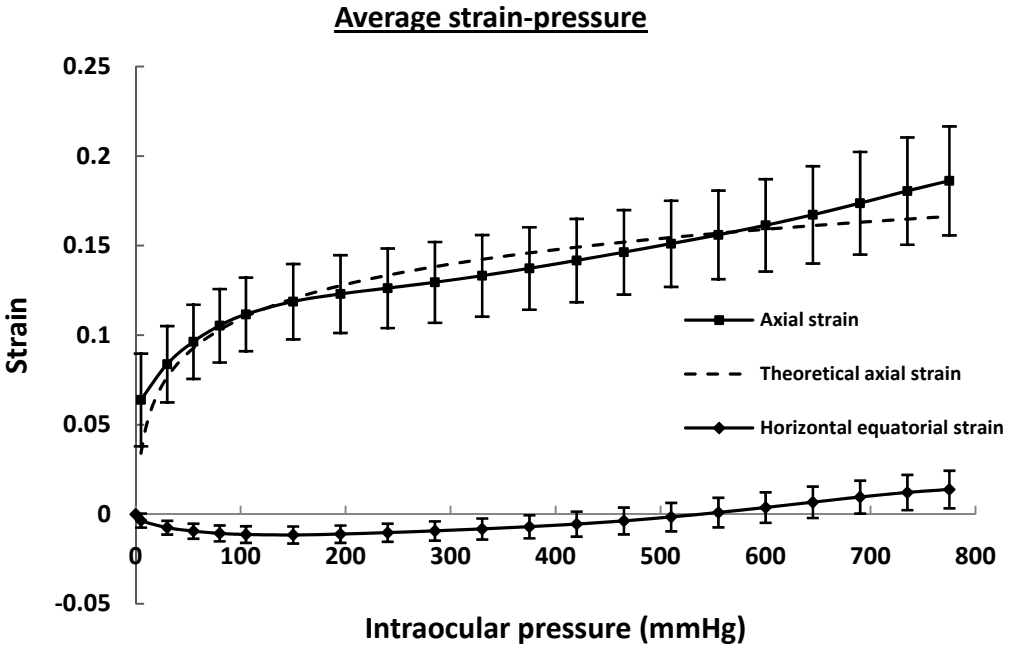

Figure 15. Average strain-pressure curve of 7-day old chick eyes (n=9, ±SD).

Figure 15 clearly shows that chick eyes do not deform equally in all directions as an exponentially stiffening sphere with constant thickness and uniform mechanical properties would under the influence of internal pressure. The fit obtained with equation (p) is not perfect, but it falls within the error bars. However, the values of A= 40.49 mmHg and α= 35.47 obtained by fitting the strain-pressure curve are quite different from the ones obtained by fitting the pressure-volume curve. Furthermore, the horizontal equatorial dimension could not be fitted with equation (p) because the exponentially stiffening sphere model does not predict contraction with increasing pressure.

2.5 Discussion

The pressure-volume and the strain-pressure curves have been presented and fitted using theoretical equations. These equations can be used to fit the data within the error of the experiment; however, values of A and α differ depending on what curve is being fitted. There are a few reasons for the discrepancy. First, fluid leaks from different openings in the eye such as Schlemm's canal and severed blood vessels, especially at higher pressures. Also, the medical tubes in the syringe pump apparatus are not perfectly rigid and expand with increasing pressure (Figure 14). The result is that the actual volume of fluid injected into the eye is less than the volume of fluid coming out of the syringe and this affects the pressure-volume curve such that chick eyes appear to be softer than they really are. The lower value of α obtained by fitting the pressure-volume curve indicates a softer eye. Obtaining A and α by fitting the strain-pressure curve is a more robust technique because strain and pressure are measured directly. In fact, the values of A and α obtained in this manner are similar to those obtained by Graebel and Van Alphen (1977) on strips of human sclera tested in simple elongation. Figure 15 clearly shows that chick eyes do not deform equally in all directions like a sphere and this suggests that chick eyes should not be assumed to be spherical and that the material constants A and α should not be calculated using the strain-pressure equation. The results presented here could not be compared with others as values of A and α for chick eyes appear to be absent from the literature. The technique used in this study could be applied to rounder eyes such as human or porcine eyes.

The deformation of chick eyes as intraocular pressure increases was accompanied by axial elongation which is in agreement with other studies in humans (Leydolt et al., 2008) and chicks (Phillips and McBrien, 2004). The axial elongation would lead to transient axial myopia and permanent myopia if the eyes were stressed beyond their elastic limit (Ethier et al., 2004). The elastic

limit of chick eyes was not determined in this study so it is not possible to tell at what pressure the chick eyes started to yield and become permanently myopic A material yields when it is subjected to a mechanical stress that exceeds its elastic limit or yield point. When the stress is removed, the material tends to return to its original shape, but permanent deformation remains. The axial elongation obtained by raising the IOP from 20 mmHg to 775 mmHg was equivalent to 25 dioptres of transient myopia and some unknown degree of permanent myopia. Also, a transient refractive error of -6.1 dioptres would be induced in chick eyes by raising the IOP to 100 mmHg. Whether chick eyes reach their yield point and become permanently myopic under an IOP of 100 mmHg is unknown. Also, the initial contraction of chick eyes in the horizontal equatorial direction is opposite to findings in humans (Atchison et al., 2004), tree shrews (Phillips and McBrien, 1995), and chicks (Irving et al., 1992) where myopic eyes are found to be larger than normal eyes in the equatorial direction. To obtain an increase in equatorial dimension in the current study, the intraocular pressure had to be increased beyond 385 mmHg, which is past the physiological range. Larger values of axial length and equatorial diameter might be obtained at physiological pressures if creep and/or fatigue were studied. For instance, Ku and Greene (1981) obtained significant amount of strain by subjecting rabbit eyes to IOP pulses of 150 mmHg over a period of 4 hours.

The fact that chick eyes deform more in the axial direction could be explained by the intrinsic material anisotropy and non-homogeneity of the chick eye. Actually, different studies in humans (Woo et al., 1972; Uchio et al., 1999) and pigs (Pierscionek et al., 2007) showed that the cornea is less stiff than the sclera which would cause the cornea to deform more than the sclera, contributing to axial deformation. In the present study, the deformation of the cornea itself was not measured, but it appeared to bulge outward as IOP increased. In addition, chicken eyes have a bony structure, the scleral ossicle, located near and posterior to the limbus (Walls, 1942) that could increase the rigidity

of the eye in the equatorial direction. However, increased rigidity in the equatorial direction would not explain why the chick eye initially shrinks in this direction. One explanation could be the oblate geometry of the chick eye (the average initial axial length was 9.12 mm and the average initial horizontal equatorial length was 12.62 mm). In fact, Phillips and McBrien (1995) constructed a basic finite element model of a tree shrew eye and found that the eye elongated in the axial direction but contracted in the equatorial direction when the intraocular pressure was increased from 0 to 20 mmHg. They modeled the tree shrew eye assuming isotropic, homogeneous, and linear elastic material properties such that the contraction in the equatorial direction could not be due to the anisotropy or non-homogeneity of the ocular tissues. The initial geometry of the tree shrew eye in their model was oblate with axial length of 7.2 mm and equatorial diameter of 8.4 mm. Furthermore, they showed that the contraction in the equatorial direction was due to the aspheric shape of the eye by comparing the finite element model of an oblate eye to a spherical eye. The oblate eye contracts in the equatorial direction whereas the spherical eye does not. Moreover, the oblate eye elongates more in the axial direction than the spherical eye when the intraocular pressure is increased from 0 to 20 mmHg.

If the geometry of the eye influences its deformation, would experimental myopia be easier to produce in animals with oblate eyes? By defining the oblateness ratio as the equatorial diameter minus the axial length over the equatorial diameter, it is possible to compare the eye shape of different animals and the amount of myopia that can be achieved experimentally. For instance, Irving et al. (1992) produced a 9.70 D myopic shift in chick eyes (oblateness ratio of 0.277) by applying -10 D goggles for 7 days while Phillips and McBrien (1995) obtained a 5.6 D myopic shift in tree shrew eyes (oblateness ratio of 0.143) using monocular deprivation of form vision for 5 days. Although the conditions of the two experiments are different, it seems to be easier to produce experimental myopia

in the more oblate eye, which is the chick eye. More research would be needed to prove this point. However, it could be argued that chicks develop higher degrees of myopia because of their fast growth rate. Gardiner (1954) showed that myopic children were in general taller than emmetropes and he suggested that their faster rate of growth was linked to their refractive error.

Following the same reasoning in humans, would people with oblate eyes be more at risk for axial deformation and myopia? Are premyopic eyes oblate in shape? In a study of ocular shape, 71% of 77 hyperopic eyes were found to be oblate in shape (Stone and Flitcroft, 2004). Although hyperopes can become myopic, there is no indication that hyperopes progress more toward myopia than emmetropes and myopes. For instance, in a study of 360 children over a 6 year period, Erismann (1871) found that 19% of children's refraction stayed stable, 28% showed an increase in myopia, and 28% presented a drift toward less hyperopia. Hyperopia is also associated with a thickening of the posterior sclera (Cheng et al., 1992) which would provide additional support and make the eye less prone to axial deformation. More research is needed to determine whether oblate eye geometry along with scleral thickness is associated with axial elongation and myopic shift in humans. The problem with current biometric measurements in humans is that they are always taken after the fact, that is, after myopia has developed. A large longitudinal study where the MRI of children eyes taken before and after myopia develops would provide valuable information on how the eye geometry evolves in myopia. While it has been argued that myopic eyes are longer in the axial direction because the bony orbital walls constrains the eye to expand more in the axial direction than in the equatorial direction (Atchison et al., 2004), the present research clearly demonstrates that for chicks, such constraints are not necessary and that the eye can expand more in the axial direction on its own.

The procedure used in this experiment is quite simple and care was taken to ensure the integrity of the measurements. Although the measurements were taken on post-mortem enucleated eyes, all measures were taken within 48 hours of death. A recent study showed that rabbit eyes can be stored for up to 72 hours in PBS at 4 ^{o}C without noticeable change in mechanical properties of the sclera (Girard et al., 2007). Also, the eyes were cannulated at the intersection of the equator and the 90 degree meridian for maximum stability and to ensure that the eyes do not rotate on the needle. This is important to obtain accurate measurements of the eye from the digital photographs. It is possible that the cyanoacrylate glue used to seal the puncture stiffened the eye and influenced the data, but care was taken to ensure no excessive use. A stiffer part of the eye would not explain the contraction in the equatorial direction and the author does not think that the use of cyanoacrylate glue significantly affected the results and the conclusions of this study.

One problem with the experiment design is that tap water injected into the eyes could have affected the results of the experiment. Because tap water is a very low concentration saline solution (hypotonic), it is absorbed by living tissues through a process known as osmosis. This process can happen very quickly. It has been shown that the water content of connective tissues changes significantly when immersed in distilled water for only 3 minutes (Chimich et al., 1992). Also, a change in the water content of living tissues affects their viscoelastic properties. For instance, Haut and Haut (1997) performed a stress relaxation test on human patellar tendons and found that specimens having a high water content (immersed in distilled water) relaxed faster than specimens having a low water content (immersed in 25% sucrose solution). Also, they found that specimens having a high water content were stiffer at a high strain rate (50%s^{-1}) but softer at a low strain rate (0.5%s^{-1}) compared with specimens having a low water content. In the present experiment, injections were administered quickly (2000 µl/min), but time was taken between injections to record pressure

and take photographs so it is difficult to evaluate the effect of tap water on chick eye rigidity. In addition, the injected tap water would have mixed with the intraocular fluid so the solute concentration of the solution in contact with the ocular tissues is unknown, but was likely higher than the tap water concentration. In the future, saline or PBS solution should be injected into the eyes so that the effect of solute concentration can be determined.

Another problem with the current experiment design is that the reference geometry of the chick eye was taken when the IOP was equal to 0 mmHg even though it is known that the normal IOP for 7-day old chicks is around 20 mmHg (Prashar et al., 2007). Basically, the geometry of a deflated eye was used to calculate the strain and this affected the axial strain curve. When the IOP was increased from 0 to 5 mmHg, the cornea bulged out considerably leading to a jump in axial length and axial strain (Figure 15). Subsequent increases in IOP did not lead to such an increase in axial length and strain. Therefore, if the reference geometry of the chick eye were taken when the IOP was 20 mmHg, the axial strain curve would shift downward. With the current data, it is not possible to use 20 mmHg as the reference because not all eyes were photographed at an IOP of 20 mmHg. In the future, the IOP of chick eyes should be set to 20 mmHg before starting the experiment. This could be done by injecting small amounts (5 µl) of saline into the eye with the syringe pump until a pressure of 20 mmHg is reached.

At last, preconditioning cycles should be performed before starting the experiment to ensure repeatable results (Conza, 2005). When soft tissues are tested in simple elongation, their stress/strain curve during the first loading cycle is different from the second loading cycle, but after a few loading cylces (preconditioning cycles), the stress/strain curve stabilizes and the mechanical behaviour is more consistent (Conza, 2005). Preconditioning can also be done with eyes. For example, Girard et

al. (2008) subjected their porcine scleral shells to twenty preconditioning cycles by varying the IOP from 5 mmHg to 15 mmHg and then allowed the specimens to rest and recover for 6 minutes before the start of the experiment. A similar preconditioning protocol could be used here with the chick eyes.

2.6 Conclusion

In conclusion, intraocular pressure increments cause axial elongation and horizontal equatorial contraction followed by expansion in chick eyes. Chick eyes prefer to deform in the axial direction as opposed to the horizontal equatorial direction. The most plausible explanation for this deformation is the oblate geometry of chick eyes which tends to naturally become more spherical as IOP increases. At high IOP, chick eyes enlarge in both directions, but are larger in the axial direction than in the horizontal equatorial direction. The maximum axial elongation would produce 25 dioptres of transient myopia under mechanical stretch alone. The natural tendency of chick eyes is to elongate under increasing IOP and this suggests that IOP could play a role in myopia onset and progression.

Chapter 3: Pressure-volume experiment with myopic eyes

3.1 Introduction

The pressure-volume experiment with myopic eyes is identical to the pressure-volume experiment with normal eyes presented in Chapter 2 except that myopic eyes were used instead of normal eyes. Myopia was experimentally induced in chicks by applying -15 D lenses in front of their right eyes and the left eye was used as control.

The purpose of this experiment was to obtain the pressure-volume behavior of experimental myopic chick eyes and compare it to the control and normal chick eyes. The slope of the pressure-volume curve is an indication of ocular rigidity and a steeper slope denotes a higher ocular rigidity. Studies in humans showed that the ocular rigidity of myopes was lower than emmetropes and hyperopes (Friedenwald, 1937; Draeger, 1959). Also, Perkins (1981) showed that the lower ocular rigidity of myopes was mainly due to their larger size and ocular volume. This result was confirmed by Greene (1985) who demonstrated theoretically that larger eyes have a lower ocular rigidity. Lower ocular rigidities have also been observed in animal models of myopia. For instance, Wang et al. (2008b) reported a significant lower ocular rigidity in myopic guinea pig eyes compared with control eyes. So, it is expected that the myopic chick eyes in the current study will have a lower ocular rigidity than the control eyes.

The second purpose was to determine the strain in the axial and horizontal equatorial directions for myopic and control eyes and compare them to the normal eyes. Myopic chick eyes are more spherical in shape than control eyes (Irving et al., 1992) and should deform differently than the control eyes.

3.2 Methods

The chicks, their environment, and the experimental procedure used in this experiment were the same as the experiment with normal eyes presented in Chapter 2 and the reader is invited to review sections 2.3.1 and 2.3.2. The only difference in this experiment is that the right eyes of chicks were made myopic experimentally. Eight chicks were obtained from a local poultry plant (Maple Leaf Poultry, New Hamburg, Ontario, Canada) on the day of hatching. Myopia was induced in the right eye of each chick by applying -15 D goggles for 7 days from the day of hatching (Figure 16). The left eye was left alone and used as control. The goggles were secured to the head of the birds using Velcro and cyanoacrylic glue. A Velcro ring was cut to match the edge of the goggle. Using forceps to hold the Velcro ring, cyanoacrylic glue was applied all around the Velcro ring except the area covered by the forceps. While holding the bird with one hand, the ring was positioned around the eye of the chick making sure that the area with no glue was aligned with the beak so that the beak was not glued. Then, the forceps were released and pressure was applied on the Velcro ring with the fingers so that the Velcro ring made contact with most of the feathers around the eye. The ring was held in this position for thirty seconds to allow the glue to dry. After 20 minutes, the goggles were applied to the Velcro ring (Figure 16). All eight chicks were examined daily to ensure that the goggles did not fall off. If goggles fell off, they were put back on immediately and the experiment was allowed to continue even though this would decrease the amount of myopia induced in the chick eye. Indeed, a study demonstrated that if chicks lost their goggles for a total duration of 3 hours each day, myopia did not develop (Schmid and Wildsoet, 1996). For the current experiment, the exact amount of myopia induced was not important as long as a noticeable amount of myopia was produced. After 7 days, the chicks were taken out of their steel brooders and the refractive state of both eyes was measured by retinoscopy with an accuracy of ±0.5 D. Wallman and Adams (1987) showed that the difference between cycloplegic and non-cycloplegic refraction in chicks was small so no cycloplegic

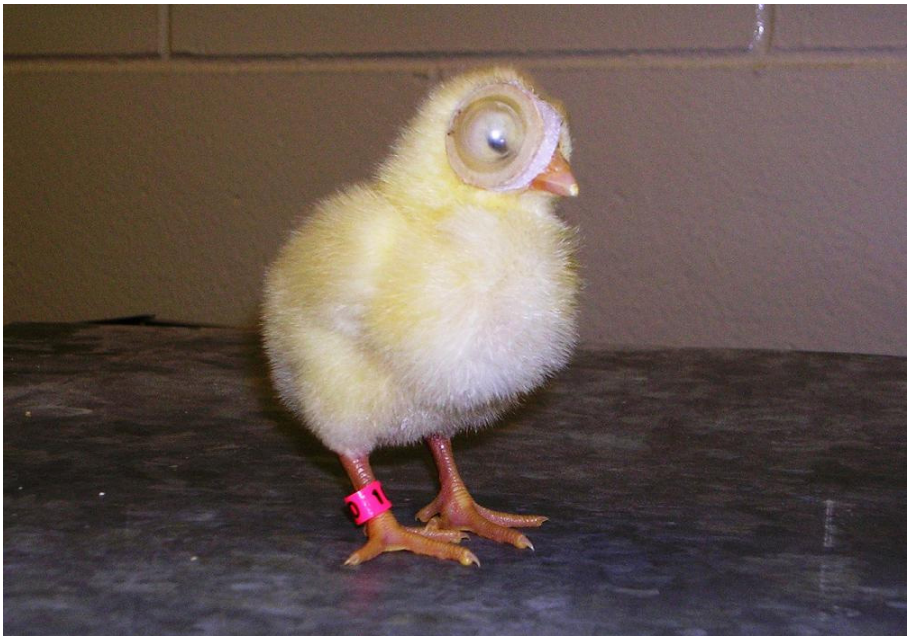

Figure 16. A -15 D goggle attached over the right eye of a chick.

drug was used during the refractive measurements. Immediately following the refractive state measurement, all chicks were sacrificed by decapitation, the eyes were removed and cleaned from extraocular fat and tissues, and they were stored in PBS solution at 4^{o}C. From this point, the pressure-volume experiment with myopic eyes employed the same syringe pump apparatus and the same procedure as described in section 2.3.2 for normal chick eyes. All myopic eyes along with all control eyes were tested to failure. Also, the results of the 10 normal chick eyes from Chapter 2 were used for comparison. Note that the myopic and control chick eye results were not fitted with the theoretical formulae from section 2.3.3.

3.3 Results

3.3.1 Refractive state

The refractive state measurements for all eyes are shown in Table 1. Note that 4 eyes were damaged during the enucleation process and were discarded. At least 5 D of myopia was induced in the right eye of all birds except bird 1, which for some reason remained highly hyperopic. The right eye of bird 1 was excluded from the results. Also, all left eyes showed 5 D of hyperopia or more and the difference in refraction between the left and the right eye was 11 D or more. The mean refraction in the right eye was -11 D and the mean refraction in the left eye was +6.9 D and the difference was significant (unpaired t-test, p=0.0003).

Table 1. Refractive error of right and left eyes.

	Refractive error Right eye (D)	**Refractive error Left eye (D)**	**Difference (D)**
Bird 1	Excluded	N.A.	N.A.
Bird 2	-13	N.A.	N.A.
Bird 3	-5	+8	13
Bird 4	-22	+7	29
Bird 5	-5	+7	12
Bird 6	-15	N.A.	N.A.
Bird 7	-6	+5	11
Bird 8	N.A.	+7.5	N.A.

3.3.2 Pressure-volume relationship

The average IOP at failure was 761 ± 57 mmHg (±SD) and 799 ± 134 mmHg for control and myopic eyes respectively and the difference was not statistically significant (unpaired t-test, p=0.57). Recall from Chapter 2 that the mean IOP at failure for normal eyes was 869 ± 95 mmHg. The mean IOP at failure for myopic eyes was not statistically different from normal eyes (unpaired t-test, p=0.24),

while the mean IOP at failure of control eyes was significantly different from normal eyes (unpaired t-test, p=0.04).

The average pressure-volume relationships for myopic, control, and normal eyes are shown in Figure 17. All pressure-volume curves are curved upwards indicating that all eyes are getting stiffer as intraocular volume increases. Also, an exponential curve fit and an F-test performed on the data revealed that the myopic and control eyes pressure-volume curves were not different ($F(2:46)=0.6503$; $p=0.526$) whereas the control and normal eyes pressure-volume curves were different ($F(2,46)=41.98$; $p<0.0001$). Also, the pressure-volume curves of myopic and normal eyes were found to be different ($F(2,46)=54.58$; $p<0.0001$). The slope of the pressure-volume curves for

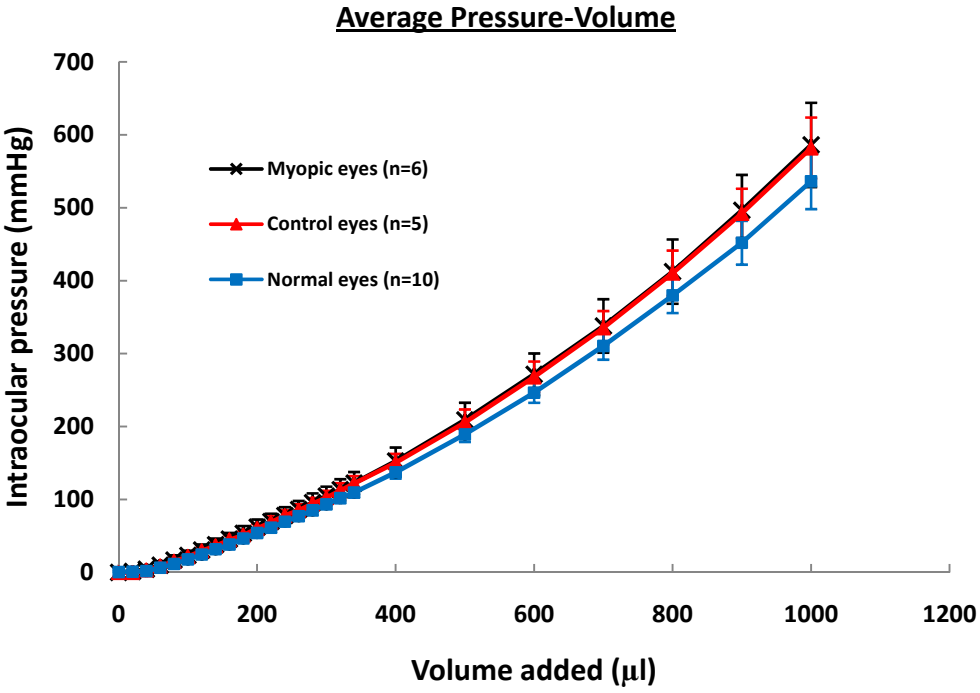

Figure 17. Average pressure-volume curve for myopic, control, and normal eyes (±SD).

myopic and control eyes was higher than the slope of the normal eyes curve which means that the ocular rigidity of myopic and control eyes was higher than the ocular rigidity of normal eyes. The F-test only compares the parameters of the exponential functions and does not take the spread into account. So, an unpaired t-test was performed on individual points on both the myopic and normal eyes curves and the results are shown in Table 2. For IOPs below 100 mmHg, the myopic and normal

Table 2. Average pressure-volume data for myopic (n=6) and normal (n=10) eyes.

Volume injected (µl)	**Myopic eyes mean IOP ±SD (mmHg)**	**Normal eyes mean IOP ±SD (mmHg)**	**Unpaired t-test P value**	**Statistically significant?**
100	23 ± 7	18 ± 6	0.1006	No
120	31 ± 8	25 ± 6	0.0953	No
140	38 ± 8	32 ± 5	0.0945	No
160	46 ± 8	38 ± 6	0.0512	Not quite
180	53 ± 10	47 ± 5	0.0884	No
200	62 ± 10	54 ± 5	0.0548	Not quite
220	70 ± 11	61 ± 6	0.0580	No
240	78 ± 11	70 ± 5	0.0533	Not quite
260	86 ± 12	77 ± 6	0.0531	Not quite
280	96 ± 13	85 ± 7	0.0508	Not quite
300	105 ± 13	93 ± 6	0.0285	Yes
320	113 ± 14	102 ± 7	0.0460	Yes
340	122 ± 15	110 ± 7	0.0361	Yes
400	152 ± 19	137 ± 9	0.0410	Yes
500	209 ± 24	189 ± 10	0.0349	Yes
600	272 ± 29	246 ± 14	0.0322	Yes
700	338 ± 37	311 ± 19	0.0667	No
800	412 ± 44	380 ± 24	0.0747	No
900	496 ± 48	452 ± 30	0.0383	Yes
1000	586 ± 58	536 ± 38	0.0552	Not quite

eyes pressure-volume curves were not statistically different, but for IOPs between 100 and 300 mmHg, the two curves were statistically different. Also, many points were almost statistically

significant as their p values were close to 0.05. It is fair to say that the lower part of the pressure-volume curves was not statistically different while the upper part was statistically different. Interestingly, the pressure-volume curves of myopic and control eyes were almost on top of each other (Figure 17) and they were not different based on the F-test. The unpaired t-test also showed that all the points on the pressure-volume curves of myopic and control eyes were not statistically different and the p value was around 0.75 (Table 3). In addition, the eyes from the same bird had similar pressure-volume curves (Figure 18) even though the right eye was myopic and larger in size.

Table 3. Average pressure-volume data for myopic (n=6) and control (n=5) eyes.

Volume injected (µl)	**Myopic eyes mean IOP ±SD (mmHg)**	**Control eyes mean IOP ±SD (mmHg)**	**Unpaired t-test P value**	**Statistically significant?**
100	23 ± 7	22 ± 5	0.7187	No
140	38 ± 8	37 ± 5	0.7739	No
300	105 ± 13	103 ± 9	0.7626	No
500	209 ± 24	206 ± 18	0.7949	No
1000	586 ± 58	582 ± 42	0.8853	No

Now, it is possible that systematic errors affected the measurements. The normal, control, and myopic eyes were not all tested at the same time and it is possible that a change in the environment or the experimental set up affected the measurements. Figure 19 shows the pressure-volume curves of chick eyes grouped by the date they were tested. There appears to be a drift in the pressure-volume curves from the different groups. The eyes tested on July 29 and July 30 were softer (less steep pressure-volume curve) than the eyes tested on October 7 and October 8. Also, the eyes tested on August 4 had a similar pressure-volume behavior compared with the eyes tested on September 9 and

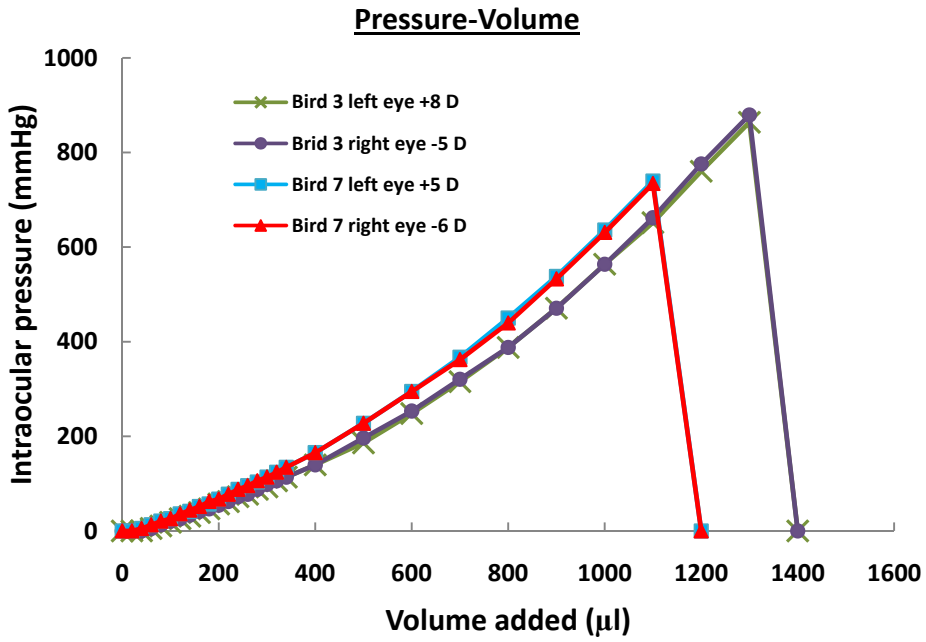

Figure 18. Individual pressure-volume curves for eyes from the same bird.

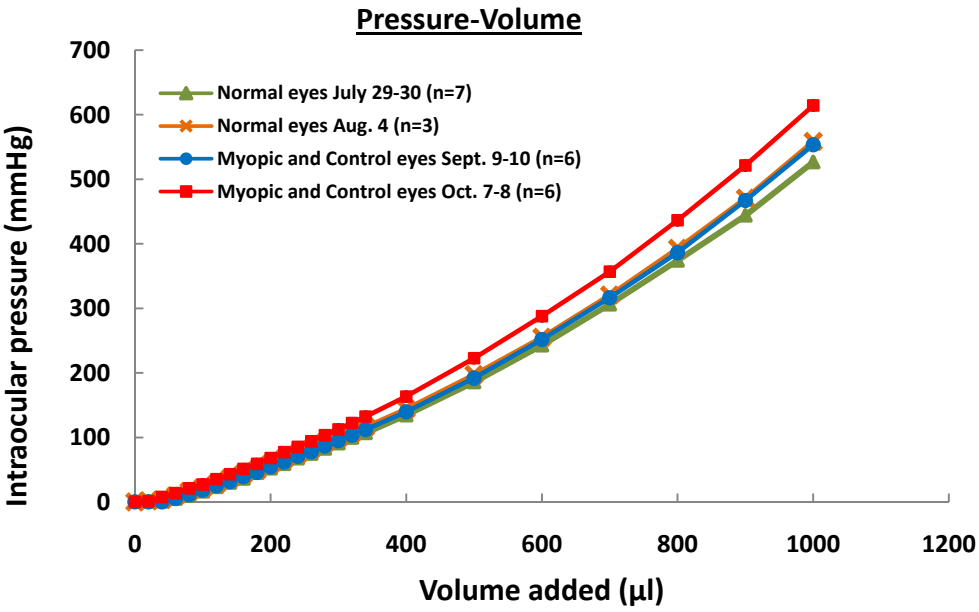

Figure 19: Pressure-volume curves of chick eyes grouped by date tested.

10. Note that there were three myopic and three hyperopic eyes in each of the myopic and control eyes groups.

3.3.3 Strain-pressure relationship

The average axial strain curves as a function of IOP for myopic, control, and normal eyes are shown in Figure 20. All three curves followed the same pattern, but the myopic eyes did not elongate as much in the axial direction with increasing IOP compared with normal and control eyes. The difference between the myopic and normal eyes was significant for all points on the curve (unpaired t-test, $p_{average}$= 0.03) whereas the difference between the myopic and control eyes was not significant for all points (unpaired t-test, $p_{average}$= 0.3472). All individual pressure points on both curves were

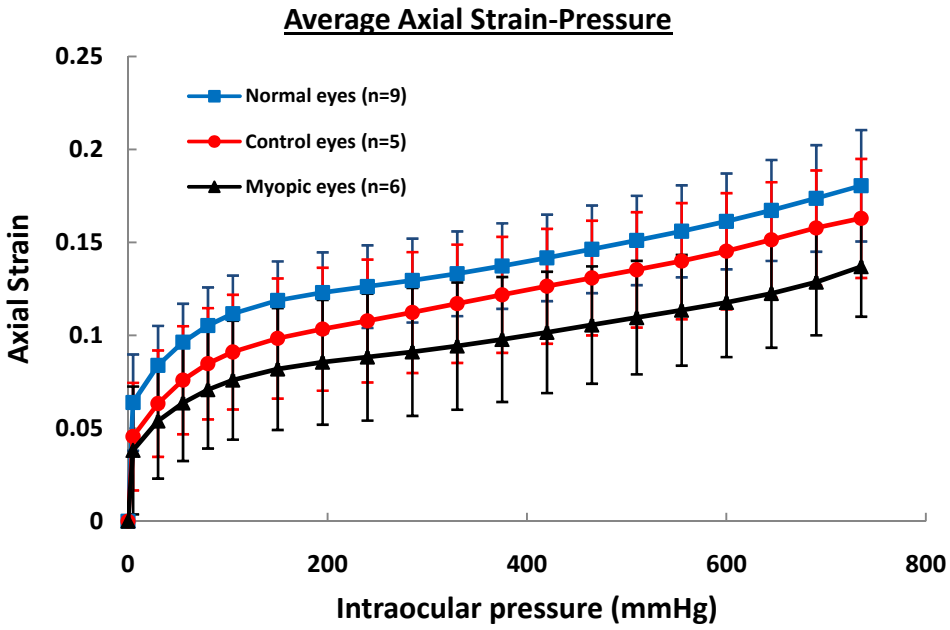

Figure 20. Average axial strain versus pressure for myopic, control, and normal chick eyes (±SD).

compared using the unpaired t-test and the p values were averaged to obtain $p_{average}$. Also, the control eyes elongated less in the axial direction than the normal eyes, but the difference was not statistically significant for all points on the curve (unpaired t-test, $p_{average}$= 0.2636).

The average horizontal equatorial strain curves as a function of IOP for myopic, control, and normal eyes are shown in Figure 21. As seen in Chapter 2, normal chick eyes initially contracted in the horizontal equatorial direction with increasing pressure and then expanded. Here, the myopic eyes did not contract as much in the horizontal equatorial direction compared with normal and control eyes. Also, the curve for the myopic eyes was shifted upwards compared with normal and control eyes. The curves for myopic and control eyes were significantly different for all points on the curves except when IOP was equal to 5 mmHg (unpaired t-test, $p_{average}$= 0.02). Similarly, the curves for myopic and normal eyes were significantly different for all points except when IOP was equal to 5 mmHg (unpaired t-test, $p_{average}$= 0.007). As seen in Figure 21, the curves for control and normal eyes were very similar and not statistically different for all points (unpaired t-test, $p_{average}$= 0.75). Also, the strain in the horizontal equatorial direction of two control eyes could not be measured adequately because the camera was out of focus and the photographs were blurry.

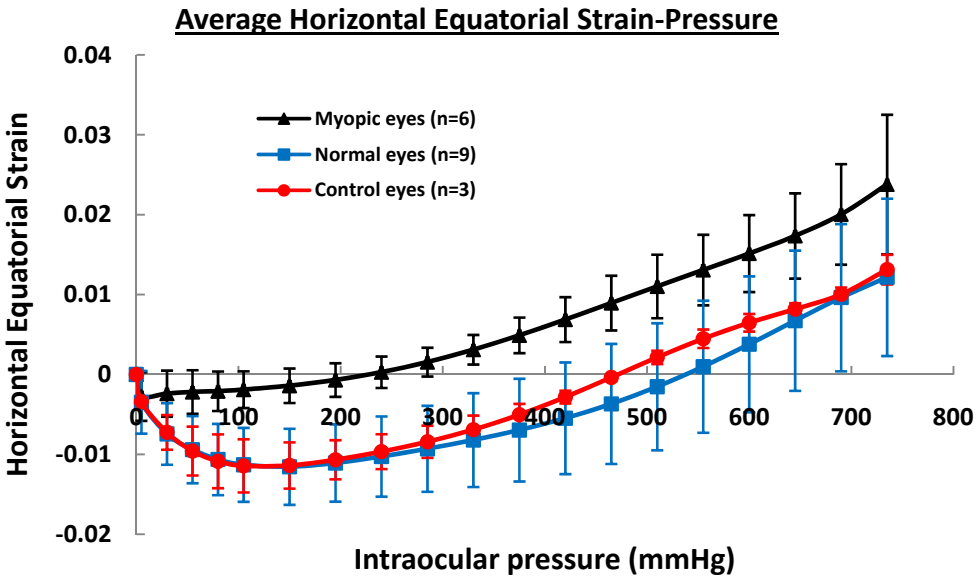

Figure 21. Average horizontal equatorial strain versus IOP for myopic, control and normal chick eyes (±SD).

3.4 Discussion

3.4.1 Pressure-volume relationship

The pressure-volume curves for myopic, control, and normal eyes have been presented and at IOP lower than 100 mmHg, the three curves were not statistically different. Similar pressure-volume curves indicate that the ocular rigidities of myopic, control, and normal eyes were similar and this result is different to findings in humans (Friedenwald, 1937; Draeger, 1959) and guinea pigs (Wang et al., 2008b) where the ocular rigidity of myopic eyes was found to be lower than control or normal eyes. Also, the fact that the right and left eye from the same bird had almost identical pressure-volume relationships mean that their ocular rigidities were almost the same even though the right myopic eyes was larger in size. Greene (1985) demonstrated theoretically that the larger eyes of human myopes have lower ocular rigidities compared with emmetropes and hyperopes. This means

that the myopic chick eyes in the current study might have had stiffer ocular tissues to compensate for their larger size such that their ocular rigidity was similar to the control eyes. If mechanical stretch were involved in myopia onset and progression, one would expect the ocular tissues of myopic eyes to be stiffer than normal because living tissues get stiffer as they stretch. Wang et al. (2008b) found that the sclera and cornea of myopic guinea pig eyes was stiffer than the sclera and cornea of control eyes, but the difference was not statistically different. Also, Phillips and McBrien (1995) tested strips of sclera from tree shrew eyes in simple elongation and found no statistical difference between the secant modulus of myopic, control, and normal scleras. However, studies in chicks showed that the cartilaginous scleral layer thickens while the fibrous scleral layer thins in eyes made myopic experimentally by form deprivation or hyperopic defocus (Gottlieb et al., 1990; Beresford et al., 2001; Xu et al., 2007). The thickening of the cartilaginous layer and the thinning of the fibrous layer were such that the overall scleral thickness did not change (Gottlieb et al., 1990). The increased thickness of the cartilaginous layer could result in increased stiffness of the sclera that would explain the similar ocular rigidities of myopic, control, and normal eyes even though the myopic eyes are larger in size.

At IOP between 100 and 300 mmHg, the pressure-volume curves of myopic and normal eyes were statistically different (unpaired t-test). The slope of the myopic pressure-volume curve was higher compared with normal eyes and this means that the ocular rigidity of myopic eyes was greater than the ocular rigidity of normal eyes. Again, the most probable explanation is the increased thickness of the cartilaginous scleral layer in experimental myopia in chicks. Also, the fact that the pressure-volume curves of myopic and control eyes were similar whereas the pressure-volume curves of control and normal eyes were different suggest that the -15 D goggle applied to the right eye also affected the left eye. Studies in chicks showed that form deprivation myopia and defocus induced

myopia in one eye also affected the refraction and the thickness of ocular tissues in the fellow control eye (Beresford et al., 2001).

The difference between the pressure-volume curves of normal, control, and myopic eyes could also be due to systematic errors. The eyes tested in July seemed to be softer than the eyes tested in October and there appears to be a drift toward more rigid eyes with time. It is possible that the gradual temperature and humidity change from the hot summer season to the cooler fall could have affected the pressure measurements or the behavior of the chick eye itself. It is known that temperature affects the mechanical properties of soft tissues. Also, the humidity level in the air can affect the water content of tissues which has an influence on the mechanical properties. Now, there is one aspect of the experiment that changed between the September and October experiments. The needle of the syringe pump apparatus was replaced by a new and identical needle. The plastic part of the needle had to be cut and glued to the medical tubing to ensure a proper fit and no leakage. It is possible that small debris got stuck into the needle which would impede the normal flow of water. This impedance would cause an increase in flow resistance and the pressure in the eye could appear higher than it is. This would explain the higher ocular rigidity of the eyes tested in October compared with the eyes tested previously. In addition, it is possible that the experimenter was getting better at performing the pressure-volume experiment and this could explain the drift seen in the data. Finally, the eyes tested on different dates were taken from different batches of chicks and it is possible that eyes from different batches behave differently during the pressure-volume experiment.

3.4.2 Strain-pressure relationship

The myopic eyes did not elongate as much in the axial direction compared with the normal eyes and the difference was significant. This could be due to the fact that the ocular rigidity of the myopic eyes was slightly higher than for the normal eyes as indicated by the steeper pressure-volume curve. A

more rigid eye is less prone to ocular deformation. Also, the myopic eyes did not contract as much in the horizontal equatorial direction as IOP initially increased compared with control and normal eyes and this is probably due to their geometry. Myopic eyes were more spherical in shape compared with control and normal eyes. A spherical eye expands equally in all direction with increasing IOP and does not contract at all whereas an oblate eye expands more in the axial direction and initially contracts in the equatorial direction. Recall from Chapter 2 that Phillips and McBrien (1995) showed that the oblate geometry of a tree shrew eye was responsible for the contraction in the equatorial direction. Overall, the deformation of the myopic eyes was closer to the deformation of a sphere under pressure because their axial and horizontal equatorial strain curves were closer together. Also, similar amounts of fluid were injected in both myopic and normal eyes before failure. This means that the volumetric deformation ($V-V_o$) or change in volume was similar for both myopic and normal eyes and this was possible because the myopic eyes ended up stretching more in the horizontal equatorial direction to compensate for the decreased axial strain. Now, if pure mechanical stretching were the mechanism of experimental myopia in the chick eye, then the ocular tissues of the myopic eyes would be pre-stressed and therefore stiffer due to the stiffening effect of stretch. Consequently, the myopic eyes would need less fluid injected before failure occurs. However, the volumetric deformation at failure of both myopic and normal eyes was similar suggesting that growth and remodeling are involved in experimental myopia in the chick. Actually, the fact that the cartilaginous scleral layer thickens in experimental myopia in chicks (Gottlieb et al., 1990) demonstrates that growth and remodeling must be involved.

The control eyes did not expand as much in the axial direction as the normal eyes and this can be explained by looking at the individual data. The pressure-volume experiment with myopic eyes was conducted with 2 batches of birds; one batch of 4 chicks in September and a second batch of 4 chicks

in October. By looking at the individual axial strain versus pressure curves, the eyes from the October birds did not elongate as much in the axial direction as the eyes from the September birds or the normal eyes. This brings the axial strain curves of the control and the myopic eyes down relative to the curve of the normal eyes. However, within each batch, all the myopic eyes elongated less in the axial direction compared with the control eyes. So, the myopic eyes did not elongate as much in the axial direction compared with the control eyes. The results in this study could not be compared with others because pressure-volume experiments with myopic chick eyes seem to be absent from the literature.

3.5 Conclusion

The myopic eyes were either similar to or more rigid than the control and normal eyes even though the myopic eyes were larger in size. The most probable explanation is the thickening of the cartilaginous layer of the sclera in chick eyes made myopic experimentally (Gottlieb et al., 1990; Beresford et al., 2001; Xu et al., 2007). Also, it is possible that systematic errors affected the pressure-volume curves of normal, control, and myopic chick eyes. In any case, a similar or higher ocular rigidity for myopic eyes compared with control and normal eyes is opposite to findings in humans and guinea pigs. Tension tests should be done on strips of chick sclera to obtain the mechanical properties of myopic, control, and normal chick eyes to better understand what causes the ocular rigidity of myopic eyes to be similar or higher than the control and normal eyes even though their size is different. Growth and remodeling is likely to be involved in experimental myopia. Finally, the myopic chick eyes did not expand as much in the axial direction and did not contract as much in the horizontal equatorial direction with increasing pressure compared with normal and control eyes. This is probably due to the more spherical shape of myopic chick eyes.

Chapter 4: Three-dimensional reconstruction

4.1 Introduction

In order to construct a finite element model of a chick eye, the geometry of the eye was required. In this chapter, the complete geometry of the corneo-scleral shell of a 7-day old chick eye was reconstructed. The corneo-scleral shell was chosen because it is the main structural element of the eye that resists the forces generated by the extraocular muscles, the ciliary muscle, and by fluctuations in intraocular pressure (McBrien and Gentle, 2003). A 7-day old chick eye was frozen and sliced with a microtome while photographs of the remaining block were taken at constant intervals. The photographs were aligned in MATLAB® (The MathWorks, Natick, USA) and then they were imported into SolidWorks® for segmentation and 3D reconstruction. The surfaces of the 3D model obtained with SolidWorks® were quite uneven so a different software was used. Mimics (The Materialise Group, Leuven, Belgium), a software used to process 2D image stacks from medical devices such as Computer Tomography (CT) and Magnetic Resonance Imaging (MRI) and to reconstruct the 3D geometry of biological structures, was chosen for the task. Mimics also allowed exporting the 3D model to the Abaqus/CAE® input file (.inp) format for finite element analysis which made the whole process relatively smooth and easy. In total, three models were constructed: two revolved 3D models in SolidWorks (model 1 and model 2) and one complete 3D model in Mimics (model 3). Chick eye # 1 was used to construct revolved model 1 and chick eye # 2 was used to produce revolved model 2 and complete model 3. Note that part of this chapter was taken from Wong et al. (in press). The content is reprinted here by the permission of the publisher (Taylor & Francis Ltd, http://www.informaworld.com).

4.2 Microtome experiment

The chicks used in this experiment were identical to the ones used in the pressure-volume experiment with normal eyes. Review section 2.3.1 for more details. Six eyes from 7-day old chicks were removed from storage and allowed to dry for 5 minutes on a piece of paper so that the external ocular surface was moist but not wet. The eyes were then painted using red tissue dye (Bradley Products Inc., Bloomington, USA) for better visualization of the exterior edge of the corneo-scleral shell. The eye was positioned on its equator onto the cutting surface of a portable freezing microtome, embedded in optimum cutting temperature (OCT) compound, and frozen with CO_2. The microtome slice thickness was set to 50 microns and the frozen OCT block was sliced until the top surface of the chick eye was identified. Then, the chick eye was sliced into thin sections in a sequential manner starting from the top. Carbon dioxide was administered at regular intervals to ensure that the eye

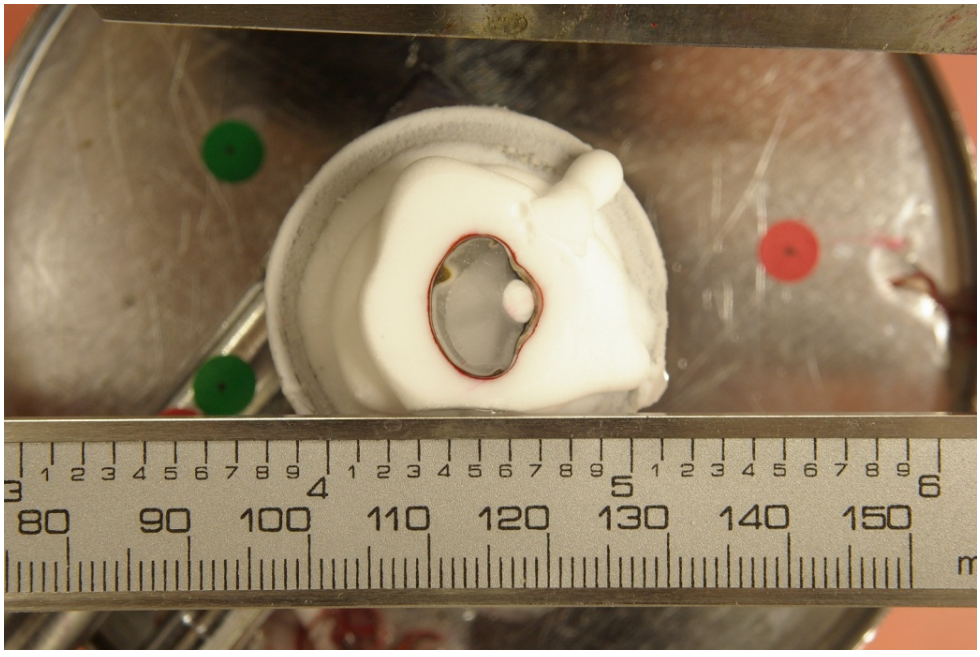

Figure 22. A chick eye section inside the microtome. The bottom scale is in mm.

remained frozen and to achieve proper hardness of the specimen for optimum sectioning. Every 5 slices (250 microns), an image of the remaining block was captured using a Pentax K100D Super digital camera (Hoya Corporation, Tokyo, Japan) having a resolution of 3008 x 2000 pixels and capable of acquiring images at a 25 microns x 25 microns spatial resolution (Figure 22). On average, a total of 47 photographs per eye were acquired.

4.3 Alignment of photographs

The microtome apparatus was reasonably stable, but vibration during the slicing process and camera jitter caused misalignments between adjacent images. Alignment of the image sequence was required to ensure accurate 3D reconstruction of the chick eye. The alignment process was carried out by Alexander Wong from the image processing group (Systems Design Engineering) at the University of Waterloo. To aid the alignment process, a series of colored markers were placed on the microtome platform (Figure 22). These markers were fixed relative to the chick eye during the entire sectioning process and acted as reference points. Also, the lighting conditions somehow changed during the experiment so an illumination-invariant alignment algorithm based on complex phase order likelihood (Wong et al., 2010) was chosen to align the photographs. The alignment algorithm was implemented in MATLAB® (The MathWorks, Natick, USA). The photographs of eye # 2 were chosen for alignment because the dataset was complete and the quality of all images was better, that is, there were minimal smearing of the red paint and no cut debris over the surface of the eye. The error in the alignment process was estimated against the ground truth alignment performed by a trained expert and was found to be less than 1% of the axial length of the chick eye.

4.4 SolidWorks® models

4.4.1 Image segmentation using SolidWorks®

Image segmentation refers to the process of dividing an image into segments and is normally used to identify parts or boundaries within an image. In the current project, image segmentation was used to extract the cornea and the sclera from the rest of the chick eye.

The aligned photographs of eye # 2 from the microtome experiment were imported on a set of parallel planes 250 µm apart in SolidWorks®. The photographs were scaled such that the size of the chick eye was true. The spline function was used to manually trace the internal and external contours of the cornea and the sclera of the chick eye on every photograph (Figure 23). The spline was a good approximation of the boundary of the corneo-scleral shell and created a smooth profile which is better for finite element analysis. It is generally more difficult to generate a good finite element mesh on a rough surface compared with a smooth surface.

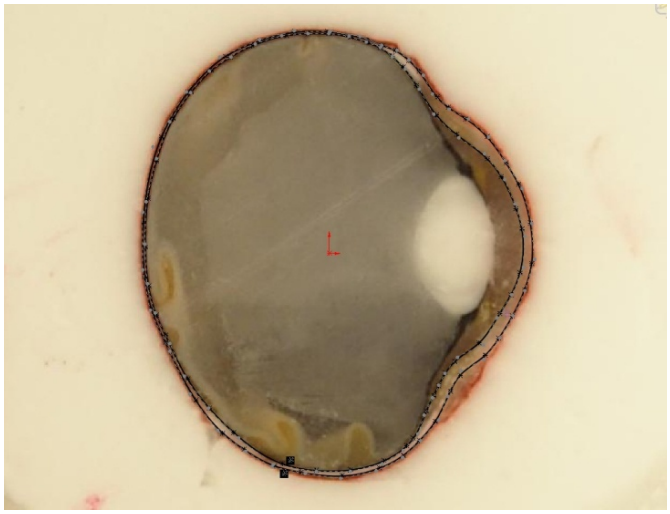

Figure 23. Segmentation using the spline function in SolidWorks®.

4.4.2 Complete 3D reconstruction

After the images were segmented, the contours of the corneo-scleral shell produced a set of parallel profiles 250 µm apart. The loft feature in SolidWorks® was used to connect the parallel profiles together and reconstruct the 3D geometry of the chick eye. The loft feature uses spline guide curves to guide the loft and connect the parallel profiles. This resulted in a 3D geometry that was not smooth (Figure 24). Chang et al. (2003) used a similar technique to reproduce the 3D geometry of a human tooth and found that using the loft feature in SolidWorks® resulted in a rough 3D model. Unfortunately, SolidWorks® does not have a smoothing function and its use for complete 3D reconstruction of the chick eye was abandoned and the Mimics software was used instead.

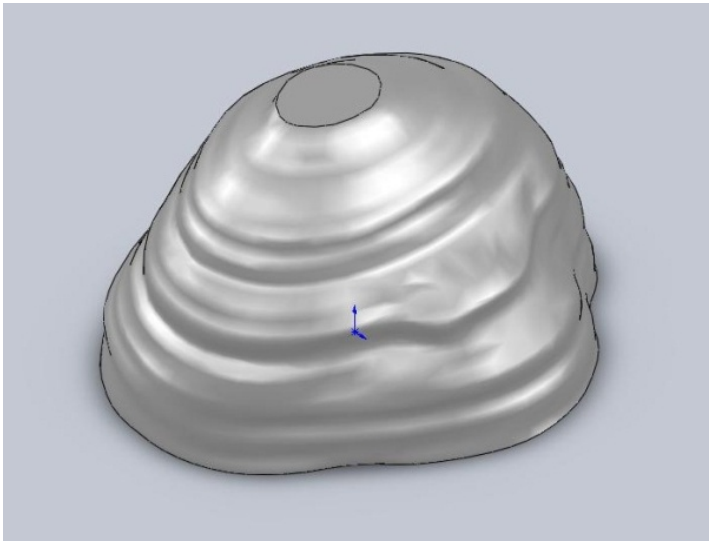

Figure 24. 3D reconstruction in SolidWorks®. Only half of the model is shown.

4.4.3 Revolved 3D models

Although the complete 3D geometry with proper thickness of the corneo-scleral shell could not be reproduced satisfactorily with SolidWorks®, the software could still be used to create a surface 3D model of the chick eye using the revolve feature. Only the midsection of the chick eye and only one

half of the external boundary of the corneo-scleral shell were used to reconstruct the geometry. The result was a body of revolution with no thickness that approximated the 3D geometry of the corneo-scleral shell. A revolved surface 3D model of both eye # 1 (model 1) and eye # 2 (model 2) was created (Figure 25). Notice how the overall geometry of the two models, and therefore the geometry of the two eyes, is different.

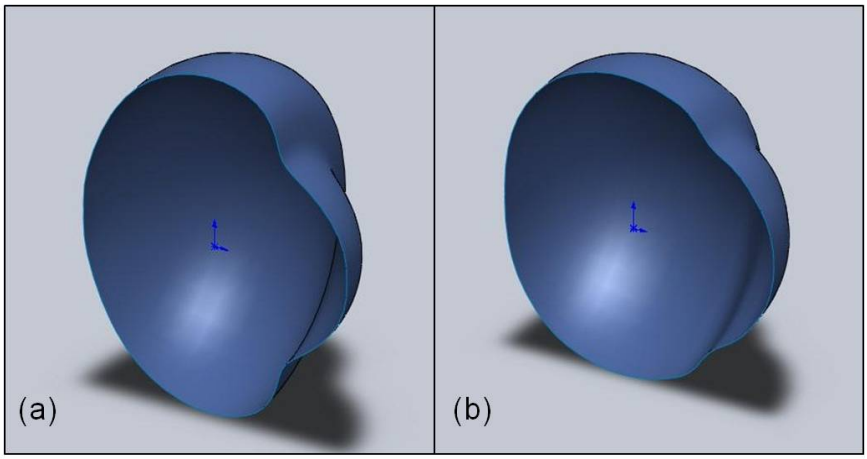

Figure 25. Revolved models of two chick eyes. (a) Model 1. (b) Model 2.

4.5 Mimics model

4.5.1 Image segmentation using Mimics

The aligned photographs of eye # 2 from the microtome experiment were imported into the Mimics software. The image resolution (3008 x 2000 pixels), pixel size (25 μm x 25 μm), and distance between the slices (250 μm) were input into the software. Mimics has a tresholding function that allows parts of an image having different pixel intensities to be identified. When the contrast between the object to be segmented and the background is good, tresholding can be used to automatically and quickly segment the desired object in the image. However, the contrast between the sclera and the rest of the eye was not constant between all the images in the sequence so that the tresholding function

could not be used. Instead, a mask was manually applied to the corneo-scleral shell on all the images using the computer mouse. Masking the images gave good results but the technique was time consuming. Masking was similar to coloring the chick eye with a crayon. A blue mask was created to mark the inner boundary of the corneo-scleral shell while a purple mask was used for the external boundary (Figure 26). At a later step, 3D models of the purple and blue masks were created and the blue 3D model was subtracted from the purple 3D model to obtain the 3D model of the corneo-scleral shell.

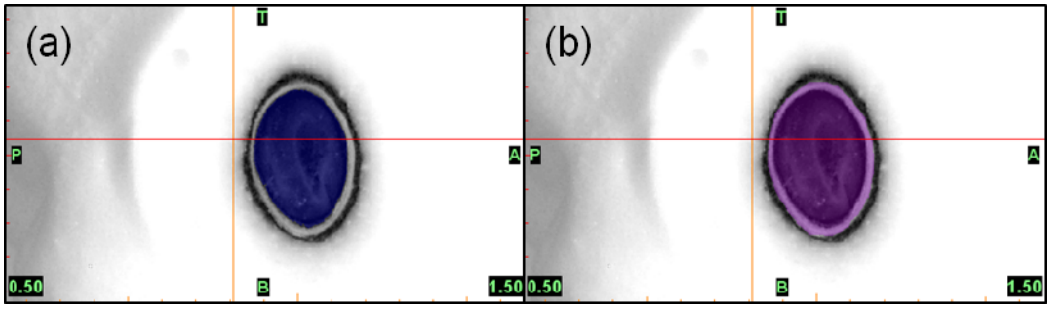

Figure 26. Chick eye section showing (a) the blue mask and (b) the purple mask.

4.5.2 3D reconstruction in Mimics

Once a blue and purple mask was applied to all the photographs in the sequence, 3D objects of the blue and purple masks were created. The Mimics software has a function to create 3D objects from masks which makes the process easy. A light wrap was applied to each 3D objects to remove small inclusions. Then, the 3D object of the blue mask was subtracted from the 3D object of the purple mask to obtain a rough 3D object of the corneo-scleral shell of chick eye # 2 (Figure 27). Note that the 3D object is made of 2 surfaces, the inner and outer surfaces of the corneo-scleral shell, and nothing in between. The smoothing function in Mimics was used to smooth the 3D object. The smooth factor was set to 0.7 and 3 iterations were needed to obtain a suitable model. Then, the smoothed model was imported into the Mimics Remesher to create the tetrahedral volume mesh.

More details about the creation of the volume mesh are given in section 5.3.1. The final smoothed 3D tetrahedral volume mesh of eye # 2 (model 3) is shown in Figure 28.

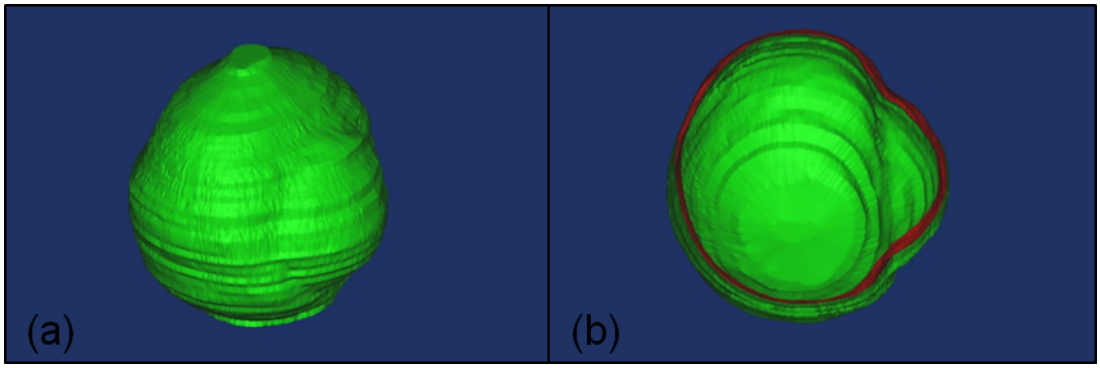

Figure 27. Initial rough 3D object of eye # 2. (a) Isometric view. (b) Cut view.

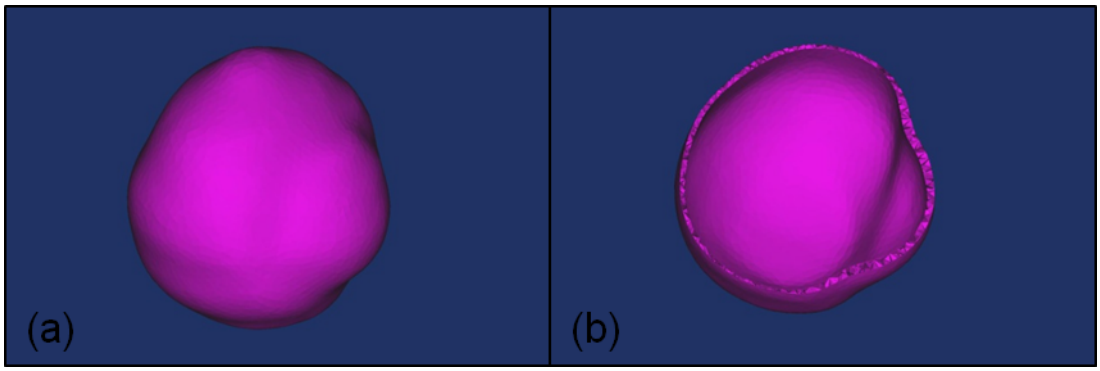

Figure 28. Final smoothed volume mesh (model 3). (a) Isometric view. (b) Cut view.

The process of smoothing the model resulted in a loss of accuracy such that the contours of the 3D model did not fit exactly the corneo-scleral shell in the photographs. Figure 29 shows the contour of the final smoothed volume mesh of eye # 2 (model 3) overlaid on top of a corresponding section photograph. It can be seen that model 3 is slightly larger and that it does not match the corneo-scleral shell perfectly. Also, the sclera is a bit too thick at the back of the eye. These geometric inaccuracies were judged to be acceptable.

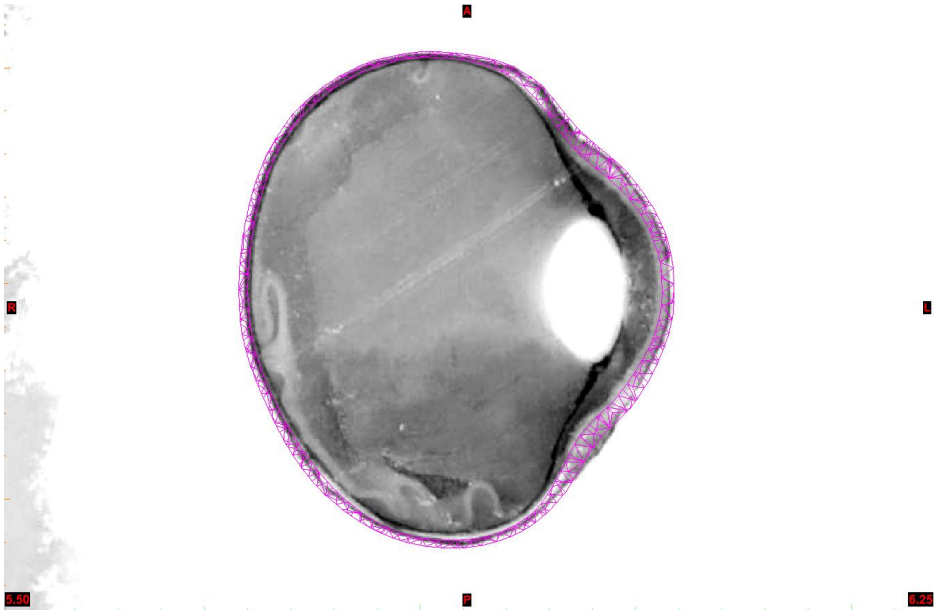

Figure 29. Fit between model 3 (pink lines) and its corresponding section photograph.

A summary of all three 3D models is shown in Table 4. Note that the Mimics model 3 and the revolved model 2 were both constructed from chick eye # 2. The revolved model 2 was created to compare it to revolved model 1 so that the effect of overall eye geometry could be studied.

Table 4: 3D models summary

	Chick eye #	**Software**	**Model type**
Model 1	1	SolidWorks®	3D revolved surface
Model 2	2	SolidWorks®	3D revolved surface
Model 3	2	Mimics	3D solid volume

4.6 Discussion

Three-dimensional reconstructions of chick eyes were presented. The revolved models do not reproduce the thickness of the corneo-scleral shell, but they are a good approximation of the overall eye geometry and can be used for finite element analysis. The complete model obtained with Mimics was reasonably good even though small geometric inaccuracies with respect to the section photographs were introduced. Manual segmentation is subjective and error in identifying the boundary of the corneo-scleral shell was present. Staining the remaining block or shining fluorescent light on it could help increase the contrast between the corneo-scleral shell and the rest of the eye so that an automatic segmentation scheme could be used. Automatic segmentation would render the process objective and would significantly speed up the method. Also, the smoothing process in Mimics caused geometric error between the 3D model and the boundary of the corneo-scleral shell as seen on the photograph. One way to minimize this error would be to improve the alignment process and decrease the distance between the slices so that less smoothing is required. Also, it was difficult to reconstruct the extremities of the chick eye because at these locations, the microtome slices through the sclera only and a higher resolution is required to capture the thickness of the sclera. Instead of using a constant distance of 250 μm between photographs for the entire eye, a smaller distance should be used near the ends of the chick eye. For instance, after the top surface of the chick eye is identified, the slice thickness could be set to 20 μm and a photograph of the remaining block could be taken every slice until the vitreous can be identified. Then, the slice thickness could be increased until the other end of the chick eye is reached.

Even if the 3D model fit the section photographs perfectly, there is no guarantee that the reconstructed model would accurately represent the real eye. The cornea has a tendency to absorb water, swell, and become opaque (Ethier et al., 2004). McCarey and Kaufman (1974) stored post-

mortem rabbit corneas in culture medium at 4^{o}C for several days and found that the thickness of the cornea increased gradually. The swelling of the cornea was not assessed in the present study, but the fact that the cornea of the chick eyes was much thicker than the sclera might indicate that swelling occurred. Also, sectioning the eye with a microtome presents a few drawbacks. First, the microtome used in this experiment was relatively old and it is possible that there was variation in slice thickness that would affect the accuracy of the 3D reconstruction. Using better and newer equipment might help improve the results. Second, the geometric accuracy of the 3D model can be compromised due to deformation of the eye that can occur during painting, mounting, freezing, and sectioning. Care was taken to ensure minimal geometrical distortion during handling. During freezing, the eye may deform and this could affect the accuracy of the model. With our current data, it was not possible to quantify the error introduced by the freezing process, but the deformations were assumed to be uniform such that the overall geometry of the eye was preserved. To quantify the accuracy of the 3D model, a laser scanner could be used to model the external surface of the eye before freezing and sectioning (Hashemi et al., 2005). Then, the model obtained with the laser scanner could be compared with the reconstructed model.

Chapter 5: Finite element analysis

5.1 Introduction

The 3D models created in chapter 4 were imported into the Abaqus/CAE® software for finite element analysis. Isotropic, homogeneous, and nearly-incompressible material properties were used to model the chick eye. Both linear elastic and exponentially stiffening material properties were used on all three models and different values were assigned to the cornea and the sclera to reflect the difference in stiffness. Note that viscoelastic effects such as creep, stress relaxation, and hysteresis were not included in the model. The pre-processing, that is, the assignment of material properties, load and boundary conditions, and meshing, for the revolved models and the Mimics model differ so they were treated separately.

5.2 Revolved models

Before any pre-processing could be done, the revolved 3D models had to be exported from SolidWorks® to Abaqus/CAE®. Many different file formats such as STEP, SAT, or IGES can be imported into Abaqus, but for this project, the IGES file format was found to work better. IGES (Initial Graphics Exchange Specification) is a neutral file format allowing the exchange of computer models between different CAD softwares. So, the native SolidWorks® .sldprt file format was converted into IGES file format using the save as function in SolidWorks®.

5.2.1 Linear elastic material properties

Once the IGES model of the chick eye was imported into Abaqus/CAE®, material properties for the cornea and the sclera were created. The material properties were isotropic, homogeneous, and nearly incompressible (ν=0.47). The value of 0.47 for Poisson's ratio was taken from a study on human scleras (Uchio et al., 1999). At first, linear elastic material properties were chosen for the model.

Linear elastic materials have a linear stress/strain relation as follow:

$$\sigma = E\varepsilon \qquad \text{(q)}$$

where σ is the stress, ε is the strain, and E is Young's modulus or simply elastic modulus of the material (Craig Jr., 2000). In a review paper, Ethier et al. (2004) reported that the Young's modulus of the corneo-scleral shell in humans was in the range of 5-13 MPa. More recently, biaxial testing on strips of human scleras showed that their stiffness was around 2.9 MPa with a range of 0.5-7.5 MPa (Eilaghi et al., 2010b). Also, uniaxial tensile testing of strips of cornea and sclera in the guinea pig revealed that the Young's modulus of the sclera was in the range of 2.09-2.56 MPa while the cornea was around 1.73-1.92 MPa (Wang et al., 2008b). In all the studies, the sclera was consistently stiffer than the cornea. No study on the material properties of the sclera or cornea in the chick could be found in the literature. So, a process of trial and error with an initial guess of 3 MPa for both the cornea and the sclera was used to find the material properties that would make the model best fit the strain versus IOP experimental data found in Chapter 2. Model 1 was used for the trial and error process and the Young's modulus for the cornea was found to be 2 MPa while the sclera was set to 5 MPa. The chick sclera is composed of a fibrous and a cartilaginous layer that would make the sclera stiffer so a larger value of Young's modulus was chosen for the sclera. The same values of Young's moduli were used for model 2 and model 3 so that the effect of geometry could be studied.

5.2.2 Exponentially stiffening material properties

Biological tissues do not exhibit a linear stress/strain behavior and a different material model must be used. Recall from section 1.4.2 that the stress/strain relation of collagen is an exponential function and can be modeled using equation (e):

$$\sigma = A[e^{\alpha\varepsilon} - 1] \qquad \text{(e)}$$

where σ is the stress, ε is the strain and A and α are material constants (Ethier et al., 2004). The sclera and the cornea contain a lot of collagen and can be modeled using equation (e). Also, these tissues stiffen exponentially as they strain and this stiffening can be seen in the pressure-volume experiment with normal eyes (Figure 12) in Chapter 2. So, equation (e) was used to generate a stress/strain table in Microsoft Excel (Microsoft Corp., Redmond, USA) for the cornea and the sclera of the chick eye. The data from the table were then imported into Abaqus/CAE® and fitted with a Marlow hyperelastic material model. For more information on the Marlow hyperelastic model, refer to the Abaqus/CAE® User's Manual (Dassault Système Simulia Corp., 2009b) and to the Abaqus Analysis User's Manual (Dassault Système Simulia Corp., 2009a). The fit between the Marlow hyperelastic model and the exponentially stiffening constitutive equation (e) was almost perfect (Figure 30). Note that equation (e) could not be entered directly into Abaqus/CAE® without extensive programming and the Marlow hyperelastic model was used to replicate the behavior of an exponentially stiffening material. The details of the Marlow hyperelastic model are not important here as long as the model fits equation (e). Also, the simulation with the Marlow hyperelastic model was stable for all strains and this is important for modeling structures undergoing large deformations like the chick eye under high IOP. Hyperelastic models are used to model the non-linear stress/strain behavior of different materials such as rubber and biological tissues. There are different hyperelastic material models, but the Marlow model was the best for approximating equation (e). Model 1 was used and the exponentially stiffening material properties (A and α values) for both the cornea and the sclera were varied until the strain in the model agreed with the experimental strain found in Chapter 2. The trial and error process was more tricky in this case because the two parameter A and α could be varied simultaneously leading to a greater number of possibilities. The values of A=40.49 mmHg and α=35.47 obtained by fitting the strain-pressure curve in Chapter 2 were used as a first guess, but this resulted in a chick eye that was a little bit too soft. Also, the A and α values were chosen in such a way that their stress/strain curve was

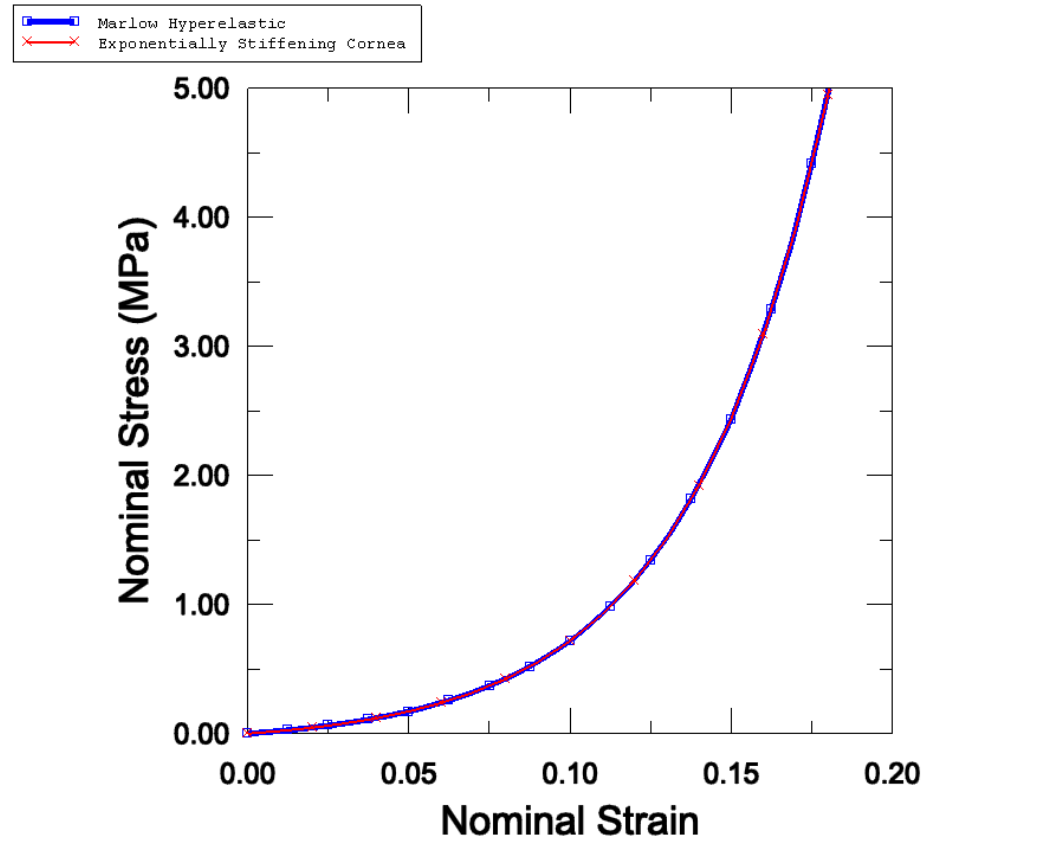

Figure 30. Exponentially stiffening cornea fitted with the Marlow hyperelastic model.

close to the linear curves (E_{cornea}= 2MPa, E_{sclera}=5 MPa) in the low strain region because the linear elastic model was good at approximating the experimental data at low values of strain. The trial and error process led to values of A=2400 mmHg and α=20 for the sclera and A=600 mmHg and α=23 for the cornea of the chick eye. Figure 31 shows the stress/strain curves for the exponentially stiffening materials and the linear elastic materials used for the cornea and the sclera. The same material properties were used for model 1, model 2, and model 3 so that the effect of eye geometry could be analyzed.

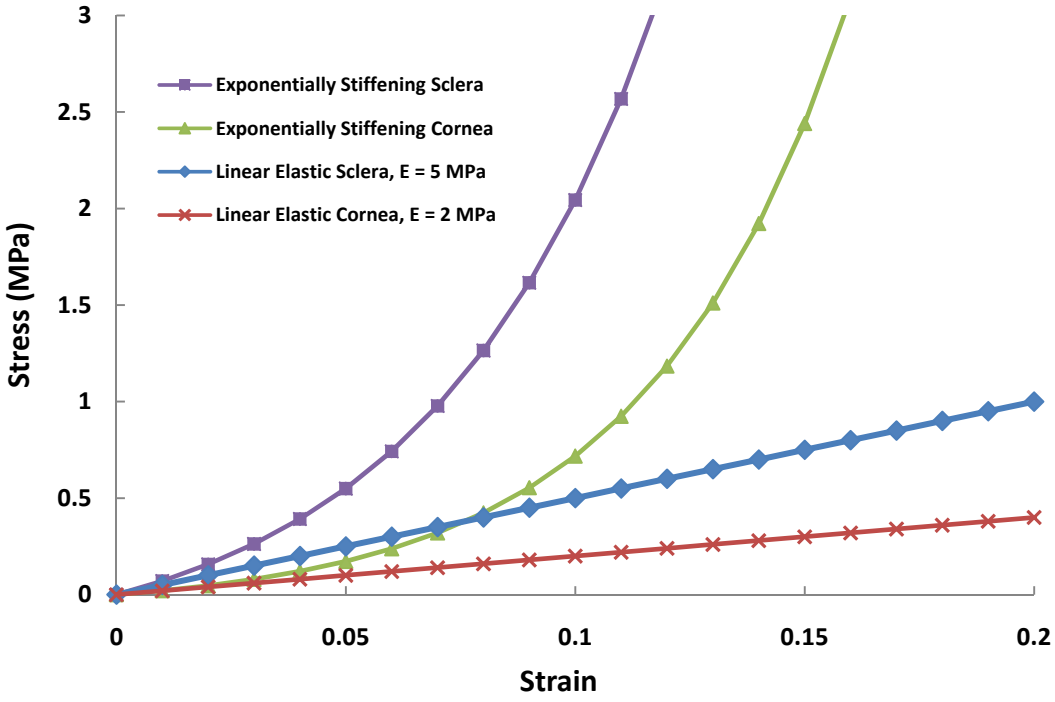

Figure 31. Material properties for the cornea and the sclera.

5.2.3 Section properties

The next step in building the finite element model was to create the section properties. Homogeneous shell sections with a thickness of 0.3 mm and 0.15 mm for the cornea and the sclera respectively were chosen for the revolved models. Measurements on frozen 7-day old chick eye sections showed that the average thickness of the cornea and the sclera were 0.3 mm and 0.15 mm respectively. The appropriate material properties were assigned to each section. Then, a partition, located at a distance of 1.8 mm from the vertex of the cornea, was created using the partition tool in Abaqus/CAE® to separate the cornea and the sclera on the 3D revolved model. This allowed different sections and different material properties to be assigned to the cornea and the sclera.

5.2.4 Geometric nonlinearity

The chick eye model subjected to high IOP underwent large deformations and suffered from geometric nonlinearity. Geometric nonlinearity in a finite element analysis occurs when large deformations cause the geometry of a structure to change so much that the overall stiffness of the structure in a given direction is affected. Material properties and geometry affects the overall stiffness of a structure in a given direction. Abaqus/CAE® has a nonlinear geometric function allowing simulations with large deformations and geometric nonlinearity to be simulated. With the nonlinear geometry function turned OFF, the revolved model of a chick eye initially contracted in the equatorial direction, kept contracting, and never expanded as IOP increased. Also, large deformations were seen in the axial direction. This is because the stiffness matrix was computed only once at the beginning of the simulation and the stiffness of the model in the axial and equatorial directions remained constant throughout the simulation. With the nonlinear geometry function turned ON, Abaqus/CAE® breaks the total load down into small load increments and computes the stiffness matrix after every increment based on the updated configuration of the model. This allows the stiffness of the model to change based on the new deformed geometry. This way, the model was capable of mimicking the deformations observed in a real chick eye. Note that the use of a hyperelastic material model in Abaqus/CAE® forces the user to use the nonlinear geometry function.

5.2.5 Load and boundary conditions

A uniform pressure was applied on the interior surface of the revolved chick eye model to simulate the effect of IOP. Simulations were performed with different pressure values to replicate the experimental data. Boundary conditions were applied to the chick eye model to avoid rigid body motion and to allow deformation in any direction. A point on the axis of symmetry at the posterior vertex of the chick eye model was constrained in all directions. This prevented rigid body motion but rigid body rotation was still present. The revolved 3D model is symmetric and, in theory, the uniform

pressure should not produce any rigid body rotation. However, inaccuracies in the finite element method led to forces and moments that caused the eye to rotate as a rigid body about the fixed node. So, a point on the symmetry axis at the vertex of the cornea was constrained in the y and z directions and was allowed to move in the x direction. This prevented rigid body rotation. The same boundary conditions were applied in a generic finite element model of a human eye (Eilaghi et al., 2010a). Also, the revolved model was cut in half to take advantage of the symmetry and reduce the number of elements used in the model. Symmetry boundary conditions (YSYMM) were used on the edge of the cut.

5.2.6 Meshing

The revolved models were uniformly meshed with 4-node linear shell elements with reduced integration (S4R). The S4R elements are robust, used in a wide range of applications, and suitable for large deformation simulations (Hibbitt et al., 1996). Also, S4R elements were used because the fully integrated S4 elements cannot be used with hyperelastic material models. Note that the chick eye and the IOP could have been modeled using axisymmetric shell elements (SAX1) and fewer elements would have been needed to achieve the same result accuracy. However, if the model were used with non axisymmetric loading such as the forces generated by the extraocular muscles, then the 3D geometry of the chick eye would be required.

A convergence study for model 1 was conducted to ensure that enough elements were used for the simulation to converge (Table 5). The intraocular pressure was kept constant at 80 mmHg and simulations were run with more and more elements. The maximum von Mises stress, the axial length, and the equatorial diameter were recorded for each simulation. The final model had 8756 elements which gave good results and a reasonable computational time. A similar mesh refinement study was conducted for model 2 and a total of 14440 elements were used.

Table 5. Convergence study for model 1.

# of elements	Max. von Mises Stress (MPa)	Axial length (mm)	Equatorial diameter (mm)	CPU time (sec)
516	0.4079	9.71442	11.9364	4
736	0.3891	9.72703	11.9311	7
1160	0.4158	9.74097	11.9251	9
2128	0.4763	9.75491	11.9170	14
4744	0.5312	9.76781	11.9152	28
8756	0.5486	9.77300	11.9138	53
19692	0.5676	9.77708	11.9124	155

5.2.7 Simulations

Simulations were performed with IOP of 5, 30, 55, 80, 105, 150, 195, 240,…, 775 mmHg to replicate the pressure-volume experiment with normal eyes. For each IOP value, the strains in the axial and equatorial directions were measured directly on the model.

5.3 Mimics model

The pre-processing for the Mimics model (model 3) was a little bit more complex and involved the use of different softwares, but once the model was imported into Abaqus/CAE®, the modeling was similar to the revolved models.

5.3.1 Meshing and partitioning in Mimics

As explained in section 4.5.2, the masks from the segmentation process were used to produce a 3D object of the chick eye. The 3D object was made of 2 surfaces; the inner and outer boundaries of the corneo-scleral shell. Then, the Mimics Remesher was used to create a triangular surface mesh on both surfaces. The smoothed 3D object still contained too much detail so the first step was to smooth the model further. Then, the Auto Remesh function was used to remesh the surfaces and improve the quality of the triangles. Very thin triangles with a low height/base ratio are not good for finite element

analysis. So, the new surface mesh contained triangles with a normalized height/base (N) ratio of 0.4 or higher which is the maximum triangle quality that Mimics can achieve. The height/base (N) ratio is normalized using $\sin 60^{o}$ so that the value for an equilateral triangle is 1. With the Auto Remesh function, it was also possible to decrease the element size so that more elements were included in the model. The element size was decreased as much as possible until the Mimics Remesher could no longer execute the task and crashed. To perform a finite element analysis with the 3D chick eye model, a volume mesh was needed. So, the surface mesh was used to build a volume mesh of tetrahedral elements using the Create Volume Mesh function. A total of 19024 four-node tetrahedral elements (C3D4) were created. Then, the surface mesh was no longer needed and deleted.

In order to apply different material properties for the cornea and the sclera, the 3D volume mesh had to be partitioned. This was done in Mimics by segmenting the cornea in all the photographs using the same segmentation tool presented in Chapter 4. A red mask of the cornea was created and used to assign different material properties. The tetrahedral elements belonging to the red mask were assigned material properties of the cornea while the rest of the model used the material properties of the sclera. There is a problem with partitioning a volume mesh; because the element size is finite, the junction between the cornea and the sclera is jagged (Figure 32). This was not a problem with the revolved models because the eye was partitioned in Abaqus before the mesh was created. After the material properties were assigned, the export function in Mimics was used to export the 3D volume mesh to the Abaqus/CAE® input file format (.inp).

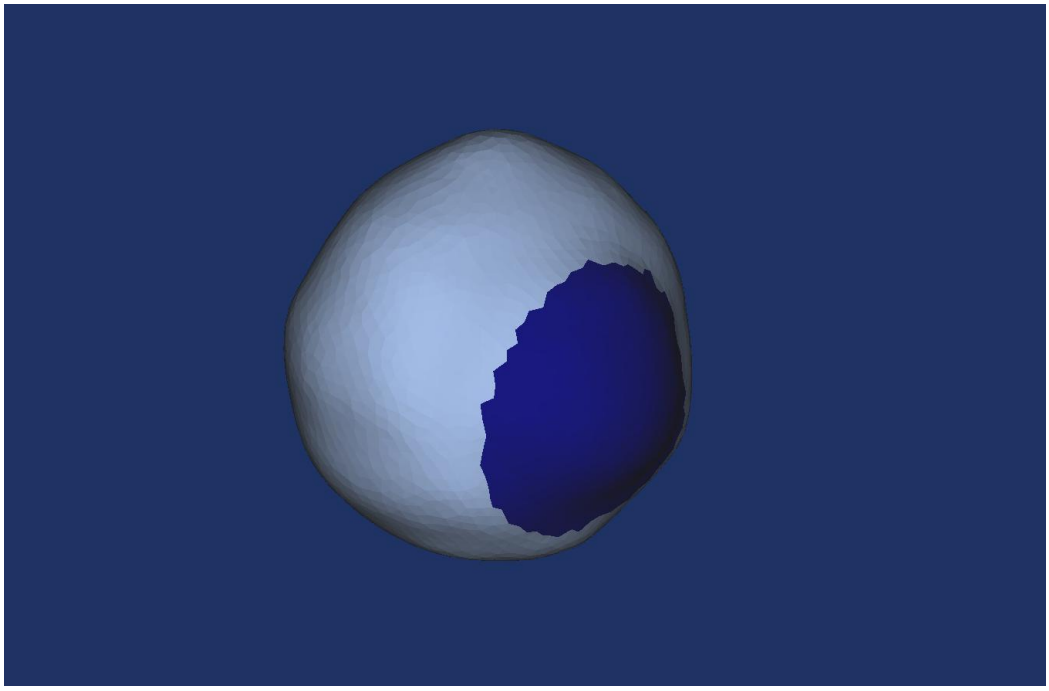

Figure 32. Material assignment for the cornea and the sclera in Mimics

5.3.2 Load and boundary conditions

The input file was imported into Abaqus/CAE®. At this point, the model was meshed and had material definition for the cornea and the sclera, but loads and boundary conditions were still required to complete the pre-processing. However, no modifications could be done to the volume mesh in Abaqus/CAE® because it was created in Mimics. It was not possible to cut the mesh or hide a few elements so that the IOP could be applied on the internal surface of the chick eye. So, the input file was imported into the Hypermesh (Altair Engineering Inc., Troy, USA) software to apply the IOP on the internal surface of the eye. Hypermesh is a pre-processing software used to mesh models from CAD softwares and export them to different finite element analysis packages. In Hypermesh, it was possible to hide the cornea and apply the IOP on each element inside the chick eye (Figure 33). Then, another input file was created and imported into Abaqus/CAE® again. The same boundary conditions

as for the revolved models were applied. That is, a node at the back of the eye was constrained in all directions and a node at the vertex of the cornea was constrained in y and z directions but allowed to move in the x direction. It was more difficult to pick a node at the center of the front and back surface because the Mimics model is not symmetric.

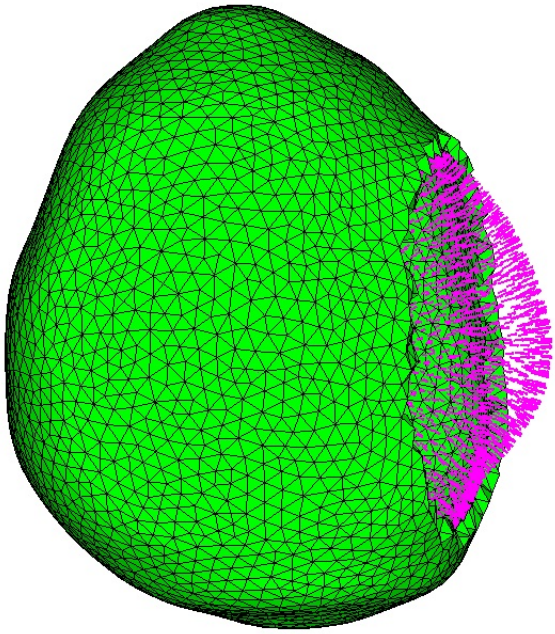

Figure 33. Pressure (pink arrows) applied inside the chick eye in Hypermesh. The cornea is hidden.

5.3.3 Simulations

The same linear and exponentially stiffening material properties used for the revolved models were used for the Mimics model. The material properties and the loads could be modified directly within Abaqus/CAE® and no more imports or exports were required. The same IOP values were used to perform the simulations with the Mimics model.

5.4 Results

A process of trial and error was used to find material properties for the cornea and the sclera using the finite element method. Figure 34 shows the exponentially stiffening stress/strain curves constructed using the values of A and α obtained with the finite element method and the A and α from fitting the pressure-volume and the strain-pressure experimental curves from Chapter 2. The values obtained by fitting the pressure-volume curve are off, but the values from fitting the strain-pressure are close to the ones obtained by the finite element method. Note that equation (e) was used to plot the stress versus strain curves.

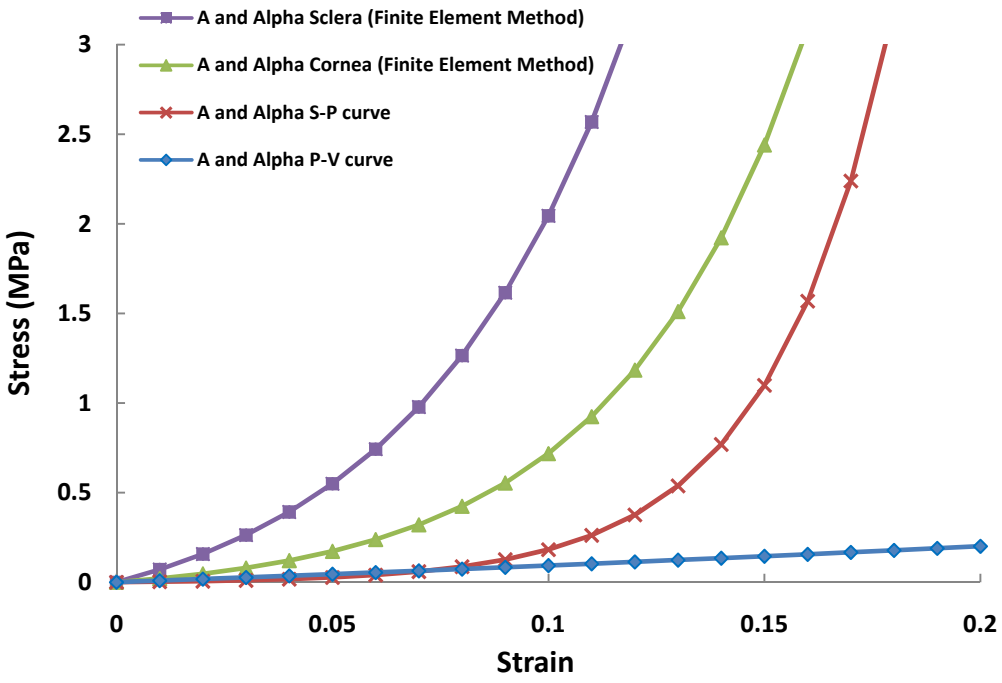

Figure 34. Comparison of A and α values obtained with the finite element method and by fitting the experimental pressure-volume and strain-pressure curves.

5.4.1 Linear elastic finite element models

The strain as a function of IOP curves for all three finite element models with linear elastic material properties are shown in Figure 35 along with the experimental strain-pressure data from Chapter 2. All three models follow the same trend, that is, they elongate more in the axial direction compared with the horizontal equatorial direction. This trend is also in agreement with the experimental data. The revolved model 1 approximates the experimental data better than the other two models. Model 1 initially contracts in the horizontal equatorial direction and up to an IOP of 105 mmHg it remains within the error of the experiment. In the axial direction, model 1 is the closest to the experimental

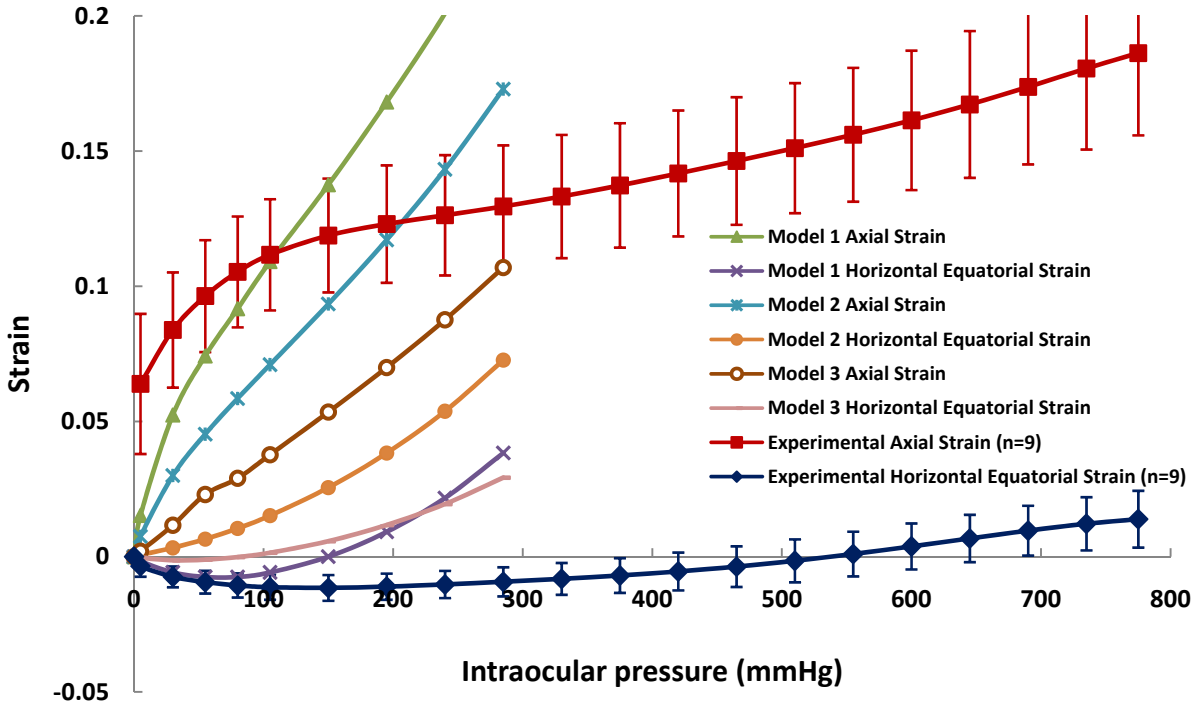

Figure 35. Linear elastic finite element models and experimental data for normal chick eyes.

data. Model 2 and model 3 do not expand as much in the axial direction. Model 2 does not even contract in the horizontal equatorial direction while model 3 barely contracts. At IOPs beyond 200 mmHg, all three linear elastic finite element models diverge from the experimental data.

5.4.2 Exponentially stiffening finite element models

A comparison of the undeformed geometry (IOP=0 mmHg) and the deformed geometry (IOP=80 mmHg) for the exponentially stiffening finite element models and a real 7-day old chick eye is shown in Figure 36. By visual inspection, the undeformed geometry of model 1 is more similar to the undeformed geometry of a real chick eye compared with model 2 and model 3. Remember that model 2 and model 3 were built from the same chick eye. Model 2 is a revolved model from the midsection photograph of eye # 2 and model 3 is the 3D reconstruction of the entire eye # 2 with proper corneo-scleral thickness all around the eye. Model 2 was constructed to compare with model 1 which is also a revolved model. Also, the deformed geometry of model 1 is closer to the deformed geometry of a real chick eye than model 2 and model 3.

The bottom colored images in Figure 36 are the contour plots of the deformed models showing the von Mises stresses. The color red on the models indicates a region of high stress while the blue is a zone of low stress. A zone of high stress can be seen on model 1 and 2 at the corneo-scleral junction. In this region, there is an inflection point where the curvature of the corneo-scleral shell is equal to zero such that the stress in the shell at that location is high. A basic knowledge of membrane shell theory is required to fully understand the latter explanation. What is important from membrane theory is that the stress in the membrane is proportional to the curvature of the membrane. A region of large curvature indicates low stress while low curvature indicates high stress. Model 3 does not have a zone of high stress near the limbus and it is probably due to the greater thickness of the corneo-scleral shell in this region. Also, all three models show that the region of lowest stress is the cornea, which is a

region of high curvature and, in the case of the chick eye, increased thickness. This means that the cornea is the part of the chick eye less susceptible to deform due to variations in IOP. From an optics point of view, this is an advantage because the cornea is responsible for roughly 70% of the total refractive power of the eye and it is important that the cornea remains stable under varying IOP for optimum vision.

The finite element models with exponentially stiffening material properties are better at approximating the experimental data than the linear elastic models (Figure 37). The strain in the horizontal equatorial direction for model 1 is within the error of the experiment for all IOP values. The strain in the axial direction for model 1 is close but not within the error of the experiment for all pressures. Model 1 is still better at approximating the experimental data than model 2 and model 3. Also, model 2 and model 3 do not expand as much in the axial direction and do not contract in the horizontal equatorial direction. Around an IOP of 450 mmHg, the experimental axial strain curve starts to curve upward indicating a softening of the eye. This is probably due to a breakage of collagen fibers within the ocular tissues. The models with exponentially stiffening material properties keep stiffening as pressure increases and are not able to capture the softening of the tissues at higher pressures.

Now, remember from Chapter 2 that the experimental strain was calculated using the geometry of a normal chick eye when the intraocular pressure was equal to 0 mmHg. In other words, a deflated chick eye was used to calculate the strain and this caused a jump in experimental axial strain (Figure 37). If the geometry of chick eyes at a normal IOP of 20 mmHg were used to calculate the axial

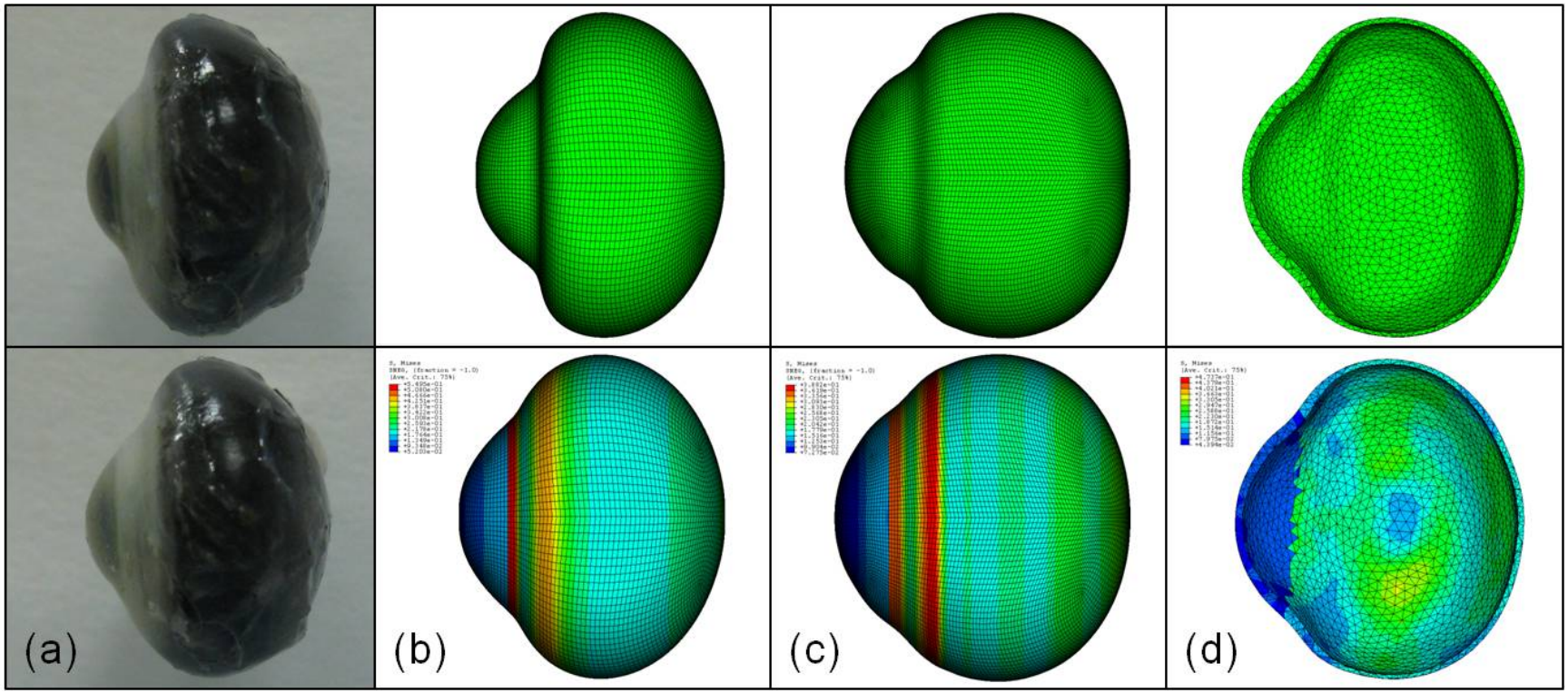

Figure 36. TOP: Undeformed (IOP=0 mmHg) and BOTTOM: deformed (IOP=80 mmHg) geometry for (a) real chick eye, (b) model 1, (c) model 2, and (d) model 3.

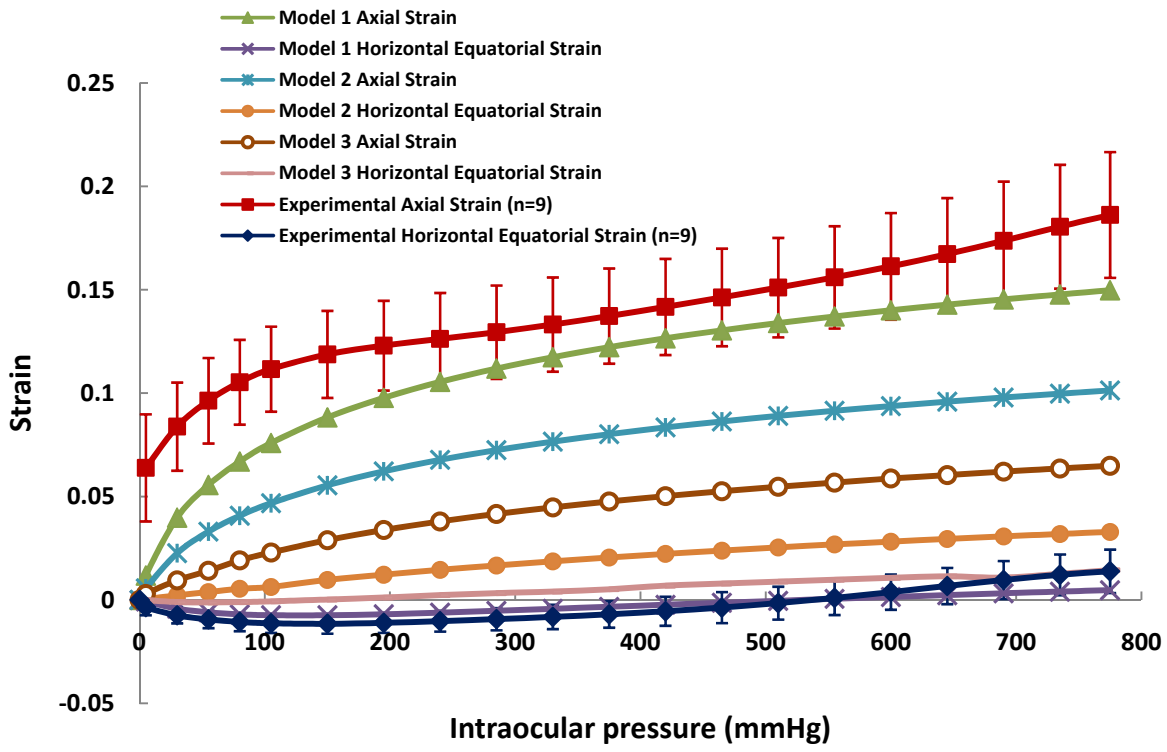

Figure 37. Exponentially stiffening finite element models and experimental data for normal chick eyes.

strain, the entire curve would move down. However, the chick eyes did not all reach a value of 20 mmHg during the pressure-volume experiment and this exact value could not be used to calculate the strain. Many chick eyes reached an IOP of 10, 12, or 15 mmHg, so the geometry of the chicks at one of these pressure values was used to recalculate the strain. The new results are shown in Figure 38. Notice that all experimental strains and finite element strains are now equal to zero around an IOP of 15 mmHg. Also, the experimental axial strain did move down and model 2 and model 3 now approximate the axial experimental data better than model 1. In the horizontal equatorial direction,

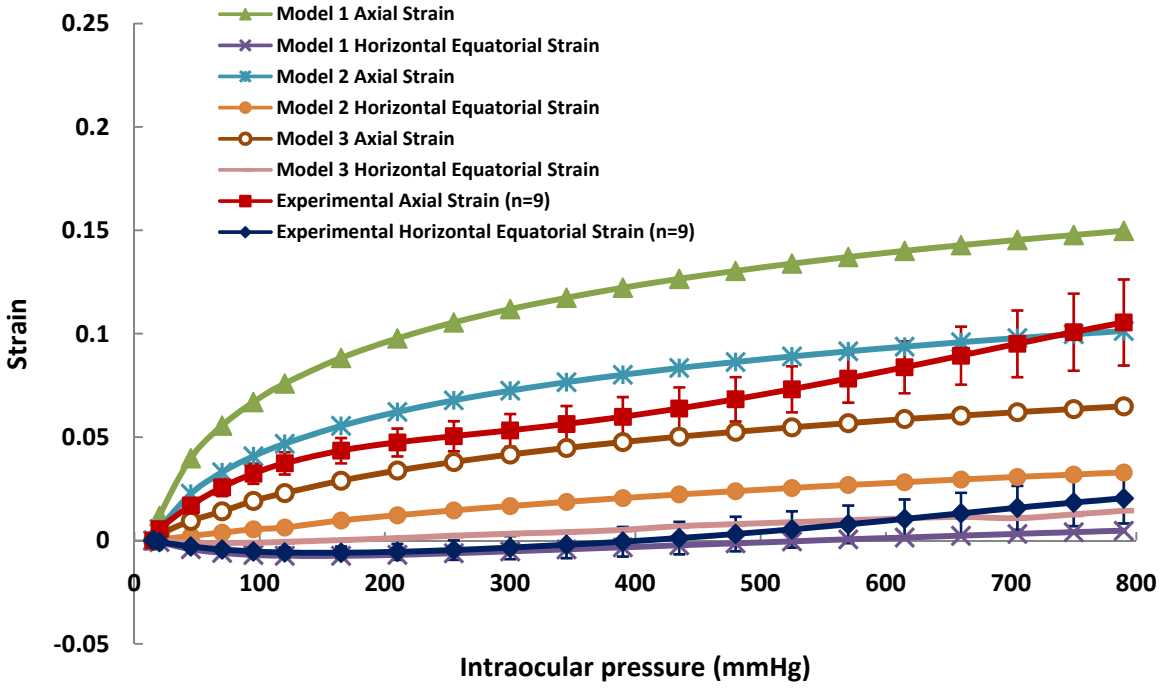

Figure 38: Exponentially stiffening finite element models and experimental strain based on normal chick eye geometries at IOPs of 10, 12, and 15 mmHg.

model 1 still approximates the experimental data better than the other two models and is within the error of the experiment up to an IOP of 600 mmHg. Model 3 does not contract as much in the horizontal equatorial direction compared with model 1, but model 3 is close to the experimental data in the horizontal equatorial direction. Overall, model 3 is the best model to approximate both the axial and horizontal equatorial strains when the reference geometry is taken at an IOP of about 15 mmHg. Note that there is a lot of variation in strain between the models even though all three models used the same material properties. This indicates that the geometry of the chick eye is an important factor in dictating its deformation under the influence of IOP.

5.5 Discussion

The results showed that non-linear material properties are very important in order to model a real chick eye appropriately, especially at higher IOP values. The linear material properties give a reasonable approximation at low IOPs, but diverge quickly at higher IOPs because they do not get stiffer with increasing strain. Also, isotropic and homogeneous material properties where used for all models and the results were close to the experimental data. The isotropic assumption was not bad considering that Eilaghi et al. (2010b) found that the sclera was nearly-isotropic away from the optic nerve canal or the extraocular muscle attachment sites. They also found that the sclera was heterogeneous, but the models were reasonably good even though heterogeneity of the sclera was not included. The fact that the models used isotropic and homogeneous material properties demonstrates that the contraction in the horizontal equatorial directions was not due to the anisotropy or heterogeneity of the chick eye. This strongly suggests that the overall oblate geometry of the chick eye causes the eye to expand more in the axial direction and to initially contract in the horizontal equatorial direction as pressure increases. This confirms the results obtained by Phillips and McBrien (1995) with their finite element model of a tree shrew eye.

There were differences in strain between the three finite element models even though the same material properties were used. For instance, the difference or gap between the axial strain curve and the horizontal equatorial strain curve for model 1 was larger compared with model 2 and model 3. The only difference between model 1 and model 2 was their overall geometry which shows that the geometry of model 1 was more prone to axial deformation than model 2. The Mimics model (model 3) appeared to be stiffer than the other two models. In other words, the gap between the axial strain curve and the horizontal equatorial strain curve for model 3 was less pronounced. This can be due to the fact that the overall geometry of eye # 2 used to construct model 3 was more spherical than eye #

1. The axial and equatorial strains for a spherical pressure vessel with constant thickness are identical because the expansion is uniform in all direction. So, a smaller gap between the axial and equatorial strain curves of model 3 indicates that eye # 2 behaved more like a sphere. Moreover, the reconstructed thickness of the posterior sclera of model 3 was a bit too thick (Figure 29) and this may have contributed to the stiffness of the eye. The cornea might have been too thick also due to corneal swelling. Also, linear tetrahedral elements (C3D4) are known to be too stiff and more elements should be used to model the chick eye (Hibbitt et al., 1996). Quadratic elements (C3D10) could also be used to improve the accuracy of the simulation. However, model 2, which is a shell model constructed from eye # 2, also appeared too stiff indicating that the more spherical geometry of eye # 2 was responsible for its deformation. The complete 3D reconstruction in Mimics should be done again with a different chick eye to better understand the effect of corneo-scleral shell thickness on eye deformation under increased IOP.

The finite element models with exponentially stiffening material properties followed the same pattern as the experimental data. When the reference geometry for calculating the experimental strain was taken when the IOP was 0 mmHg, model 1 was better at approximating the experimental data. However, the experimental axial strain calculated in this manner is overinflated. The finite element models were constructed based on the geometry of a chick eye at a normal IOP, not a deflated chick eye. Thus, the strain for the finite element models was calculated using the geometry of a chick eye at a normal IOP. So, the finite element models strains should not be compared to the original experimental strain calculation. When the reference geometry at 10, 12, and 15 mmHg was used for the calculation, the experimental strain curve in the axial direction moved down and model 3 was the better approximation, but still appeared too stiff. Now, it is difficult to say if model 3 appeared too stiff for the reasons explained earlier or because of the overall geometry of the eye used for

reconstruction. It would be interesting to redo the complete 3D reconstruction in Mimics with a different chick eye to better understanding the effect of eye geometry and corneo-scleral shell thickness on eye deformation under increased IOP. Also, because the eye geometry affects the strain, it is difficult to have confidence in the material properties extracted using the finite element model. The material properties extracted are probably in the right range, but tension testing should be done on strips of chick sclera and cornea to confirm the results.

There were a few modeling problems that might have affected the accuracy of the finite element models. First, only the corneo-scleral shell was modeled and the effect of the lens, the scleral ossicles, the choroid, the retina, and other ocular tissues was not included. These eye components would add rigidity to the chick eye such that the material properties for the cornea and the sclera obtained using the finite element method are probably stiffer than they really are. Also, a uniform pressure was applied to the internal surface of the eye in all models and this might not be the case in a real eye for a pressure gradient has been shown to exist across the lens during accommodation (Young, 1981). In addition, the geometry of the models was reconstructed from an eye having an IOP of about 20 mmHg. The normal IOP of 20 mmHg means that the ocular tissues of the chick eye are normally pre-stressed. However, in the finite element models, the reconstructed geometry corresponded to an IOP of 0 mmHg. It is difficult to include the pre-stressed condition in the finite element models without knowing the stress free geometry. One possibility would be to puncture the chick eye before freezing it so that the deflated geometry of the chick eye is obtained. This does not guarantee that the deflated geometry of the chick eye is stress free. For instance, when arteries are cut in the longitudinal direction, they spring open even though there is no blood in them (Humphrey, 2008). This shows that residual stresses are present in the arterial walls and the same could happen with ocular tissues.

Including the pre-stressed condition in the models would require using slightly softer material properties because of the stiffening effect of tissues with strain.

5.6 Conclusion

The geometry of the finite element models had a large effect on the axial and horizontal equatorial strain curves. The finite element models with linear elastic material properties gave a reasonable approximation at low IOP values. At higher IOPs, exponentially stiffening material properties were required to properly model the chick eye. Due to the variation in eye shape, it was difficult to extract the material properties of the corneo-scleral shell with precision. Tension testing with strips of chick sclera and cornea should be performed to gain more knowledge about the material properties of the chick sclera and cornea.

Chapter 6: Conclusions and future work

6.1 Conclusions

Intraocular pressure increments cause axial elongation and horizontal equatorial contraction followed by expansion in normal chick eyes. Normal chick eyes prefer to deform in the axial direction as opposed to the horizontal equatorial direction. The strains obtained using the finite element method are similar to the experimental data and this suggests that the oblate geometry of chick eyes is responsible for their deformation. At high IOP, normal chick eyes enlarge in both directions, but are larger in the axial direction than in the horizontal equatorial direction. The maximum axial elongation of normal chick eyes would produce 25 dioptres of transient myopia under mechanical stretch alone. The natural tendency of chick eyes is to elongate under increasing IOP and this suggests that IOP could play a role in myopia onset and progression. However, it is unlikely that IOP is the only factor and the experiment with myopic eyes showed that growth and remodelling are likely to be involved in experimental myopia. The overall geometry of myopic eyes, which is more spherical than normal eyes, makes them less prone to axial elongation and equatorial contraction. The method for 3D reconstruction of the corneo-scleral shell of a chick eye presented in Chapter 4, although not perfect, does not require expensive equipment such as MRI and can be implemented in any lab. Exponentially stiffening material properties are important to properly model the deformation of a chick eye subjected to high IOP. The finite element models showed that the geometry of the chick eye greatly affects its deformation under increased IOP.

6.2 Future work

As noted in the previous chapters, the pressure-volume experiment and the 3D modeling of the chick eye could be improved in many ways. First, at the beginning of the pressure-volume experiment, the IOP of the chick eye should be adjusted to a normal pressure of 20 mmHg and the eye dimensions at that pressure should be taken as the reference dimensions for the calculation of strain. Also, saline should be injected into the chick eyes instead of water. More rigid medical tubing should be used for the syringe pump apparatus to minimize the effect of tube expansion on the pressure-volume curves of chick eyes. It would be interesting to use a different chick eye and redo the entire 3D reconstruction process and finite element analysis and compare the new results with model 3. Also, the slice thickness for the microtome experiment could be set to 50 μm so that more details are included in the model and less smoothing would be required in Mimics.

More testing could be done to gain more knowledge about the material properties of the corneo-scleral shell of chick eyes. Biaxial testing of corneal and scleral strips from chick eyes could be performed to obtain anisotropy and heterogeneity data. The non linear material properties obtained from the biaxial test could be compared to the material properties obtained with the FEM trial and error process. Also, the elastic limit of chick eyes could be determined to gain knowledge about the level of strain required for permanent myopia to occur. For instance, the IOP of a post-mortem chick eye could be increased from 20 mmHg to 40 mmHg and then brought back down to 20 mmHg again. The axial length and the equatorial dimension would be measured initially at 20 mmHg, then at 40 mmHg, and again at 20 mmHg. If there is permanent deformation, then the elastic limit of the eye has been surpassed. If not, then the experiment has to be repeated with a higher IOP until the elastic limit of the eye is found. Furthermore, viscoelastic properties could be included in the model. A creep test could be performed on the whole chick eye by raising the IOP to a certain value and keeping it

constant for a period of time. Then, the axial and equatorial dimension would be measured periodically. Fluid would have to be injected into the eye every now and then to maintain a constant IOP and compensate for fluid leakage. Finally, fatigue could be tested by subjecting the chick eye to cycles of high and low IOPs for a certain period of time.

The applications for a finite element model of the chick eye as it relates to myopia are numerous. The muscles forces of the extraocular muscles and the ciliary muscle could be simulated to study the effect of convergence and accommodation on eye geometry. Also, different parameters could be varied sequentially to investigate their effect on eye geometry. For instance, the length of the extraocular muscle force line could be varied to verify if the extraocular muscle attachment width has an effect on ocular stress and deformation. Also, the material properties of the cornea and the sclera could be changed to investigate their effect on eye shape. This way, the parameters that would render the eye more prone to eye elongation and myopia could be identified.

Finally, future finite element models should be constructed using human eyes. The ultimate goal is to find out what causes myopia in humans and find solutions to prevent it. The anatomical differences between chicken and human eyes make it difficult to apply the results of the chick eye model to humans. Using MRI, it would be possible to reconstruct the 3D geometry of live human eyes. A longitudinal study could be conducted where the MRI of children is taken before and after they become myopic. The initial eye geometry of those who remained emmetropic and those who became myopic could be modeled and compared. Then, the finite element method could be used to simulate close work and verify how the initial eye geometry of those who became myopic and those who remained emmetropic react and deform.

References

Adams, D.W., McBrien, N.A., 1992. Prevalence of myopia and myopic progression in a population of clinical microscopists. Optom. Vis. Sci. 69, 467-473.

Allen, P.M., O'Leary, D.J., 2006. Accommodation functions: Co-dependency and relationship to refractive error. Vision Res. 46, 491-505.

Armaly, M.F., Rubin, M.L., 1961. Accommodation and applanation tonometry. Arch. Ophthalmol. 65, 415-423.

Atchison, D.A., Jones, C.E., Schmid, K.L., Pritchard, N., Pope, J.M., Strugnell, W.E., Riley, R.A., 2004. Eye shape in emmetropia and myopia. Invest. Ophthalmol. Vis. Sci. 45, 3380-3386.

Au Eong, K.G., Tay, T.H., Lim, M.K., 1993. Education and myopia in 110 236 young Singaporean males. Singapore Med. J. 34, 489-492.

Beresford, J.A., Crewther, S.G., Kiely, P.M., Crewther, D.P., 2001. Comparison of refractive state and circumferential morphology of retina, choroid, and sclera in chick models of experimentally induced ametropia. Optom. Vis. Sci. 78, 40-49.

Bloom, R.I., Friedmann, I.B., Chuck, R.S., 2010. Increasing rates of myopia: the long view. Curr. Opin. Ophthalmol. Article in Press.

Bonomi, L., Marchini, G., Marraffa, M., Bernardi, P., De Franco, I., Perfetti, S., Varotto, A., Tenna, V., 1998. Prevalence of glaucoma and intraocular pressure distribution in a defined population. Ophthalmology. 105, 216-223.

Callister Jr., W.D., 2003. Materials Science and Engineering an Introduction, sixth ed. John Wiley & Sons, Inc., New York.

Chang, K.H., Magdum, S., Khera, S.C., Goel, V.K., 2003. An advanced approach for computer modeling and prototyping of the human tooth. Ann. Biomed. Eng. 31, 621-631.

Cheng, H.M., Singh, O.S., Kwong, K.K., Xiong, J., Woods, B.T., Brady, T.J., 1992. Shape of the myopic eye as seen with high-resolution magnetic resonance imaging. Optom. Vis. Sci. 69, 698-701.

Chimich, D., Shrive, N., Frank, C., Marchuk, L., Bray, R., 1992. Water content alters viscoelastic behavior of the normal adolescent rabbit medial collateral ligament. J. Biomech. 25, 831-837.

Conza, N., 2005. Part 3: Tissue preconditioning. Exp. Techniques. 29, 43-46.

Craig Jr., R.R., 2000. Mechanics of Materials, second ed. John Wiley & Sons, New York.

Dassault Système Simulia Corp., 2009a. Abaqus Analysis User's Manual, Providence, RI.

Dassault Système Simulia Corp., 2009b. Abaqus/CAE User's Manual, Providence, RI.

Dirani, M., Tong, L., Gazzard, G., Zhang, X., Chia, A., Young, T.L., Rose, K.A., Mitchell, P., Saw, S.M., 2009. Outdoor activity and myopia in Singapore teenage children. Br. J. Ophthalmol. 93, 997-1000.

Draeger, J., 1959. Untersuchungen über den rigiditätskoeffizienten. Doc. Ophthalmol. 13, 431-486.

Edwards, M.H., Brown, B., 1993. Intraocular pressure in a selected sample of myopic and nonmyopic Chinese children. Optom. Vis. Sci. 70, 15-17.

Edwards, M.H., Brown, B., 1996. IOP in myopic children: the relationship between increases in IOP and the development of myopia. Ophthalmic Physiol. Opt. 16, 243-246.

Eilaghi, A., Flanagan, J.G., Simmons, C.A., Ethier, C.R., 2010a. Effects of scleral stiffness properties on optic nerve head biomechanics. Ann. Biomed. Eng. 38, 1586-1592.

Eilaghi, A., Flanagan, J.G., Tertinegg, I., Simmons, C.A., Brodland, G.W., Ethier, C.R., 2010b. Biaxial mechanical testing of human sclera. J. Biomech. 43, 1696-1701.

Erismann, F., 1871. Ein Beitrag zur Entwickelungs - Geschichte der Myopie, gestützt auf die Untersuchung der Augen von 4358 Schülern und Schülerinnen. Graefes Arch. Clin. Exp. Ophthalmol. 17, 1-79.

Ethier, C.R., Johnson, M., Ruberti, J., 2004. Ocular biomechanics and biotransport. Annu. Rev. Biomed. Eng. 6, 249-273.

Fendalton Eye Clinic, 2010. Myopia. Retrieved 18 Sept. 2010. <http://lasik.co.nz>.

Ferrer, E., 2006. Trabecular meshwork as a new target for the treatment of glaucoma. Drug News Perspect. 19, 151-158.

Friberg, T.R., Lace, J.W., 1988. A comparison of the elastic properties of human choroid and sclera. Exp. Eye Res. 47, 429-436.

Friedenwald, J.S., 1937. Contribution to the theory and practice of tonometry. Am. J. Ophthalmol. 20, 985-1024.

Fung, Y.C., 1993. Biomechanics: Mechanical Properties of Living Tissues, second ed. Springer-Verlag, New York.

Gabelt, B.T., Kutuzova, G.D., Kiland, J.A., Hennes-Beann, E.A., Kim, C.B.Y., Deluca, H.F., Kaufman, P.L., 2010. Vitamin D effects on intraocular pressure in nonhuman primates. Poster session presented at: The 2010 ARVO annual meeting. May 2-6. Fort-Lauderdale, FL.

Gardiner, P.A., 1954. The relation of myopia to growth. The Lancet. 263, 476-479.

Girard, M., Suh, J.K.F., Hart, R.T., Burgoyne, C.F., Crawford Downs, J., 2007. Effects of storage time on the mechanical properties of rabbit peripapillary sclera after enucleation. Curr. Eye. Res. 32, 465-470.

Girard, M.J.A., Downs, J.C., Burgoyne, C.F., Suh, J.K.F., 2008. Experimental surface strain mapping of porcine peripapillary sclera due to elevations of intraocular pressure. J. Biomech. Eng. 130, 041017-1-041017-6.

Glasser, A., Howland, H.C., 1996. A history of studies of visual accommodation in birds. Q. Rev. Biol. 71, 475-509.

Goldschmidt, E., 1968. On the etiology of myopia. An epidemiological study. Acta. Ophthalmol. Suppl. 98, 1-172.

Gottlieb, M.D., Joshi, H.B., Nickla, D.L., 1990. Scleral changes in chicks with form-deprivation myopia. Curr. Eye Res. 9, 1157-1165.

Graebel, W.P., Van Alphen, G., 1977. The elasticity of sclera and choroid of the human eye, and its implications on scleral rigidity and accommodation. J. Biomech. Eng. 99, 203-208.

Greene, P.R., 1980. Mechanical considerations in myopia: relative effects of accommodation, convergence, intraocular pressure, and the extraocular muscles. Am. J. Optom. Phys. Opt. 57, 902-914.

Greene, P.R., 1985. Closed-form ametropic pressure-volume and ocular rigidity solutions. Am. J. Optom. Phys. Opt. 62, 870-878.

Grosvenor, T., 1987. A review and a suggested classification system for myopia on the basis of age-related prevalence and age of onset. Am. J. Optom. Physiol. Opt. 64, 545-554.

Grosvenor, T., 1989. Myopia: what can we do about it clinically? Optom. Vis. Sci. 66, 415-419.

Gwiazda, J., 2009. Treatment options for myopia. Optom. Vis. Sci. 86, 624-628.

Gwiazda, J., Thorn, F., Bauer, J., Held, R., 1993a. Emmetropization and the progression of manifest refraction in children followed from infancy to puberty. Clin. Vision Sci. 8, 337-344.

Gwiazda, J., Thorn, F., Bauer, J., Held, R., 1993b. Myopic children show insufficient accommodative response to blur. Invest. Ophthalmol. Vis. Sci. 34, 690-694.

Gwiazda, J., Thorn, F., Held, R., 2005. Accommodation, accommodative convergence, and response AC/A ratios before and at the onset of myopia in children. Optom. Vis. Sci. 82, 273-278.

Hall, S.J., 2007. The Biomechanics of Human Bone Growth and Development, in: Basic biomechanics, fifth ed. The McGraw-Hill Companies, New York, pp. 87-117.

Hashemi, J., Chandrashekar, N., Cowden, C., Slauterbeck, J., 2005. An alternative method of anthropometry of anterior cruciate ligament through 3-D digital image reconstruction. J. Biomech. 38, 551-555.

Haut, T.L., Haut, R.C., 1997. The state of tissue hydration determine the strain-rate-sensitive stiffness of human patellar tendon. J. Biomech. 30, 79-81.

Hibbard, R.R., Lyon, C.S., Shepherd, M.D., McBain, E.H., McEwen, W.K., 1970. Immediate rigidity of an eye. I. Whole, segments and strips. Exp. Eye Res. 9, 137-143.

Hibbitt, Karlsson & Sorensen, Inc., 1996. Getting Sarted with ABAQUS/Standard, Pawtucket, RI.

Howstuffworks.com, 2010. The human eye. Retrieved 29 Sept. 2010. <http://healthguide.howstuffworks.com/eye-picture.htm>.

Humphrey, J.D., 2008. Vascular adaptation and mechanical homeostasis at tissue, cellular, and sub-cellular levels. Cell Biochem. Biophys. 50, 53-78.

Hutton, D.V., 2004. Fundamentals of Finite Element Analysis, first ed. The McGraw-Hill Companies, Boston.

Inal, K., 2008. Finite Element Methods - ME559 Course Notes, University of Waterloo.

Ingber, D.E., 1997. Tensegrity: The architectural basis of cellular mechanotransduction. Annu. Rev. Physiol. 59, 575-599.

Irving, E.L., 1993. Optically induced ametropia in young chickens. PhD thesis, University of Waterloo.

Irving, E.L., Callender, M.G., Sivak, J.G., 1991. Inducing myopia, hyperopia, and astigmatism in chicks. Optom. Vis. Sci. 68, 364-368.

Irving, E.L., Sivak, J.G., Callender, M.G., 1992. Refractive plasticity of the developing chick eye. Ophthalmic Physiol. Opt. 12, 448-456.

Jensen, H., 1992. Myopia progression in young school children and intraocular pressure. Doc. Ophthalmol. 82, 249-255.

Katz, J.L., Meunier, A., 1990. A generalized method for characterizing elastic anisotropy in solid living tissues. J. Mater. Sci. Mater. Med. 1, 1-8.

Kiskis, A.A., Markowithz, S.N., Morin, J.D., 1985. Corneal diameter and axial length in congenital glaucoma. Can. J. Ophthalmol. 20, 93-97.

Ku, D.N., Greene, P.R., 1981. Scleral creep in vitro resulting from cyclic pressure pulses: applications to myopia. Optom. Vis. Sci. 58, 528-535.

Kuo, P.L., Li, P.C., Li, M.C., 2001. Elastic properties of tendon measured by two different approaches. Ultrasound Med. Biol. 27, 1275-1284.

Le Grand, Y., El Hage, S.G., 1980a. Description of the Human Eye, in: Physiological optics, first ed. Springer, Berlin, pp. 25-42.

Le Grand, Y., El Hage, S.G., 1980b. Optics of the Eye, in: Physiological optics, first ed. Springer, Berlin, pp. 57-69.

Lee, A.J., Saw, S.M., Gazzard, G., Cheng, A., Tan, D.T.H., 2004. Intraocular pressure associations with refractive error and axial length in children. Br. J. Ophthalmol. 88, 5-7.

Leydolt, C., Findl, O., Drexler, W., 2008. Effects of change in intraocular pressure on axial eye length and lens position. Eye. 22, 657-661.

Lyon, C., McEwen, W.K., Shepherd, M.D., 1970. Ocular rigidity and decay curves analyzed by two nonlinear systems. Invest. Ophthalmol. Vis. Sci. 9, 935-945.

Mallen, E.A.H., Kashyap, P., Hampson, K.M., 2006. Transient axial length change during the accommodation response in young adults. Invest. Ophthalmol. Vis. Sci. 47, 1251-1254.

Manny, R.E., Deng, L., Crossnoe, C., Gwiazda, J., 2008. IOP, myopic progression and axial length in a COMET subgroup. Optom. Vis. Sci. 85, 97-105.

Mayer, D.L., Hansen, R.M., Moore, B.D., Kim, S., Fulton, A.B., 2001. Cycloplegic refraction in healthy children aged 1 through 48 months. Arch. Ophthalmol. 119, 1625-1628.

McBrien, N.A., Adams, D.W., 1997. A longitudinal investigation of adult-onset and adult-progression of myopia in an occupational group: Refractive and biometric findings. Invest. Ophthalmol. Vis. Sci. 38, 321-333.

McBrien, N.A., Gentle, A., 2003. Role of the sclera in the development and pathological complications of myopia. Prog. Retin. Eye Res. 22, 307-338.

McBrien, N.A., Moghaddam, H.O., Reeder, A.P., 1993. Atropine reduces experimental myopia and eye enlargement via a nonaccommodative mechanism. Invest. Ophthalmol. Vis. Sci. 34, 205-215.

McCarey, B.E., Kaufman, H.E., 1974. Improved corneal storage. Invest. Ophthalmol. Vis. Sci. 13, 165-173.

McFadden, S.A., Howlett, M.H.C., Mertz, J.R., 2004. Retinoic acid signals the direction of ocular elongation in the guinea pig eye. Vision Res. 44, 643-653.

Moses, R.A., Lurie, P., Wette, R., 1982. Horizontal gaze position effect on intraocular pressure. Invest. Ophthalmol. Vis. Sci. 22, 551-553.

Mutti, D.O., Mitchell, G.L., Hayes, J.R., Jones, L.A., Moeschberger, M.L., Cotter, S.A., Kleinstein, R.N., Manny, R.E., Twelker, J.D., Zadnik, K., 2006. Accommodative lag before and after the onset of myopia. Invest. Ophthalmol. Vis. Sci. 47, 837-846.

Mutti, D.O., Mitchell, G.L., Moeschberger, M.L., Jones, L.A., Zadnik, K., 2002. Parental myopia, near work, school achievement, and children's refractive error. Invest. Ophthalmol. Vis. Sci. 43, 3633-3640.

Neath, P., Roche, S.M., Bee, J.A., 1991. Intraocular pressure-dependent and-independent phases of growth of the embryonic chick eye and cornea. Invest. Ophthalmol. Vis. Sci. 32, 2483-2491.

Nguyen, T.D., Jones, R.E., Boyce, B.L., 2008. A nonlinear anisotropic viscoelastic model for the tensile behavior of the corneal stroma. J. Biomech. Eng. 130, 1-10.

Nomura, H., Ando, F., Niino, N., Shimokata, H., Miyake, Y., 2004. The relationship between intraocular pressure and refractive error adjusting for age and central corneal thickness. Ophthalmic Physiol. Opt. 24, 41-45.

Perkins, E.S., 1981. Ocular volume and ocular rigidity. Exp. Eye Res. 33, 141-145.

Phillips, J.R., Khalaj, M., McBrien, N.A., 2000. Induced myopia associated with increased scleral creep in chick and tree shrew eyes. Invest. Ophthalmol. Vis. Sci. 41, 2028-2034.

Phillips, J.R., McBrien, N.A., 1995. Form deprivation myopia: elastic properties of sclera. Ophthalmic Physiol. Opt. 15, 357-362.

Phillips, J.R., McBrien, N.A., 2004. Pressure-induced changes in axial eye length of chick and tree shrew: significance of myofibroblasts in the sclera. Invest. Ophthalmol. Vis. Sci. 45, 758-763.

Pierscionek, B.K., Asejczyk-Widlicka, M., Schachar, R.A., 2007. The effect of changing intraocular pressure on the corneal and scleral curvatures in the fresh porcine eye. Br. J. Ophthalmol. 91, 801-803.

Pinsky, P.M., van der Heide, D., Chernyak, D., 2005. Computational modeling of mechanical anisotropy in the cornea and sclera. J. Cataract Refract. Surg. 31, 136-145.

Prashar, A., Guggenheim, J.A., Erichsen, J.T., Hocking, P.M., Morgan, J.E., 2007. Measurement of intraocular pressure (IOP) in chickens using a rebound tonometer: Quantitative evaluation of variance due to position inaccuracies. Exp. Eye Res. 85, 563-571.

Puell-Marin, M.C., Romero-Martin, M., Dominguez-Carmona, M., 1997. Intraocular pressure in 528 university students: effect of refractive error. J. Am. Optom. Assoc. 68, 657-662.

Quinn, G.E., Berlin, J.A., Young, T.L., Ziylan, S., Stone, R.A., 1995. Association of intraocular pressure and myopia in children. Ophthalmology. 102, 180-185.

Read, A.S., Collins, M.J., Becker, H., Cutting, J., Ross, D., Savill, A.K., Trevor, B., 2010. Changes in intraocular pressure and ocular pulse amplitude with accommodation. Br. J. Ophthalmol. 94, 332-335.

Rose, K., Smith, W., Morgan, I., Mitchell, P., 2001. The increasing prevalence of myopia: implications for Australia. Clin. Exp. Ophthalmol. 29, 116-120.

Rose, K.A., Morgan, I.G., Ip, J., Kifley, A., Huynh, S., Smith, W., Mitchell, P., 2008. Outdoor activity reduces the prevalence of myopia in children. Ophthalmology. 115, 1279-1285.

Rosenfield, M., Gilmartin, B., 1998. Myopia and Nearwork, 1st ed ed. Butterworth-Heinemann, Oxford.

Schaeffel, F., Glasser, A., Howland, H.C., 1988. Accommodation, refractive error and eye growth in chickens. Vision Res. 28, 639-657.

Schaeffel, F., Howland, H.C., 1988. Visual optics in normal and ametropic chickens. Clin. Vision Sci. 3, 83-98.

Schmid, K.L., Hills, T., Abbott, M., Humphries, M., Pyne, K., Wildsoet, C.F., 2003. Relationship between intraocular pressure and eye growth in chick. Ophthalmic Physiol. Opt. 23, 25-33.

Schmid, K.L., Wildsoet, C.F., 1996. Effects on the compensatory responses to positive and negative lenses of intermittent lens wear and ciliary nerve section in chicks. Vision Res. 36, 1023-1036.

Sigal, I.A., Flanagan, J.G., Tertinegg, I., Ethier, C.R., 2004. Finite element modeling of optic nerve head biomechanics. Invest. Ophthalmol. Vis. Sci. 45, 4378-4387.

Sivak, J.G., 2004. Through the lens clearly: Phylogeny and development. The proctor lecture. Invest. Ophthalmol. Vis. Sci. 45, 740-747.

Sperduto, R.D., Seigel, D., Roberts, J., Rowland, M., 1983. Prevalence of myopia in the United States. Arch. Ophthalmol. 101, 405-407.

Stone, R.A., Flitcroft, D.I., 2004. Ocular shape and myopia. Ann. Acad. Med. Singapore. 33, 7-15.

Tamm, E., Lütjen-Drecoll, E., Jungkunz, W., Rohen, J.W., 1991. Posterior attachment of ciliary muscle in young, accommodating old, presbyopic monkeys. Invest. Ophthalmol. Vis. Sci. 32, 1678-1692.

Tarrant, J., Severson, H., Wildsoet, C.F., 2008. Accommodation in emmetropic and myopic young adults wearing bifocal soft contact lenses. Ophthalmic Physiol. Opt. 28, 62-72.

Thale, A., Tillmann, B., 1993. The collagen architecture of the sclera - SEM and immunohistochemical studies. Ann. Anat. 175, 215-220.

Thale, A., Tillmann, B., Rochels, R., 1996. Scanning electron-microscopic studies of the collagen architecture of the human sclera - normal and pathological findings. Ophthalmologica. 210, 137-141.

Tomlinson, A., Phillips, C.I., 1970. Applanation tension and axial length of the eyeball. Br. J. Ophthalmol. 54, 548-553.

Troilo, D., Nickla, D.L., Wildsoet, C.F., 2000. Choroidal thickness changes during altered eye growth and refractive state in a primate. Invest. Ophthalmol. Vis. Sci. 41, 1249-1258.

Uchio, E., Ohno, S., Kudoh, J., Aoki, K., Kisielewicz, L.T., 1999. Simulation model of an eyeball based on finite element analysis on a supercomputer. Br. J. Ophthalmol. 83, 1106-1111.

Vitale, S., Cotch, M.F., Sperduto, R., Ellwein, L., 2006. Costs of refractive correction of distance vision impairment in the United States, 1999-2002. Ophthalmology. 113, 2163-2170.

Vitale, S., Ellwein, L., Cotch, M.F., Ferris, F.L.I.I.I., Sperduto, R., 2008. Prevalence of Refractive Error in the United States, 1999-2004. Arch. Ophthalmol. 126, 1111-1119.

Vitale, S., Sperduto, R.D., Ferris, F.L.I.I.I., 2009. Increased prevalence of myopia in the United States between 1971-1972 and 1999-2004. Arch. Ophthalmol. 127, 1632-1639.

Wallman, J., Adams, J.I., 1987. Developmental aspects of experimental myopia in chicks: susceptibility, recovery and relation to emmetropization. Vision Res. 27, 1139-1163.

Wallman, J., Winawer, J., 2004. Homeostasis of eye growth and the question of myopia. Neuron. 43, 447-468.

Walls, G.L., 1942. Birds, in: Walls, G.L. (Ed.), The vertebrate eye and its adaptive radiation. The Cranbrook Institute of Science, Bloomfield Hills, Michigan, pp. 641-662.

Wang, T.J., Chiang, T.H., Wang, T.H., Lin, L.L.K., Shih, Y.F., 2008a. Changes of the ocular refraction among freshmen in National Taiwan University between 1988 and 2005. Eye. 23, 1168-1169.

Wang, X., Chen, W., Li, Y., 2008b. Biomechanical properties of experimental myopia in the guinea pig. ICBBE. , 1825-1827.

Weizhong, L., Zhikuan, Y., Wen, L., Xiang, C., Jian, G., 2008. A longitudinal study on the relationship between myopia development and near accommodation lag in myopic children. Ophthalmic Physiol. Opt. 28, 57-67.

Wildsoet, C., Wallman, J., 1995. Choroidal and scleral mechanisms of compensation for spectacle lenses in chicks. Vision Res. 35, 1175-1194.

Wong, A., Clausi, D.A., Fieguth, P., 2010. CPOL: Complex phase order likelihood as a similarity measure for MR-CT registration. Med. Image Anal. 14, 50-57.

Wong, A., Genest, R., Chandrashekar, N., Choh, V., Irving, E.L., in press. Automatic system for three-dimensional reconstruction of the chick eye based on digital photographs. Computer Methods in Biomechanics and Biomedical Engineering.

Wong, T.Y., Foster, P.J., Hee, J., Ng, T.P., Tielsch, J.M., Chew, S.J., Johnson, G.J., Seah, S.K.L., 2000. Prevalence and risk factors for refractive errors in adult Chinese in Singapore. Invest. Ophthalmol. Vis. Sci. 41, 2486-2494.

Wong, T.Y., Klein, B.E.K., Klein, R., Knudtson, M., Lee, K.E., 2003. Refractive errors, intraocular pressure, and glaucoma in a white population. Ophthalmology. 110, 211-217.

Woo, S.L.Y., Kobayashi, A.S., Schlegel, W.A., Lawrence, C., 1972. Nonlinear material properties of intact cornea and sclera. Exp. Eye Res. 14, 29-39.

Xu, J., Ma, L.W., Liu, L.M., Xu, Y.C., 2007. Relationship of refractive status, axial length, and scleral metamorphic change in chicken form deprivation eyes. Ophthalmologica. 7, 400-403.

Xu, L., Li, J., Zheng, Y., Cui, T., Zhu, J., Yang, H., Ma, B., Jonas, J.B., 2005. Intraocular pressure in northern China in an urban and rural population: The Beijing eye study. Am. J. Ophthalmol. 140, 913-915.

Young, F.A., 1981. Primate myopia. Am. J. Optom. Physiol. Opt. 58, 560-566.

Young, F.A., Lear, G.A., Baldwin, W.R., West, D.C., Box, R.A., Harris, E., Johnson, C., 1969. The transmission of refractive errors within Eskimo families. Am. J. Optom. Arch. Am. Acad. Optom. 46, 676-685.

Young, F.A., Pullman, W.A., Leary, G.A., 1987. The mechanism of visual accommodation and its role in refraction (abstract). Am. J. Optom. Physiol. Opt. 64, 10.

Appendix A: Spherical membrane theory

In this appendix, the spherical membrane theory is used to derive equations to relate pressure to volume and strain to pressure for a sphere of constant thickness and homogeneous and isotropic material properties. The calculation for obtaining the pressure-volume relation follows the development of Greene (1985) while the strain-pressure relation was derived by the author.

A.1 Normal displacement of the membrane wall

A membrane subjected to a biaxial state of stress (σ_1 and σ_2) will deform according to the following formulae:

$$\varepsilon_1 = \frac{\sigma_1 - \nu\sigma_2}{E}$$

$$\varepsilon_2 = \frac{\sigma_2 - \nu\sigma_1}{E} \tag{1}$$

Here, ν is Poisson's ratio and E is the Young's modulus of the membrane. The membrane is assumed to be isotropic and homogeneous. Now, for the case of a spherical membrane, the stress distribution is uniform such that $\sigma_1 = \sigma_2 = \sigma$ and $\varepsilon_1 = \varepsilon_2 = \varepsilon$. Equation (1) reduces to:

$$\varepsilon = \frac{\sigma(1-\nu)}{E} \tag{2}$$

When the stress-strain curve of a material is nonlinear, it is useful to use the tangent modulus $E_t(\sigma)$ and small increments of stress and strain. Equation (2) takes the form of:

$$d\varepsilon = \frac{d\sigma(1-\nu)}{E_t(\sigma)} \tag{3}$$

Now, the following equation can be used to relate the stress σ in the spherical membrane and the internal pressure p:

$$\sigma = \frac{pr}{2t} \tag{4}$$

In equation (4), r is the inner radius of the spherical membrane and t is its thickness. Similarly, equation (4) can be used to relate a small stress increment dσ to a small pressure increment dp:

$$d\sigma = \frac{r}{2t}dp \tag{5}$$

Also, the normal strain increment dε of a spherical membrane of radius r is related to the normal deflection dw of the wall by:

$$d\varepsilon = \frac{dw}{r} \tag{6}$$

Now, if we combine equations (3), (5), and (6) we get:

$$d\varepsilon = \frac{dw}{r} = \frac{d\sigma(1-\nu)}{E_t(\sigma)} = \frac{r(1-\nu)}{2tE_t(\sigma)}dp \tag{7}$$

We can solve equation (7) for dw as a function of dp to obtain:

$$dw = \frac{r^2(1-\nu)}{2tE_t(\sigma)}dp \tag{8}$$

The eye is modeled as an exponentially stiffening spherical membrane whose constitutive relation is given by:

$$\sigma = A[e^{\alpha\varepsilon} - 1] \tag{9}$$

Note that the eye is assumed to have uniform thickness and material properties. Also, the thickness t is assumed to remain constant during inflation. Now, the total normal displacement of the spherical

membrane wall can be found by integrating equation (8):

$$w = \frac{r^2(1-\nu)}{2t}\int_0^p \frac{dp}{E_t(p)} \tag{10}$$

Here, we assumed that the membrane radius r and the thickness t vary so little with pressure p that they are almost constant, and can therefore be taken out of the integral. Now, we need an expression for $E_t(p)$ in order to evaluate the integral. Let's start with the definition of tangent modulus and the constitutive relation, equation (9):

$$E_t(\sigma) = \frac{d\sigma}{d\varepsilon} = \frac{d(A[e^{\alpha\varepsilon}-1])}{d\varepsilon} = A\alpha e^{\alpha\varepsilon} = \alpha(Ae^{\alpha\varepsilon} - A + A) = \alpha(\sigma + A) \tag{11}$$

By substituting equation (4) into equation (11), we can find a relation for $E_t(p)$ as follow:

$$E_t(p) = \alpha\left(\frac{rp}{2t} + A\right) \tag{12}$$

At this point, we need to insert equation (12) into equation (10) and perform the integration:

$$w = \frac{r^2(1-\nu)}{2t}\int_0^p \frac{dp}{\alpha\left(\frac{rp}{2t}+A\right)} = \frac{r^2(1-\nu)}{2t\alpha}\int_0^p \frac{rdp}{2tA(\frac{rp}{2tA}+1)}.\frac{2t}{r}$$

$$\int \frac{du}{u} = ln|u| + C$$

$$w(p) = \frac{r(1-\nu)}{\alpha}\ln\left|\frac{\mathrm{rp}}{2\mathrm{tA}} + 1\right| \tag{13}$$

Equation (13) gives us the normal deflection of the spherical membrane wall as a function of pressure and parameters r, t, α, A, and ν.

A.2 Pressure-volume relation

To obtain a pressure-volume relation, we first start with an expression of volume as a function of pressure. We know that the volume at a given pressure is equal to the initial volume plus the volume due to the wall deflection:

$$V(p) = V_o + 4\pi r^2 w(p) \tag{14}$$

Substituting equation (13) into equation (14), we obtain:

$$V(p) = V_o + \frac{4\pi r^3(1-\nu)}{\alpha} ln\left|\frac{rp}{2tA} + 1\right|$$

Note that $4\pi r^3 = 3V_0$:

$$\frac{\alpha(V - V_o)}{3V_o(1-\nu)} = ln\left|\frac{rp}{2tA} + 1\right|$$

Inverting the equation to obtain pressure as a function of volume:

$$e^{\frac{\alpha(V-V_o)}{3V_o(1-\nu)}} = \frac{rp}{2tA} + 1$$

$$p(V) = \frac{2tA}{r}\left[e^{\frac{\alpha(V-V_o)}{3V_o(1-\nu)}} - 1\right] \tag{15}$$

A.3 Strain-pressure relation

To obtain a strain-pressure relation for an exponentially stiffening sphere, we need to substitute equation (4) into equation (9) and solve for the strain:

$$\varepsilon(p) = \frac{1}{\alpha}\ln\left|\frac{\mathrm{rp}}{2\mathrm{tA}} + 1\right| \tag{16}$$

Glossary

Accommodation

The change in optical power of the eye to focus light coming from objects of different distances.

Anisotropic material

A material whose mechanical properties at a given point vary with direction of loading.

Convergence

The coordinated and simultaneous inward movement of both eyes in an attempt to maintain a single visual image when looking at an object.

Defocus

The state of an optical system that is out of focus, that is, an optical system focused in front or behind the plane of focus.

Dioptre

A unit of measure of the optical power of a lens or an optical system. Is equal to the reciprocal of the focal length of the lens or optical system measured in metres.

Dioptric power

The degree to which a lens or an optical system bends light as it passes through it; commonly measured in dioptres. Also referred to as optical power or refractive power.

Elastic limit

See yield point.

Emmetrope

A person with emmetropia (no refractive error).

Emmetropia

The state of the non-accommodated eye in which the optical power of the eye matches its axial length such that parallel rays of light entering the eye are focus precisely on the retina. The result is a clear image.

Heterogeneous material

A material whose mechanical properties vary from point to point.

Homogeneous material

A material whose mechanical properties do not vary from point to point.

Hyperope

A person affected by hyperopia.

Hyperopia

A refractive error that occurs when the non-accommodated eye focuses parallel rays of light behind the retina. Near objects appear blurry.

Hyperopic defocus

The state of the eye in which rays of light are focused behind the retina.

Incompressible material

A material whose volume does not diminish when subjected to a force or pressure.

Isotropic material

A material whose mechanical properties at a given point do not vary with direction of loading.

Marlow hyperelastic material model

A material definition used to model elastic and highly nonlinear materials such as rubber. It uses a strain energy potential (rather than Young's modulus and Poisson's ratio) to relate strain to stress in the material.

Myope

A person affected by myopia.

Myopia

A refractive error that occurs when the non-accommodated eye focuses parallel rays of light, coming from far objects, in front of the retina. Distance objects appear blurry.

Myopic defocus

The state of the eye in which rays of light are focused in front of the retina.

Optical power

The degree to which a lens or an optical system bends light as it passes through it; commonly measured in dioptres. Also referred to as dioptric power or refractive power.

Optical system

A system composed of optical devices (lenses, mirrors, prisms, and other devices) arranged in a prescribed manner to refract, reflect, disperse, polarize, absorb, or somehow act on light.

Refraction

The bending of light as it passes through two media of different refractive index.

Refractive error

An optical defect of the non-accommodated eye in which parallel rays of light are not focused exactly on the retina.

Refractive index

A measure of the speed of light in a substance. Is equal to the ratio of the speed of light in a vacuum to the speed of light in the substance under consideration.

Refractive power

The degree to which a lens or an optical system bends light as it passes through it; commonly measured in dioptres. Also referred to as dioptric power or optical power.

Retinoscopy

A method for determining the refractive error of the eye.

Strain

A measure of deformation of a body under applied stresses. Engineering strain is equal to the ratio of elongation to the initial dimension of the body.

Stress

A measure of the average internal force per unit area within a body. The internal forces are produced in response to externally applied forces on a body and the result is deformation of the body's geometry. The unit of stress in the International System of Units is the Pascal (Pa) which is equal to one newton (unit of force) per square meter (unit of area).

Von Mises Stress

An equivalent stress quantity based on the maximum-distortion-energy theory that takes into account the principal stresses in all directions caused by combined loading. The von Mises Stress is commonly used to predict the yielding of ductile materials under combined loading using the yield point from a simple tension test.

Yield point

The stress level at which permanent deformation starts to occur in a given material. Prior to the yield point, the deformation is elastic and the material returns to its original geometry after the applied stress is removed. Beyond the yield point, a portion of the deformation remains after removal of the applied stress.

Copyrighted material

Permission to use Figure 5.

Dear Reno,

Thank you for your interest in our copyrighted material and for your e-mail requesting permission to reproduce the Fig. 1 from our journal Drugs News and Perspectives 2006; 19(3): 152 in your master thesis entitled *"Effect of Intraocular Pressure on Chick Eye Geometry, Finite Element Modeling, and Myopia"*.

Permission is granted with the understanding that you will give appropriate credit and include the following text in your credit line:

Drugs News Perspect 2006; 19(3): 151-158. Copyright © 2006 Prous Science, S.A. All rights reserved.

Please note that this permission is a nonexclusive grant limited to the specific use, format and edition specified on a one-time only or life-on-an-edition basis.

Best regards,

Ana Ballesteros
Pharma Services
Thomson Reuters
Ph . +34-93-459 2220; ext. 600
ana.ballesteros@thomsonreuters.com

Permission to use part of the Wong et al. (in press) article.

Hello Reno.

You can use part of your article in your thesis, so long as you use the original text as it was accepted by CMBBE and cite CMBBE as the source.

You can cite the paper as 'in press' instead of by date of publication, as it has not yet been published.

As far as we're concerned, you don't need a permission note. All we ask is that you cite CMBBE as the source. If you publish your thesis or something based on it the publisher might ask for a permission note, in which case this email should suffice.

Regards,

Chris Longhurst

Chris.Longhurst@tandf.co.uk